THREE-DIMENSIONAL KINEMATIC ANALYSIS OF SPINE MOTION

By

BRYAN PRESTON CONRAD

A DISSERTATION PRESENTED TO THE GRADUATE SCHOOL
OF THE UNIVERSITY OF FLORIDA IN PARTIAL FULFILLMENT
OF THE REQUIREMENTS FOR THE DEGREE OF
DOCTOR OF PHILOSOPHY

UNIVERSITY OF FLORIDA

2009

To my girls

ACKNOWLEDGMENTS

I thank my committee for providing thoughtful feedback and insight. Dr. Horodyski has helped to keep the project focused on the clinical goals and applications of measuring spine motion and has also shared her extensive experience with statistical analysis. In every interaction I have had with him, Dr. Fregly has been a source of inspiration and encouragement. I also appreciate his background in optimization techniques and for letting me borrow three computers and a corner of his lab to do several thousand registrations this past summer. Dr. Zheng has given me a great deal of advice on many aspects of kinematics, image analysis and computer programming. The many interactions I have had with him in the Biomechanics and Motion Analysis lab have gone a long way in shaping my understanding of how to apply engineering principles in a medical environment. I thank Dr. Banks for giving me the opportunity to work on an interesting, significant and challenging project. His arrival at UF when I was desperately seeking a thesis advisor and project was serendipitous. I am incredibly grateful that he suggested that it might be interesting to study spine kinematics; despite the challenges (or maybe because of them), I cannot imagine working on a more rewarding project.

I also appreciate the interaction and frequent feedback from my fellow graduate students. Bo, JD and Dr. David have done an excellent job of representing the engineering contingent in the OSMI. The development of my image registration code was greatly assisted by the contributions of Shang, who laid the groundwork with JointTrack 2.0. I also appreciate the various insights and suggestions of Nick, Tim, Ben, and the many undergraduate students that have worked in the lab over the years.

I also thank my high school calculus teacher, Anastasia Bilotta, who infected me with a passion for math and a zeal for solving difficult problems.

I thank my family for the support and encouragement they have provided during my exceedingly long tenure as a graduate student. I started this journey the same year I married Suzanne and I assured her when we got married that there was no possibility of me ever pursuing a doctorate degree. Although this was not part of the bargain when she married me, she has been a constant source of encouragement and help at every step of the process. She has displayed an incredible level of selflessness in giving me the time necessary to complete this work, I could not have completed this degree without her help. Along the way we have been blessed with two daughters. Adeline is very curious about this “book” I am writing and would like me to read it to her when I am done. Esther has taken a keen interest in my laptop and has been trying to help me by “typing” a few lines for me every time I turn my back on her.

TABLE OF CONTENTS

page

ACKNOWLEDGMENTS 4

TABLE OF CONTENTS 6

LIST OF TABLES 8

LIST OF FIGURES 9

LIST OF ABBREVIATIONS 12

ABSTRACT 13

CHAPTER

1 INTRODUCTION 15

Clinical Motivation 15
Spine Anatomy 16
Hypothesis 17
Specific Aims 18

2 MEASUREMENT OF CERVICAL DISC REPLACEMENT KINEMATICS USING MODEL TO IMAGE REGISTRATION 19

Introduction 19
Clinical Motivation 19
Purpose 20
Methods 22
Image Registration Tool 22
Experimental Setup 23
Data Analysis 24
Results 25
Discussion 31

3 VALIDATION OF A METHOD TO REGISTER A 3D CT VOLUME TO A SINGLE PLANE 2D FLUOROSCOPIC IMAGE USING DIGITALLY RECONSTRUCTED RADIOGRAPHS 34

Introduction 34
Clinical Motivation 34
Medical Image Registration 34
Purpose 35
Methods 37
Digitally Reconstructed Radiographs 37

Perspective Projection Geometry 43
Registration Algorithm 44
Image Metric 45
Mean squares 46
Normalized correlation metric 48
Normalized cross correlation 50
Gradient correlation 51
Gradient difference 55
Mutual information 57
Mutual information and gradient correlation 59
Optimizer 61
Starting Positions 62
Results 63
Discussion 67
Conclusion 72

4 MEASUREMENT OF SPINE KINEMATICS BY REGISTERING LATERAL FLUOROSCOPY IMAGES TO DIGITALLY RECONSTRUCTED RADIOGRAPHS 73

Introduction 73
Review of Current Methods for Measuring Spine Motion 74
Purpose 76
Methods 77
Specimen Preparation 77
Experimental Protocol 77
Imaging Protocol 80
Data Analysis 81
Software Development 82
Results 85
Discussion 104

5 CONCLUSION 108

LIST OF REFERENCES 109

BIOGRAPHICAL SKETCH 117

LIST OF TABLES

Table		page
2-1	RMS errors for image based measurements compared to marker based measurements.	25
2-2	Precision for image based measurements compared to marker based measurements.	26
2-3	Bias for image based measurements compared to marker based measurements.	26
3-1	Analysis of registration errors for each pose parameter.	66
3-1	Specimen properties.	81
4-1	Average RMS Errors for translations.	102
4-2	Average RMS Errors for rotations.	102
4-3	Average bias for translations.	102
4-4	Average bias for rotations.	103
4-5	Average precision for translations.	103
4-6	Average precision for rotations.	103

LIST OF FIGURES

Figure page

2-1 CAD model of the Synthes Pro-Disc C cervical arthroplasty implant. 24

2-2 Absolute segmental rotation (in degrees) of the superior implant. 26

2-3 Absolute segmental rotation (in degrees) of the superior implant. 27

2-4 Rotation errors (in degrees) of the superior implant. 28

2-5 Absolute segmental rotation (in degrees) of the inferior implant. 29

2-6 Absolute segmental rotation (in degrees) of the inferior implant. 30

2-7 Rotation errors (in degrees) of the inferior implant. 31

2-7 Surface model projections of a cervical spine arthroplasty implant. 32

2-8 Surface model projections of a cervical spine arthroplasty implant. 33

3-1 Diagram of the work flow during the registration process. 35

3-2 Diagram of the radiographic projection geometry. 39

3-3 Diagram of the DRR projection geometry. 40

3-4 Texture mapping. 41

3-5 DRRs of a thoracolumbar spine specimen 42

3-6 DRRs of a cervical spine specimen. 42

3-7 Example of a fluoroscopic image of the thoracolumbar spine. 43

3-8 The projection geometry of the radiographic imaging equipment. 44

3-9 Schematic diagram of the registration process. 45

3-10 Plots of the MS metric function versus pose. 47

3-11 Plots of the NC metric function versus pose. 49

3-12 Plots of the NCC metric function versus pose. 51

3-13 Changing the amount of image blur. 52

3-14 An example of edge images from the fluoroscopic image. 53

3-15 Plots of the NCC metric function versus pose. 54

3-16 Plots of the GD metric function versus pose 56
3-17 Example of Mutual information. 58
3-18 Plots of the MI metric function versus pose. 59
3-19 Plots of the GC+MI metric function versus pose. 60
3-20 Percentage of successful registrations. 64
3-21 For registrations that were successful. 65
3-22 Three orthogonal views of a surface model a spinal vertebrae 68
4-1 Definition of the motion capture reference frame. 78
4-2 Definition of the anatomical reference frame. 79
4-3 Image of the fluoroscopic testing setup. 79
4-4 Screen capture of pyTrack software. 83
4-5 Diagram of the pyTrack data structure. 84
4-6 Segmental rotation (in degrees) of the superior vertebrae. 86
4-7 Segmental rotation (in degrees) of the superior vertebrae 87
4-8 Segmental rotation (in degrees) tracking errors of the superior vertebrae. 88
4-9 Segmental translation (in mm) of the superior vertebrae. 89
4-10 Segmental translation (in mm) of the superior vertebrae. 90
4-11 Segmental translation tracking errors (in mm) of the superior vertebrae. 91
4-12 Segmental rotation (in degrees) of the inferior vertebrae. 92
4-13 Segmental rotation (in degrees) of the inferior vertebrae. 93
4-14 Segmental rotation tracking errors (in degrees) of the inferior vertebrae. 94
4-15 Segmental translation (in mm) of the inferior vertebrae. 95
4-16 Segmental translation (in mm) of the inferior vertebrae. 96
4-17 Segmental translation tracking errors (in mm) of the inferior vertebrae 97
4-18 Relative joint angles (in deg) calculated from image based motion data. 98

4-19 Relative joint angles (in deg) calculated from marker based motion data..... 99

4-20 Relative joint translations (in mm) calculated from image based motion data. . 100

4-21 Relative joint translations (in mm) calculated from marker based motion data. 101

4-18 Lateral bending motion presents challenges with a lateral fluoroscopic view. .. 104

LIST OF ABBREVIATIONS

3D	Three Dimensional
CT	Computerized Tomography
DRR	Digitally Reconstructed Radiograph
MRI	Magnetic Resonance Imaging
PET	Positron Emission Tomography
SPECT	Single Photon Emission Computed Tomography
US	Ultrasound
MSE	Mean Square Error
NCC	Normalized Correlation Coefficient
GD	Gradient Difference
GC	Gradient Correlation
MI	Mutual Information
ACDF	Anterior Cervical Discectomy and Fusion
mTRE	mean Target Registration Error

Abstract of Dissertation Presented to the Graduate School
of the University of Florida in Partial Fulfillment of the
Requirements for the Degree of Doctor of Philosophy

THREE-DIMENSIONAL KINEMATIC ANALYSIS OF SPINE MOTION

By

Bryan Preston Conrad

December 2009

Chair: Scott A. Banks
Major: Biomedical Engineering

Motion is an important function of the human spine and accurate measurement of that motion is critical to assessing spinal health and the effect of treatments. There is a great need for tools that allow accurate 3D intervertebral spine motion to be measured *in vivo*. The purpose of this study is to develop a method for registering a 2D radiograph with a 3D CT scan for the purpose of measuring 3D motion in the spine. This goal was achieved in three phases. The first phase of this project evaluated the accuracy of a fluoroscopic object recognition technique to measure the 3D position and orientation of a cervical disc arthroplasty implant. Although the experimental uncertainties of the proposed technique have been extensively analyzed with respect to the measurement of knee implant motions, the size, geometry, and type of motion of spine implants requires that these uncertainties be determined specifically for spine components. These uncertainties were determined using a cadaver model. The second phase of this project developed and evaluated the static accuracy and capture range of a novel 2D/3D image registration methodology using existing gold standard data. Digitally reconstructed radiographs were used in the registration algorithm to take advantage of the internal contours and density variation of the bony anatomy. In the

third phase of this project, the uncertainties of measuring dynamic 3D kinematics of cervical vertebrae were determined. The tools developed in this project will allow clinicians and researchers to accurately quantify the performance of the normal spine as well as new implants designed to restore motion to the spine. This methodology also has applications for other joints, such as the shoulder, ankle, knee and hip.

CHAPTER 1
INTRODUCTION

Clinical Motivation

"The purpose of the human musculoskeletal system is to support the body and allow motion. If we didn't need to move, we would have roots and photosynthesize."(1) Motion is a critical function of the body. Measuring motion is important to understanding the function of the joints of the body. There are many disabilities that can adversely affect joints in the body and understanding the motion of those joints can provide an avenue to restore the proper function of the joint. Range of joint motion often is used as an indicator of the extent of disability caused by joint disease. Likewise, changes in motion provide a valuable outcome measure to assess the effectiveness of clinical interventions. Although many orthopaedic therapies attempt to restore normal joint motion, in some cases it is not clear how to measure or even evaluate "normal" joint motion. The situation of clinically measuring spine kinematics is so muddled that not only is there disagreement over how much motion is desirable, but there is also controversy over how to define whether any motion exists at all. Some authors have suggested that less than 2-4 deg of motion constitutes a "fusion", while others hold that a "fusion" must be demonstrate less than 1 deg of motion. These differences are likely attributable to the large uncertainties associated with currently available motion measurement tools.

There are numerous challenges that must be addressed to perform accurate measurements of skeletal motion. Most joints must be evaluated in 3-dimension (3D) motion to fully appreciate their full function. While it can be convenient and useful to sometimes model them as such, joints generally do not behave as simple mechanical

linkages like a hinge, ball-socket or universal joint. The most complete model of joint motion requires that it be modeled as a 6-degree of freedom joint. It is also difficult to measure skeletal motion externally due to the paradoxical motion of the overlying soft tissue. While these challenges are encountered when performing kinematic measurements for every joint in the body they are perhaps most acute when measuring spine motion.

The fundamental purpose of this project is to develop, validate and utilize a method to accurately measure spinal motion. There are three specific requirements that drive this research project:

- Intervertebral motion – it is critical to measure motion at each functional spinal unit, between adjacent vertebrae, so that dysfunction and treatments can be evaluated at the point of application.
- Three-dimensional – it is necessary to measure spine motion in three dimensional space, so that the full functional range of motion of the spine can be evaluated.
- *in vivo* – it is important to measure spine motion in a clinical setting using non-invasive methods, so that the full physiological environment (including active muscle forces) can be tested.

Spine Anatomy

A brief review of spine anatomy as it relates to the purpose of this research study is presented below, much more detailed works (such as (2)) are available with greater depth than is possible here. The human spine is a unique structure consisting of 24 individual bones. Of these 24 bones there are seven cervical vertebrae, twelve thoracic vertebrae and five lumbar vertebrae. While the vertebrae in each region share common characteristics, each bone has a unique geometry that defines the type and amount of motion is allowable at that level. In the upper cervical spine, C1 and C2 differ significantly in structure and function from the rest of the cervical spine and are

generally treated separately. C1, also called the atlas, articulates with the occiput of the skull and allows only flexion and extension motions. The C2 vertebra, also known as the axis, forms a pivot which articulates with C1 to allow nearly planar axial rotation. The remainder of the cervical, thoracic and lumbar vertebrae (C3-L5), have three points of motion between each level, the intervertebral disc and the right and left facets. At each level the angle of the facet joints dictates the amount and direction of motion allowed. Oblique in the cervical spine to allow freedom for flexion-extension, lateral bending and axial rotation; nearly vertical and parallel to the frontal plane in the thoracic spine to restrict all motion except for lateral bending; and nearly vertical and oriented parallel to the sagittal plane in the lumbar spine to allow flexion-extension. The articulations in the spine present a complex kinematic environment where motions are coupled. For example: as the cervical spine rotates axially, it also bends laterally. When cervical spine motion is being evaluated, it is therefore valuable to account for motions in all three dimensions. Because the individual vertebrae reside deep within surrounding soft tissue, there are very few external landmarks that can be used to quantify intervertebral motion, which limits the use of external sensors for measuring intervertebral spine motion.

Hypothesis

The purpose of this project is to quantify the 3D motions of the human spine for both normal anatomy as well as for implanted devices. The specific hypothesis that drives this work is that model to image registration can be used to accurately measure the kinematics of the spine. The conception of this project was inspired from the following observations. First, single plane fluoroscopy and 2D/3D registration have been used for over 15 years to quantify the in vivo motions of knee arthroplasty

components(3-12). Second, more recently, this technique has been extended so that not only can metallic objects be registered, but bone models can be tracked as well. Third, advances in imaging and computing allow higher resolution images to be acquired, which is critical for tracking the relatively smaller bones of the spine. The specific aims are designed to provide a comprehensive evaluation of the accuracy of applying a 2D/3D registration algorithm to measuring spine motion.

Specific Aims

The specific aims of this research project were:

- Specific Aim 1. Determine the accuracy of a fluoroscopic object recognition technique to measure the 3D position and orientation of a cervical disc arthroplasty implant using existing model based registration methods. Although the experimental uncertainties of the proposed technique have been extensively analyzed with respect to the measurement of knee implant motions, the size, geometry, and type of motion of spine implants requires that these uncertainties be determined specifically for spine components. A cadaver model was used to quantify the uncertainty of this method.

- Specific Aim 2. Determine the accuracy of a fluoroscopic model registration technique to measure the 3D position and orientation of the vertebrae. Digitally reconstructed radiographs were used in the registration algorithm to take advantage of the internal contours and density variation of the bony anatomy. This phase of the research project developed of a set of software tools that enable 2D/3D registration of spinal vertebrae. The experimental uncertainties for registering static images were determined for the image registration process. Existing static gold standard data were used for this phase of the project.

- Specific Aim 3. Characterize the 3D motion of vertebrae during dynamic motion. The final aim is to demonstrate an *in vitro* application of a 2D/3D registration algorithm for measuring dynamic spine motions and to evaluate the uncertainties of measuring vertebral kinematics using image registration. The technique developed in Specific Aim 2 was utilized in a cadaver study to measure dynamic intervertebral kinematics in the spine. The ultimate results of this project is to generate a unique set of tools that can be used to measure 3D segmental spine motion in vivo.

CHAPTER 2
MEASUREMENT OF CERVICAL DISC REPLACEMENT KINEMATICS USING MODEL TO IMAGE REGISTRATION

Introduction

Clinical Motivation

Anterior cervical discectomy and fusion (ACDF) currently are the gold standard for treating the symptoms of radiculopathy and myelopathy. Although ACDF has favorable short-term results, recent data suggests that in the long-term, fusion adversely affects adjacent vertebral levels. It is suspected that by eliminating motion at one level, increased stress and motion is induced at adjacent levels, which leads to degeneration. Cervical arthroplasty has been introduced as an alternative to fusion to preserve motion at operated levels. Although several clinical trials are underway to evaluate the effectiveness of various cervical disc replacement implants, important biomechanical parameters remain to be addressed. The combination of concern over the long-term consequences of spinal arthrodesis and the proliferation of motion preserving spinal technology has created an acute need for accurate measurements of 3-dimensional spine motion.

Symptoms of cervical spondylosis include pain and motor dysfunction caused by impingement of the nerve roots (radiculopathy) or spinal cord (myelopathy). Patients with cervical spondylosis are typically treated conservatively at first. If the patient's symptoms are unresponsive to conservative treatment, surgery may be indicated, in which case, ACDF can be used to provide decompression to the nerves and spinal cord. Although excellent 2 year clinical results have been reported for ACDF, recent results from longer term studies are sobering. Hillibrand has documented a cumulative 2.9% per year rate of repeated operation at segments adjacent to a fusion resulting in

approximately 26% of patients requiring an additional fusion by 10 years(13). Goffin(14) recently reported that 92% of patients with cervical interbody fusion eventually displayed signs of adjacent segment degeneration (follow-up 60-187 months).

While the mechanism responsible for adjacent level degeneration has not been clearly defined, it is often postulated to be a result of altered biomechanics of the spine caused by the fusion(15). Another widely held theory is that the adjacent degeneration is a continuation of the natural history of the disease process(16). However, in the study by Goffin et al.(14), younger trauma patients without history of pre-existing degenerative disc disease had similar rates of adjacent degeneration to older patients with spondylosis or disc herniation. This finding suggests that biomechanical factors play an important role in understanding and potentially alleviating adjacent disc degeneration.

Cervical disc replacements have been designed to maintain motion in the cervical spine while allowing decompression of nerve roots and the spinal cord. The goal of cervical arthroplasty is to maintain normal neck kinematics, thereby avoiding increased stresses on levels adjacent to the surgery. Although several clinical trials are underway to evaluate the effectiveness of various cervical disc replacement implants(17-21), important biomechanical parameters remain to be addressed.

Purpose

Motion measurement is critical for evaluating clinical modalities. The increasing use of motion preserving devices in the spine has highlighted the need for accurate kinematic measurement tools to evaluate the performance of these new implants. Single plane fluoroscopy has been used for over 15 years to quantify the in vivo motions of total knee replacement implants, with reported accuracies of 0.5-1.0 deg for rotations.

The purpose of this phase of the research project was to determine the accuracy and feasibility of using a fluoroscopic image registration technique to measure the 3D position and orientation of a cervical disc arthroplasty implant.

Methods

Image Registration Tool

We propose to utilize techniques that we have previously implemented and validated on numerous studies of knee implants(8,12,22-27) to measure 3D motion of spinal arthroplasty components in the cervical spine. Radiographic images are produced when x-rays pass through space and are attenuated by the patient's anatomy before striking a sensitive medium to cause a chemical or electrical reaction. The x-ray beam emanates from a single point in space, creating a perspective projection of the object. The location of the x-ray source with respect to the image plane can be measured and the same projection can be reproduced on a computer. Computer aided design (CAD) models of implant designs can be obtained from the manufacturer or reverse engineered and used to create projections of the implant based on a perspective projection model. The position and orientation of the CAD model can be modified until the computer generated projections of the model match the views obtained from patients – thus determining the position and orientation of the objects in 3D space. A number of groups around the world have used shape matching techniques for determining implant motion from single-plane radiographic views, studying a range of joints and activities including gait(4) , stair-climbing(3), and deep knee bends(7). Although the details of the methods vary, measurement precision for each moving segment is typically 0.5mm-1.0mm for implant motions parallel to the image plane and 0.5°-1.0° for all rotations(22). For the current experiment, used an existing tool developed in our laboratory to measure spine arthroplasty kinematics.

Experimental Setup

A four-camera optical motion capture system (Motion Analysis Corp, Santa Rosa, CA) was used to establish the “true” position and orientation of each cervical vertebrae during the dynamic test. In our lab, this motion capture system has demonstrated a positional accuracy of less than 0.2 mm for a volume of 1 m^3. Three reflective tracking fiducial markers were attached to specific anatomical landmarks on each cervical vertebrae to allow them to be visualized with the optical motion capture system.

Three cadaveric cervical spines that have been implanted with a cervical disc arthroplasty were obtained for this experiment. Three dimensional CAD surface models of the cervical disc arthroplasty implants were obtained from the manufacturer (Figure 2-1). Each cadaver spine was manually manipulated through a range of motions while simultaneously recording both fluoroscopic images and optical motion capture of the spine. The position and orientation of each cervical vertebrae and the implant was determined using both the optical system and the fluoroscopic technique. For the fluoroscopic data, the position and orientation of the implants was determined using existing model to image registration software (JointTrack 1.0, previously developed in our lab). The accuracy of the position and orientations determined by the fluoroscopic measurements were evaluated against the “true” values obtained from the optical motion capture system.

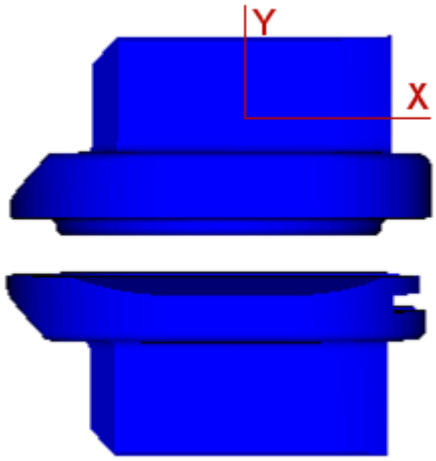

Figure 2-1. CAD model of the Synthes Pro-Disc C cervical arthroplasty implant that was evaluated for this experiment.

Data Analysis

For the error analysis, the absolute position and orientation of the two vertebrae was calculated for both measurement techniques. The position and orientation at each frame, *i,* was determined with respect to the neutral pose, which was defined as the first frame of the trial.

$$^{neutral}\mathrm{A}_i = \left(^{fluoro}\mathrm{A}_{neutral}\right)^{-1} \times {}^{fluoro}\mathrm{A}_i$$

$$^{neutral}\mathrm{A}_i = \left(^{mocap}\mathrm{A}_{neutral}\right)^{-1} \times {}^{mocap}\mathrm{A}_i$$

Where A is a 4 x 4 homogenous transformation matrix. These absolute poses were determined for both the mocap and fluoroscopic techniques, and used to calculate the uncertainties between the two measurement systems.

Motion capture data was collected at a rate of 60 frames/s and the fluoroscope captured images at a rate of 7.5 frames/s. To ensure that the motion capture and fluoroscopic data are comparable in terms of temporal resolution, the fluoroscopic

results were resampled at a rate of 60 Hz using an interpolation algorithm. The data sets were temporally synchronized by performing a linear regression between the mocap and fluoroscopic data. The fluoroscopic data was shifted in the time domain until the R^2 of the linear regression was maximized. This method optimized the alignment between the two data sets..

Experimental errors were determined by measuring the deviation of the fluoroscopic calculated absolute position and orientation data from the motion capture values. Differences were calculated for each frame of data and averaged to determine mean errors. Root mean square (RMS) errors were calculated to determine the experimental uncertainties.

Results

The disc replacement implants were placed at three different levels in the cervical spine (C3-C4, C4-C5, C6-C7). The absolute rotations of each implant were calculated during each motion trial (flexion-extension trial, lateral bending trial, and axial rotation trial) using both the image based measurement technique (Figures 2-1 and 2-4) and for the marker based "gold-standard" technique (Figures 2-2 and 2-5) The experimental uncertainties for calculating the absolute range of motion of each implant were 0.23 ± 1.68^{o} for flexion-extension, 0.13 ± 1.73^{o} for lateral bending, and -1.95 ± 3.36^{o} for axial rotation. (Tables 2-1 to 2-3, and Figures 2-3 and 2-6).

Table 2-1. RMS errors for image based measurements compared to marker based measurements.

Trial	Flexion Extension (deg)	Lateral Bending (deg)	Axial Rotation (deg)
AR	1.49	1.70	4.42
FE	2.17	1.50	1.59
LB	2.19	3.54	8.03
Grand Total	1.95	2.25	4.68

Table 2-2. Precision for image based measurements compared to marker based measurements.

Trial	Flexion Extension (deg)	Lateral Bending (deg)	Axial Rotation (deg)
AR	1.16	1.33	4.18
FE	2.11	0.96	1.40
LB	1.78	2.90	4.50
Grand Total	1.68	1.73	3.36

Table 2-3. Bias for image based measurements compared to marker based measurements.

Trial	Flexion Extension (deg)	Lateral Bending (deg)	Axial Rotation (deg)
AR	0.53	0.28	0.62
FE	-0.08	0.51	-0.47
LB	0.24	-0.39	-6.01
Grand Total	0.23	0.13	-1.95

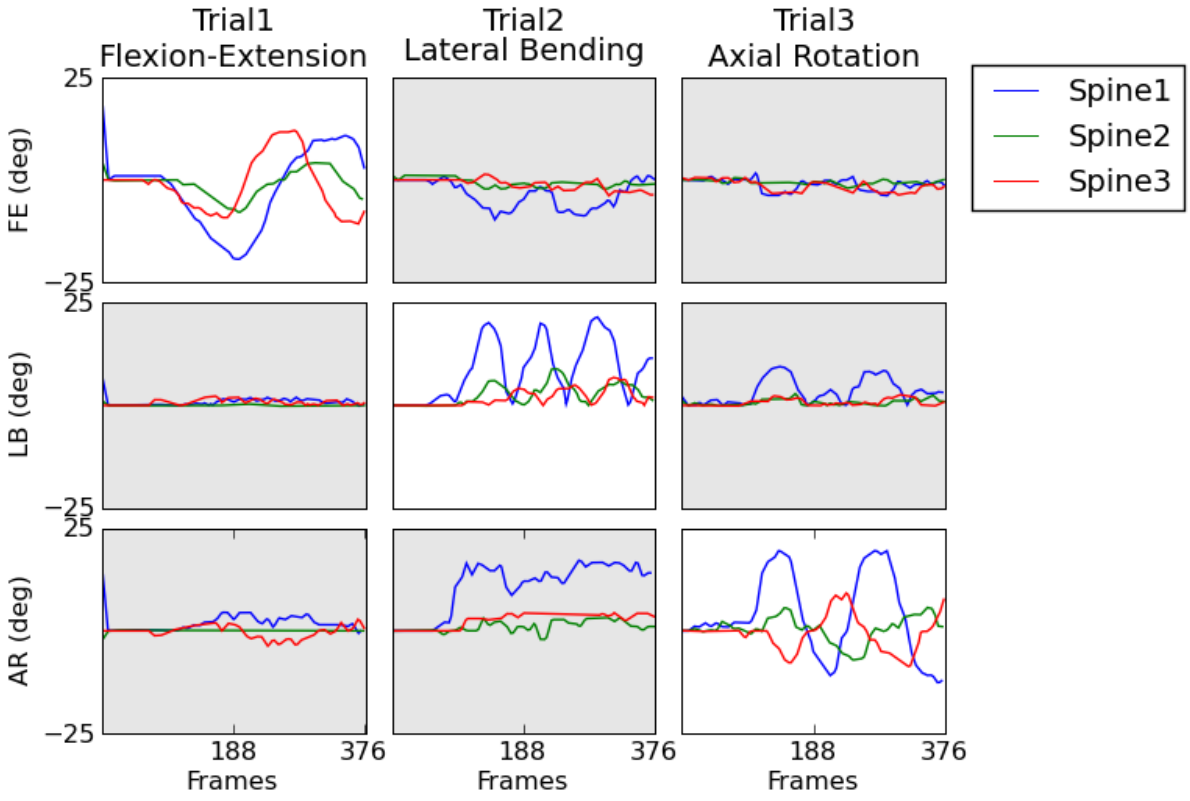

Figure 2-2. Absolute segmental rotation (in degrees) of the superior implant of each spine specimen in primary direction of motion (white background) and the off-axis motions (grey background), measured using optical marker based motion tracking.

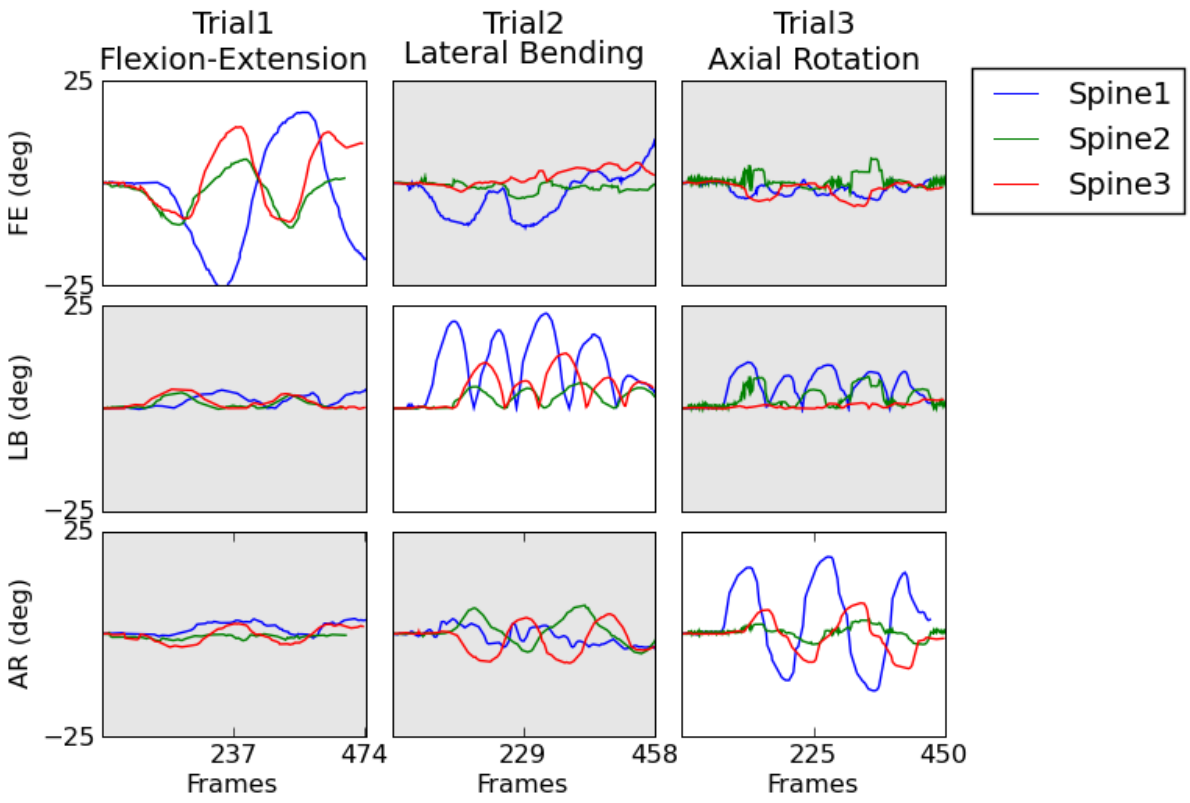

Figure 2-3. Absolute segmental rotation (in degrees) of the superior implant of each spine specimen in primary direction of motion (white background) and the off-axis motions (grey background), measured using optical marker based motion tracking.

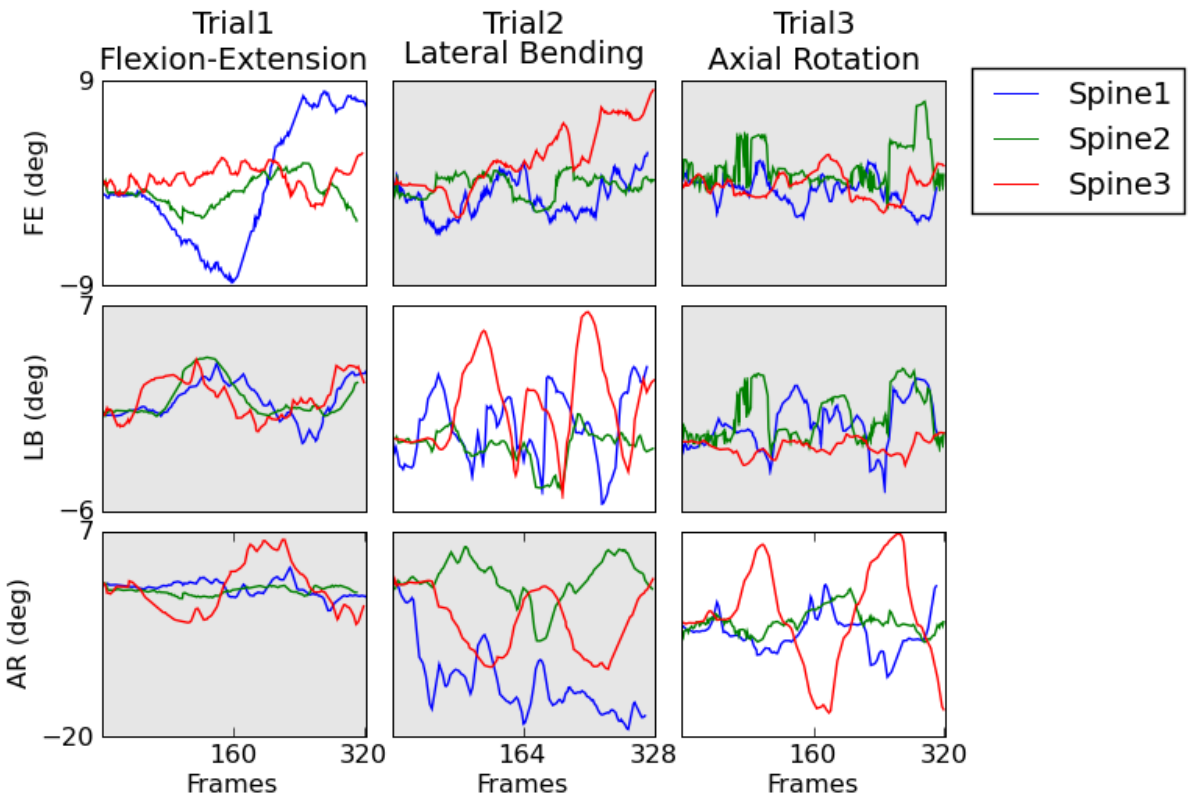

Figure 2-4. Rotation errors (in degrees) of the superior implant of each spine specimen in primary direction of motion (white background) and the off-axis motions (grey background), calculated by subtracting the optical marker based results from the image based results.

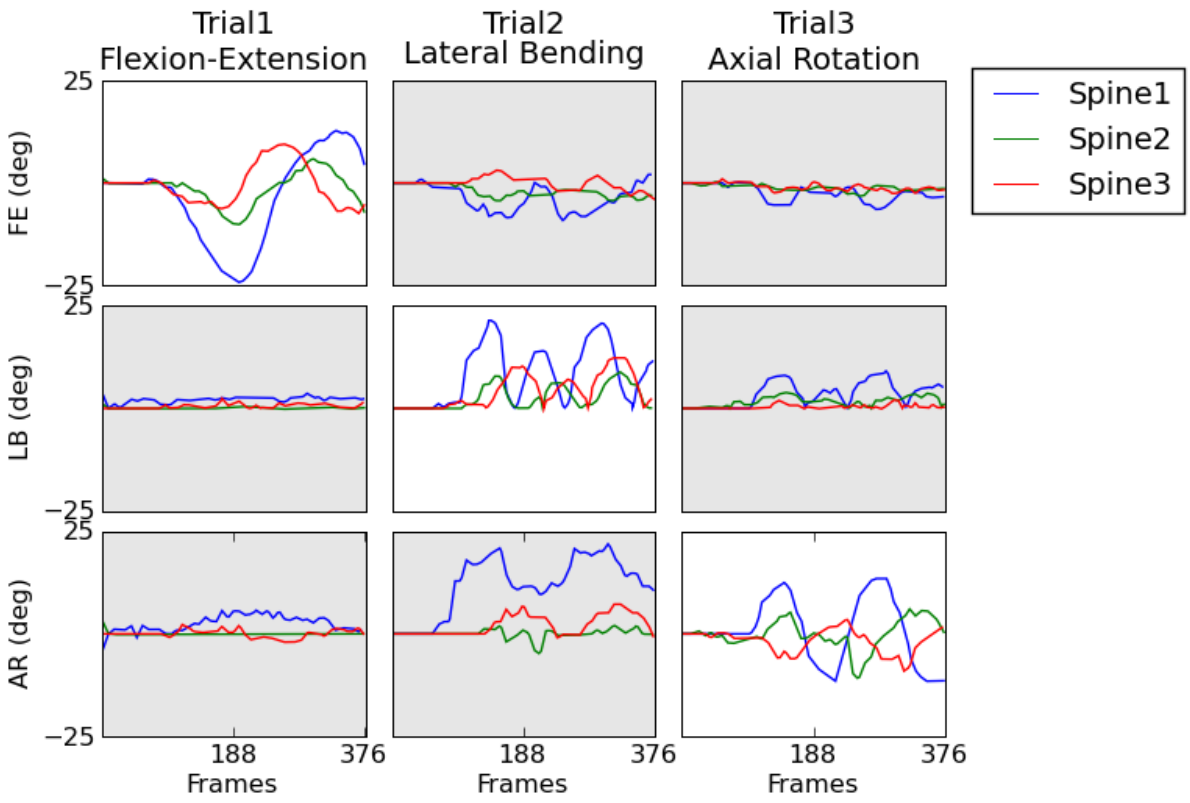

Figure 2-5. Absolute segmental rotation (in degrees) of the inferior implant of each spine specimen in primary direction of motion (white background) and the off-axis motions (grey background), measured using image based motion tracking.

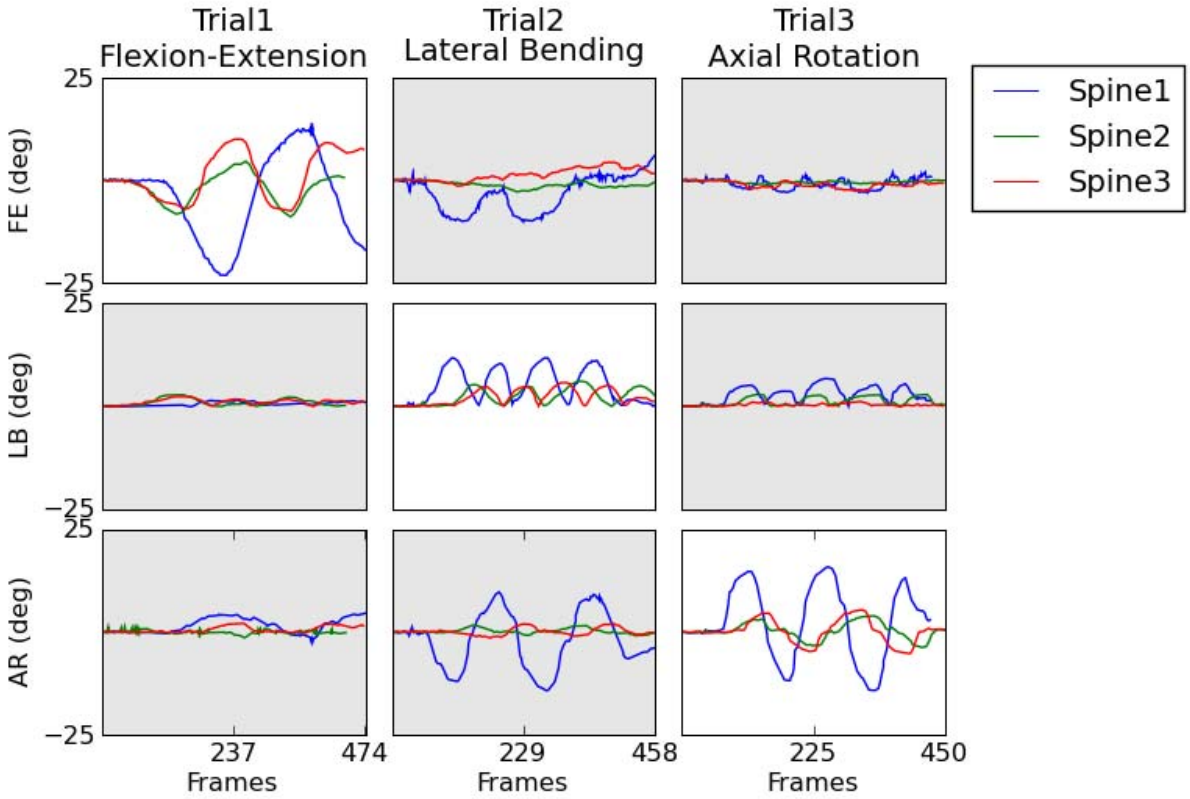

Figure 2-6. Absolute segmental rotation (in degrees) of the inferior implant of each spine specimen in primary direction of motion (white background) and the off-axis motions (grey background), measured using optical marker based motion tracking.

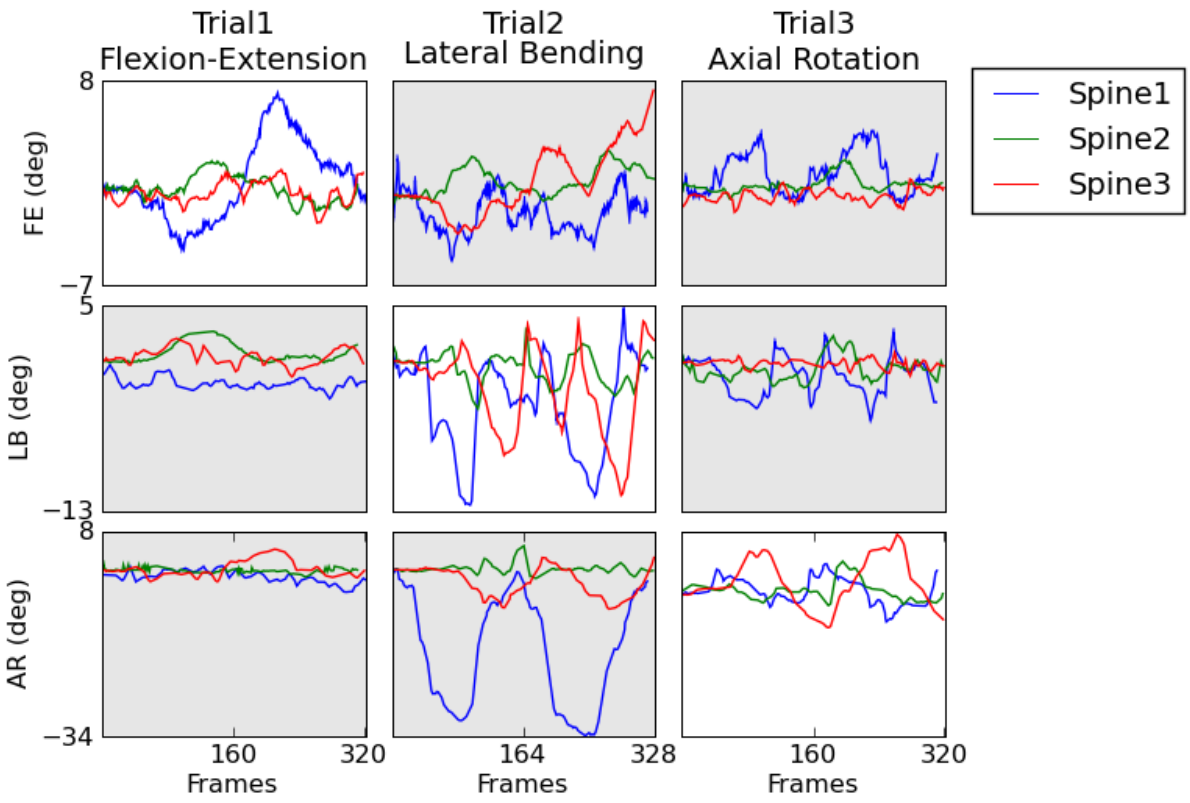

Figure 2-7. Rotation errors (in degrees) of the inferior implant of each spine specimen in primary direction of motion (white background) and the off-axis motions (grey background), calculated by subtracting the optical marker based results from the image based results.

Discussion

While analyzing the data for this experiment, it was discovered that the size and geometry of the implant made axial rotation and lateral bending pose estimations unreliable. The implant models are fairly symmetric in these planes and large changes in the rotation of the implant were not readily discernable from the projection image (Figures 2-7 and 2-8). In these two figures, the implant was rotated from -5 to +5 degrees about the X and Y axes. These changes in orientation have very little affect on the shape of the projection and make it very difficult to accurately match the implant shape to the fluoroscopic projection. The small size (63 x 26 pixels) of the implant with

respect to the full fluoroscopic field of view (1024 x 1024 pixels) also make it difficult to detect measure the motion of the implant.

These results demonstrate that single plane fluoroscopy can be a useful tool for quantifying the dynamic flexion-extension motion of spinal implants. However, there are limitations to this method that make it unfeasible for evaluating axial rotation and lateral bending from a single sagittal plane fluoroscopic image. In addition to the problems in measuring X and Y rotations, this method requires surface models for registration, which make it difficult to apply to tracking vertebrae.

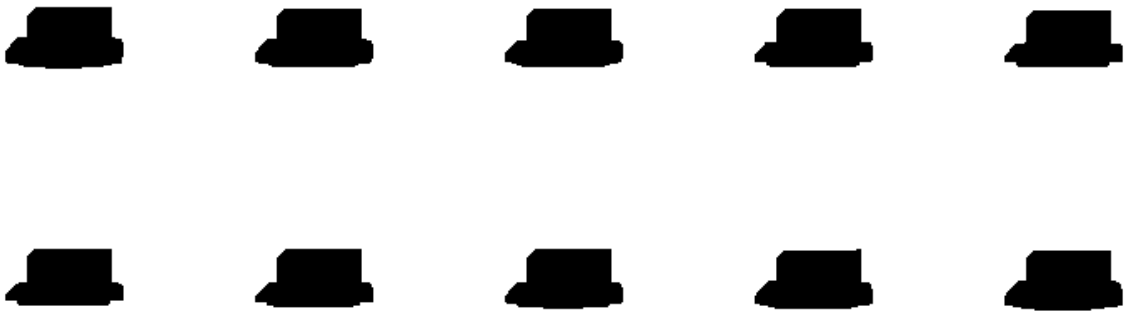

Figure 2-7. Surface model projections of a cervical spine arthroplasty implant rotated about the X-axis (axis oriented toward the right). The top left image is at -5 deg, and the bottom right image is at +5 deg of rotation.

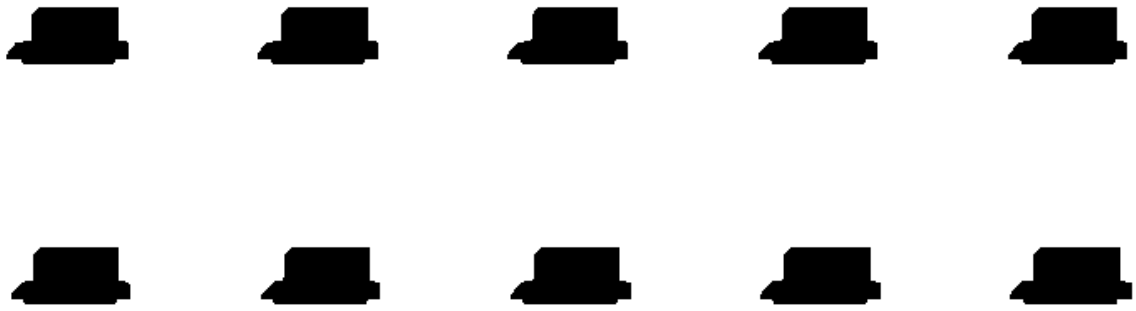

Figure 2-8. Surface model projections of a cervical spine arthroplasty implant rotated about the Y-axis (axis oriented up). The top left image is at -5 deg, and the bottom right image is at +5 deg of rotation.

CHAPTER 3
VALIDATION OF A METHOD TO REGISTER A 3D CT VOLUME TO A SINGLE PLANE 2D FLUOROSCOPIC IMAGE USING DIGITALLY RECONSTRUCTED RADIOGRAPHS

Introduction

Clinical Motivation

The ability to accurately track the motion of the spine is a valuable tool for diagnosing the extent of spinal disorders and assessing the functionality of motion preserving implants. However, a standardized method for quantifying spine motion has not yet been embraced by the clinical or research communities.

Medical Image Registration

The rapid development of new functional and anatomical imaging modalities, has presented clinicians and researchers with the challenge of integrating a wide array of data into a useful format. Images can be acquired using CT, MRI, positron emission tomography (PET), single photon emission computed tomography (SPECT), Ultrasound (US), X-Ray, video (from arthroscope, laryngoscope, or laparoscope). Depending on the imaging modality, the dimensionality of the images could be 2D, 3D (spatial), 3D (temporal sequence of 2D images), or 4D (temporal sequence of 3D images). Furthermore, the images may be acquired from the same patient at different times, from different patients, or even from an atlas of standard images. Further complexity is introduced due to the fact that the images are often captured at different resolutions, have different fields of view and have different geometric distortions based on the imaging equipment.

A number of excellent and thorough reviews have been written on the topic of medical image registration, for example Vandenelsen(28), Maintz(29) and Hill(30). For different applications of image registration, the problem statement is unique and will

dictate the nature of the solution. One of the most common applications is for alignment and integration of two or more 3D images acquired using different imaging modalities. Another area of active research is the challenge of aligning 3D CT image to a 2D fluoroscopic image. This problem has several applications in the intraoperative setting, where it can be used to visualize anatomic structures as well as to guide instruments and radiation therapy. We describe a technique for applying 2D/3D image registration to measure the position and orientation of spinal vertebrae, which can be used to measure dynamic motion in the spine.

Purpose

A diagram of the work flow for the image registration process is presented in Figure 3-1.

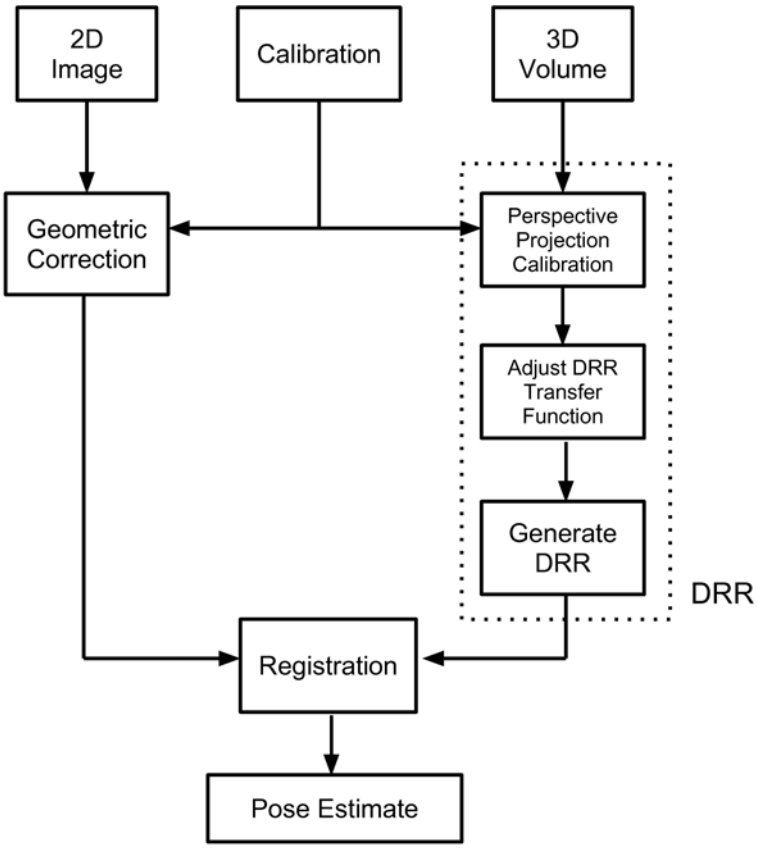

Figure 3-1. Diagram of the work flow during the registration process.

In this chapter, we will describe a method that will allow the 3D kinematics of an individual vertebrae to be measured from single plane lateral fluoroscopic images. The key element of this method is to use digitally reconstructed radiographs (DRRs) created from a computed tomography (CT) volume to register the fluoroscopic images. When the CT volume is optimally aligned, the DRR image has a maximum similarity to the fluoroscopic image. Although the ultimate intention is to use this tool for the measurement of dynamic spine motion, the goal of this phase of the research project is to assess the uncertainties of measuring the position and orientation of static images. In the next chapter, we will evaluate the uncertainties associated with measuring dynamic spine motion. The required accuracy for clinical use is highly dependent on the application. Based on similar studies in the literature, a threshold for clinical accuracy was set at 2mm in-plane mean Target Registration Error (mTRE) for this study. We chose mTRE as an outcome measure because it provides a scalar value that represents the position and orientation errors of the 3D volumes transformed into 2D position distances in the projection plane. While it is represented as a distance, it is a function of the position and orientation of the 3D volume.

Methods

The requirements of the current project are to develop, validate and utilize a pose estimation tool that can:

- Measure position and orientation in 3D
- Measure position and orientation of individual vertebrae
- Have sufficient accuracy for clinical and research use (<2mm mTRE errors)
- Be non-invasive, and appropriate for *in vivo* populations

Digitally Reconstructed Radiographs

DRRs have been used in clinical applications for surgical planning since at least 1990(31). They have also been utilized extensively in surgical navigation to register a pre-operative CT scan to an intra-operative fluoroscopic image(32-38), thus allowing the location of internal anatomic structures to be determined relative to external landmarks. Motion analysis can then be used to track instruments that are introduced to the operative field and allow the surgeon to visualize their position and orientation with respect to internal anatomy.

DRRs are created by projecting a 3D image volume onto a 2D image plane (Figures 3-2 and 3-3). There are several methods for performing this projection. Ray-casting, for example, is a fairly common projection algorithm. Ray-casting works by calculating a series of lines or rays that originate from each pixel location in the image plane and travel through the volume, toward the perspective focus. Along the path of the ray, each pixel value encountered in the volume is summed to determine the pixel value at the location where the ray originates from the imaging plane. Ray-casting can produce images that look very similar to actual radiographs because the computational method is analogous to the physical process of creating radiographic images.

Radiographs are produced by emitting photons from a point source and detecting the amount of energy received by the image detector. Any objects that are encountered by the photons along their path attenuate the beam and result in lower energy being detected at the image intensifier. While ray-casting can produce high-quality, realistic images, the calculation is computationally intensive, especially for large images. An alternative to ray-casting is to use 3D texture mapping(39) methods which can take advantage of hardware accelerated graphics(40-43) processing units on modern graphics cards. Texture mapping calculates a 2D image slice from any different viewpoint, reorienting the volume to the desired position and orientation, and then re-slicing the volume along the direction of projection (Figure 3-4). By using hardware accelerated texture mapping, the generation of DRR images can be accomplished significantly faster than the CPU based ray-casting method. Render speed affects image registration since, at each new pose, a new DRR image must be rendered. Texture mapping results in some image artifacts that are not present in ray-cast images, but for the current research project, these artifacts were determined to be acceptable (Figure 3-5 and Figure 3-6), when compared to fluoroscopic images (Figure 3-7). The use of texture mapping to produce DRRs allowed us to achieve reasonable performance (each registration took approximately 60-90s).

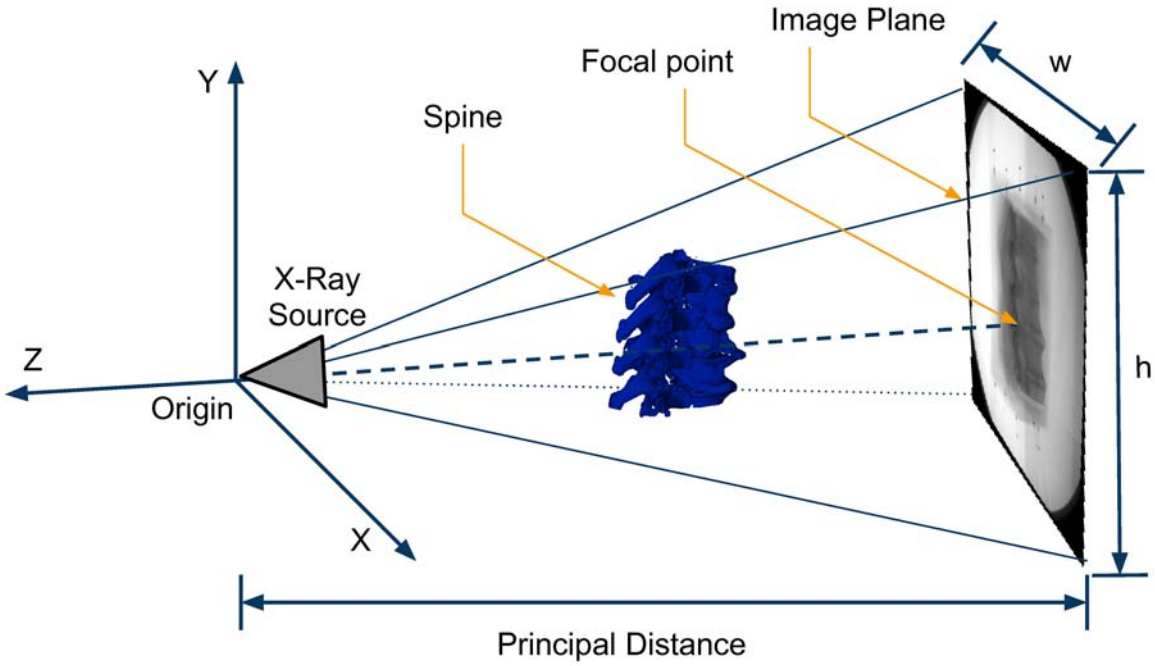

Figure 3-2. Diagram of the radiographic projection geometry. The object being imaged, a thoracolumbar spine in this example, is placed between the x-ray source and the detector, or image intensifier, which forms the image plane. By using a calibration procedure, the imaging geometry of a specific radiography device can be obtained.

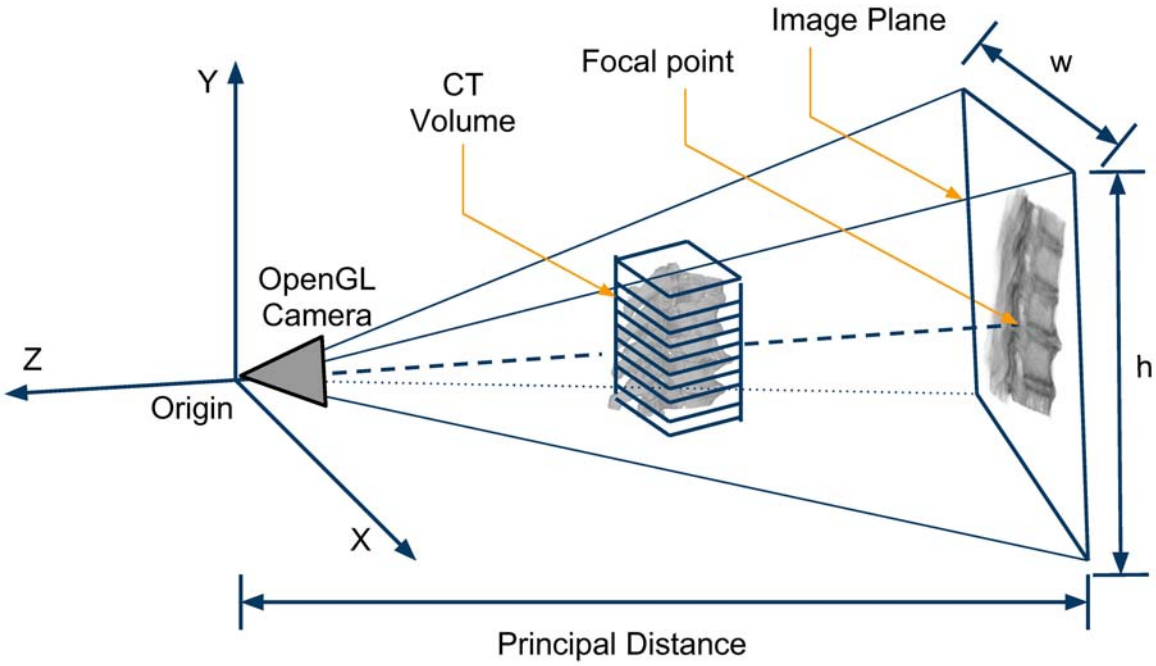

Figure 3-3. Diagram of the DRR projection geometry. Using the projection geometry derived from the calibration of the x-ray device, a computer graphics scene can be constructed to produce DRRs with matching perspective projections to the x-ray images. The differences between this virtual setup and the radiographical setup described in Figure 3-3 is that instead of an x-ray source, an openGL camera is used, and instead of an anatomical object being imaged, a projection is created digitally from an existing CT scan. The pixel spacing and dimensions of the DRR are controlled to match the x-ray image.

A comparison of the render time for ray-casting and texture mapping algorithms was performed by rendering the same 3D volume 20 times and calculating the average time required to project a 512x512 pixel image. On an Intel® Core™2 Duo CPU T5550 running at 1.83GHz with a NVIDIA GeForce 8400M GS graphics card, ray-casting took an average time of : 0.84 $\pm$ 0.22 seconds (average frame rate: 1.26 $\pm$ 0.27 frames/second) and texture mapping took: an average time of: 0.15 $\pm$ 0.04 seconds (average frame rate: 7.18 $\pm$ 1.41 frames/second). On an Intel® Core™2 Duo CPU T9400 running at 2.53GHz with a NVIDIA Quadro FX 770M graphics card, ray-casting

took an average time of : 0.37 ± 0.01 seconds (average frame rate: 2.73 ± 0.08 frames/second) and texture mapping took: an average time of: 0.03 ± 0.01 seconds (average frame rate: 30.41 ± 3.86 frames/second). The ray-casting rendering, which is performed on the CPU, scales roughly with the speed of the processor (1.83GHz vs. 2.53GHz), where the 2.53GHz processor rendered the volume 2.2 times faster than the 1.83GHz processor. However, the texture mapping rendering which is performed on the graphics card scales with GPU performance (1033 vs. 5297 in 3DMark06 benchmark), where the Quadro FX 770M card rendered the volume 4.2 times faster than the 8400M GS card.

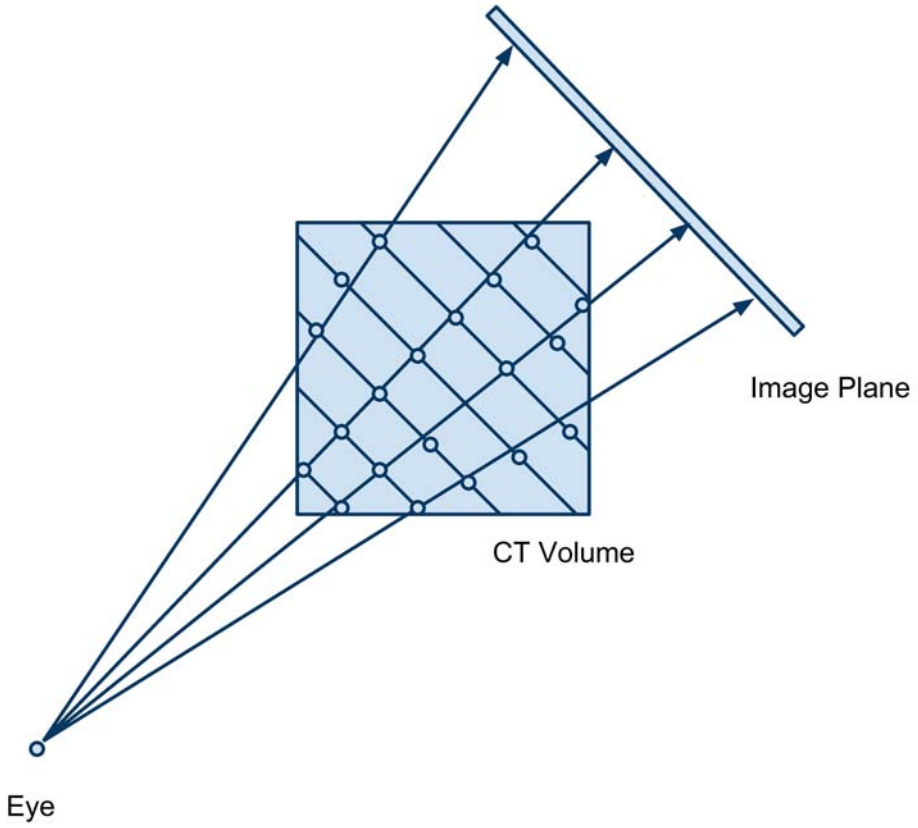

Figure 3-4. Texture mapping reslices the CT volume, so that the resulting grid is parallel to the image plane. The image data is interpolated and mapped onto the resampled grid and the contribution of each voxel to the image is calculated using the graphics hardware. Texture mapping is significantly faster than using software based ray-casting methods to render a 3D volume.

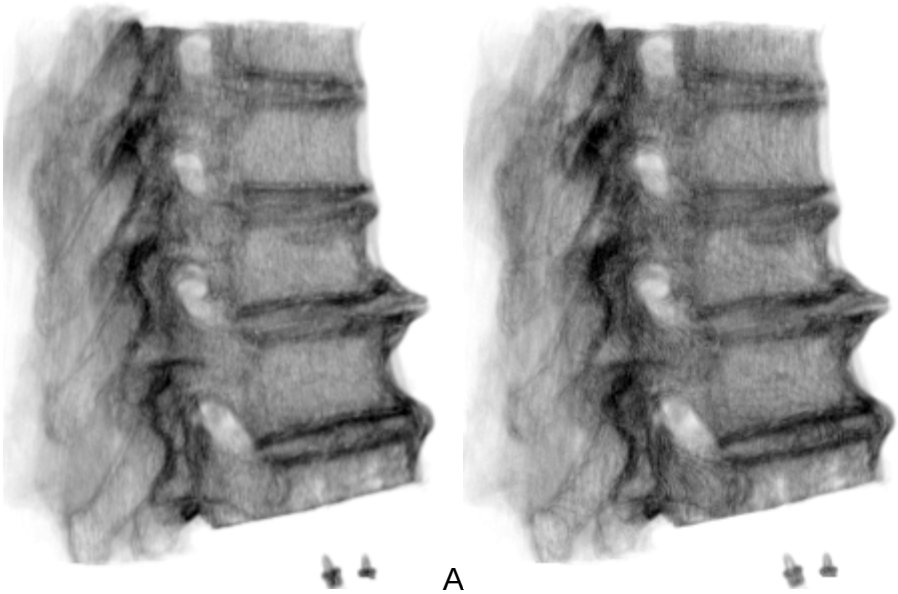

A B

Figure 3-5. DRRs of a thoracolumbar spine specimen generated using two different rendering techniques. A) Ray-casting B) Texture mapping. In the texture mapped image, there are slight “wood grain” artifacts due to interpolation between pixels. The mean frame rate for 20 renderings using the ray-cast mapper was 1.85 +/- 0.10 fps, the mean frame rate for 20 renderings using the texture mapper was: 8.15 +/- 0.37 fps

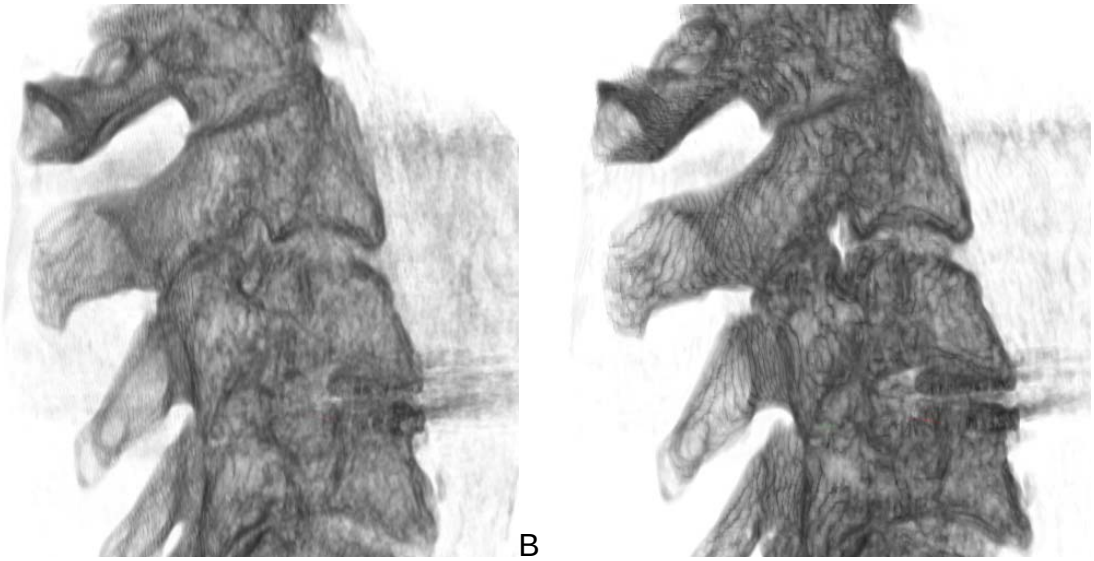

A B

Figure 3-6. DRRs of a cervical spine specimen generated using two different rendering techniques. A) Ray-casting B) Texture mapping. In the texture mapped image, there are slight “wood grain” artifacts due to interpolation between pixels.

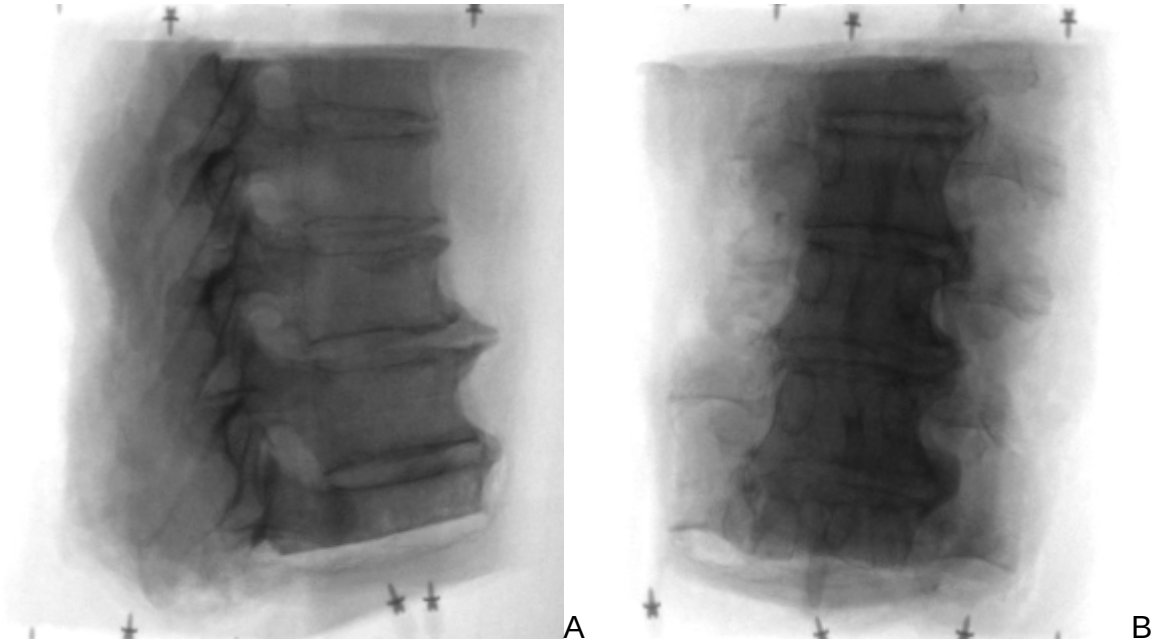

Figure 3-7. Example of a fluoroscopic image of the thoracolumbar spine A) lateral view and B) anterior view.

Perspective Projection Geometry

In order for DRR images to match fluoroscopic images, it is critical that the perspective projection parameters are established. The parameters that need to be determined from the radiographic imaging equipment in order for the DRR images to have the same geometrical projections as the radiographic images are the principal point, principal distance and pixel spacing(44) (Figure 3-8). The principal distance is the length of the line from the x-ray source to the image plane, perpendicular to the image plane. The principal point is the point in the image plane at which a perpendicular line extending from the image plane will intersect the x-ray source. Pixel spacing is the physical size of the image pixels in the horizontal and vertical directions.

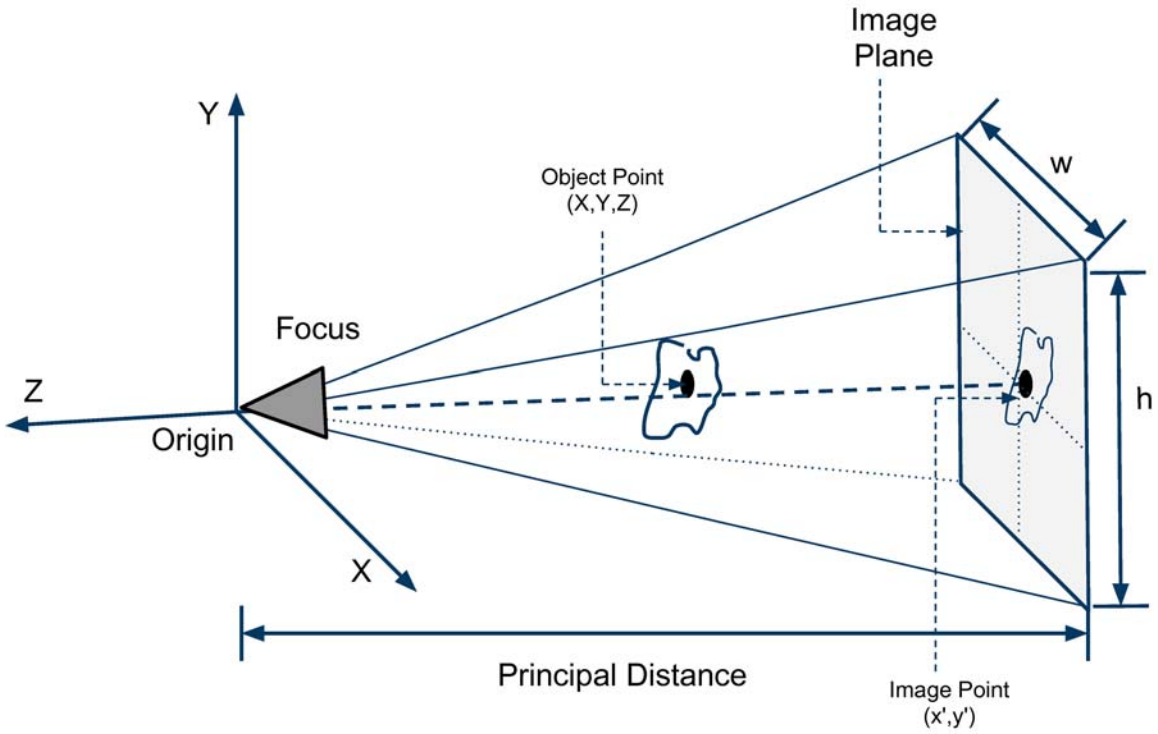

Figure 3-8. The projection geometry of the radiographic imaging equipment. The principal distance, x and y offset and pixel size are required to create DRR projections that match the images captured from the fluoroscopic system.

Registration Algorithm

The registration algorithm ties together the necessary components of the registration and manages the flow of data from DRR, metric, transform, and optimizer. A basic framework for the registration algorithm used in this work is presented below (Figure 3-9). The process begins with the two input images that are to be registered, a 2D image from the fluoroscopic device and a 3D CT (or MRI) volume.

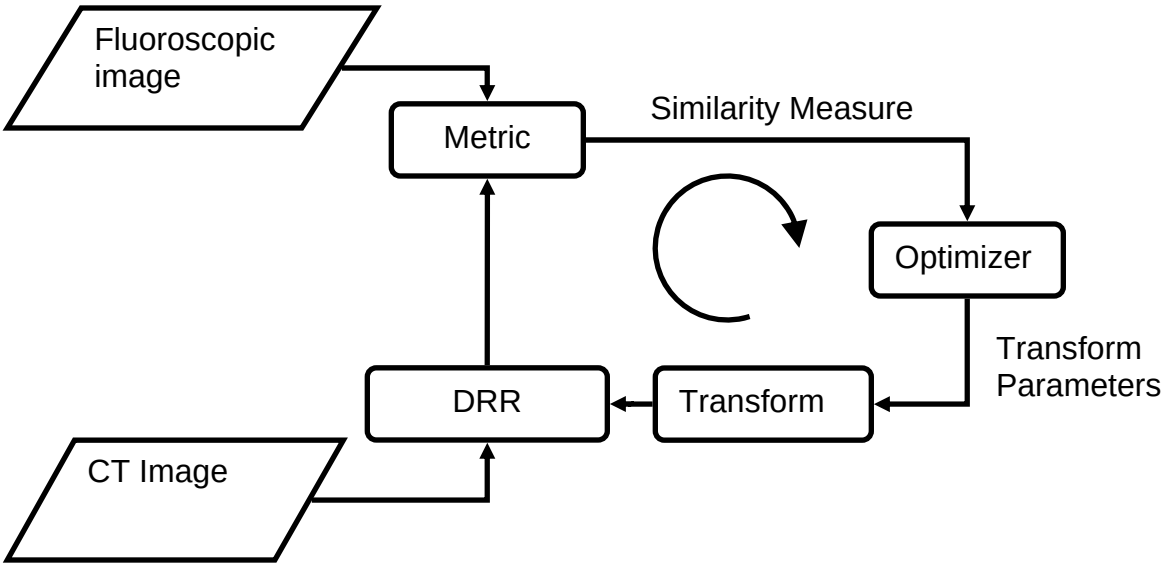

Figure 3-9. Schematic diagram of the registration process (adapted from the ITK Software Guide(45)). The five basic components are: Input images, metric, DRR, optimizer and transform.

Image Metric

A key step in the registration of a 3D volume to a 2D image is defining a measure that returns a value which represents the similarity between two images. This measure is called a similarity measure or image metric, and the two terms will be used interchangeably. For this project the similarity measurement is calculated on two 2D images (fluoroscopic image and DRR image). The inputs to the metric function are the two images and the output is a scalar value representing the similarity of the two images. The most important characteristic of the image metric function is that it returns a minimum value when the two images are optimally aligned. A wide variety of image similarity metrics have been described in the literature[31,32,48,49,80,83,84,85] for different image registration applications. The choice of an image metric heavily depends on the details of the registration being performed. Factors that can affect the

image metric include: image resolution, image size and imaging modality (CT, MRI, ultrasound, etc). The ability of the metric to accurately quantify spatial alignment between two images depends on the intrinsic properties of the images. An ideal metric is sensitive to differences in structural position, but robust to noise and occlusions. All of the image metrics considered for this project use the pixel intensity values from the fixed and DRR images as inputs. The different image metrics that were considered for this experiment are presented below.

Mean squares

One of the simplest image similarity measures is the mean squares (MS) metric (52,45).

$$MS(A,B) = \frac{1}{N}\sum_{i=1}^{N}(A_i - B_i)^2$$

Where:

A_i is the i-th pixel in the fixed image

B_i is the i-th pixel in the DRR image

N is the total number of pixels considered

The mean squares metric is equal to 0 when the two images are identical. This metric has a fairly large capture range(45), but does not perform well when images are taken from different modalities, because it assumes that the pixel intensities between two homologous points in the compared images match exactly. This measure has been shown to be the optimum similarity metric when two images differ only by Guassian noise(53).

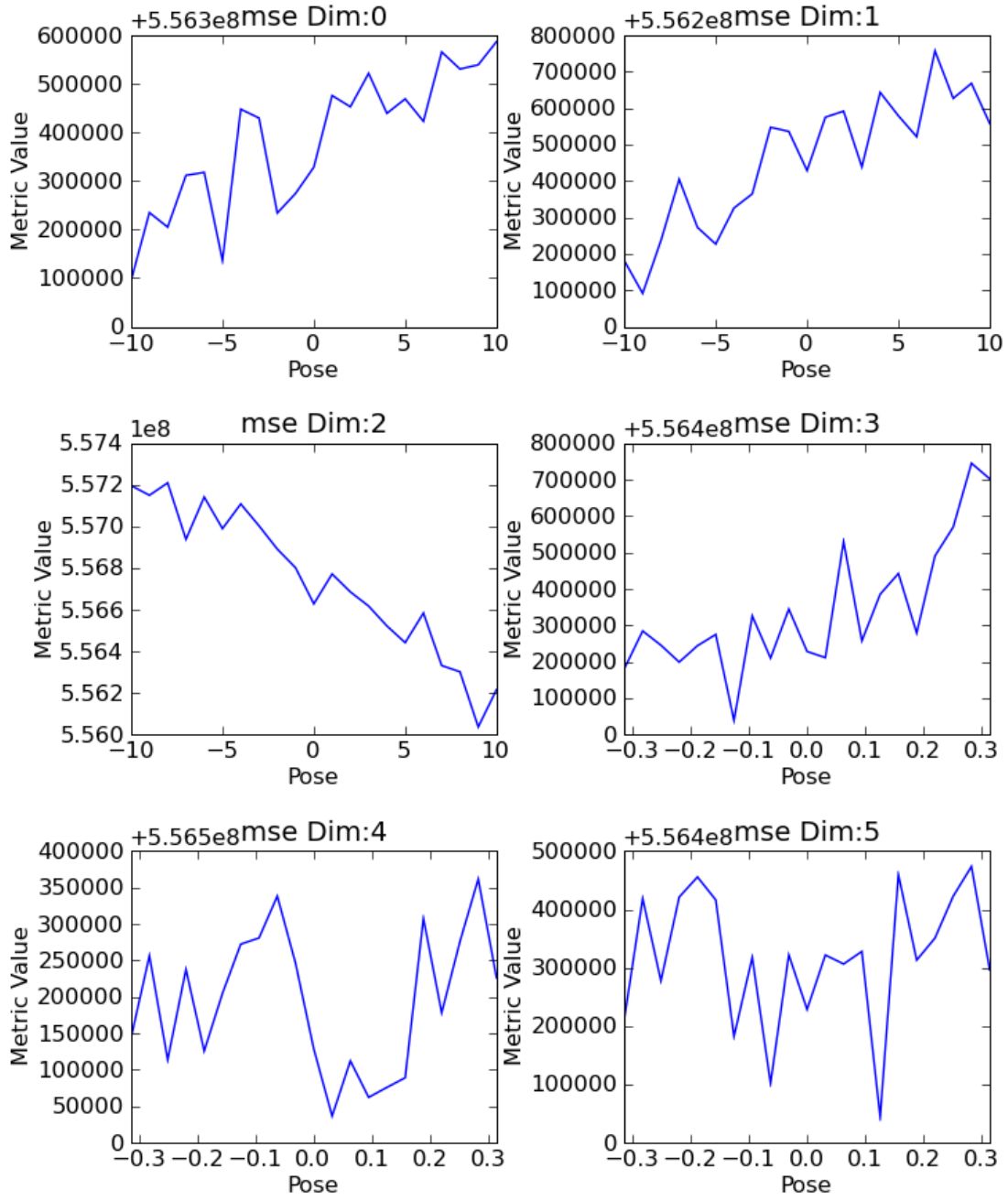

Figure 3-10. Plots of the MS metric function versus pose. Dimensions 0-2 correspond to X, Y and Z translations, and dimensions 3-5 correspond to rotations about the X, Y and Z axes. Translations are in mm, and rotations are in radians.

Normalized correlation metric

The normalized correlation (NC) metric(45) accommodates linear shifts in pixel intensity between two images by calculating the product of two homologous pixels and normalizing it by the geometric mean of the sum of squares for each image.

$$NC(A,B) = -1 \times \sum_{i=1}^{N} \frac{A_i \times B_i}{\sqrt{\sum_{i=1}^{N} A_i^2} \times \sqrt{\sum_{i=1}^{N} B_i^2}}$$

Where:

Ai is the i-th pixel of the fixed image

Bi is the i-th pixel of the DRR image

N is the number of pixels considered

NC is a better choice than MS when there is a shift in pixel intensities between two images, because the pixel magnitude is normalized for each image.

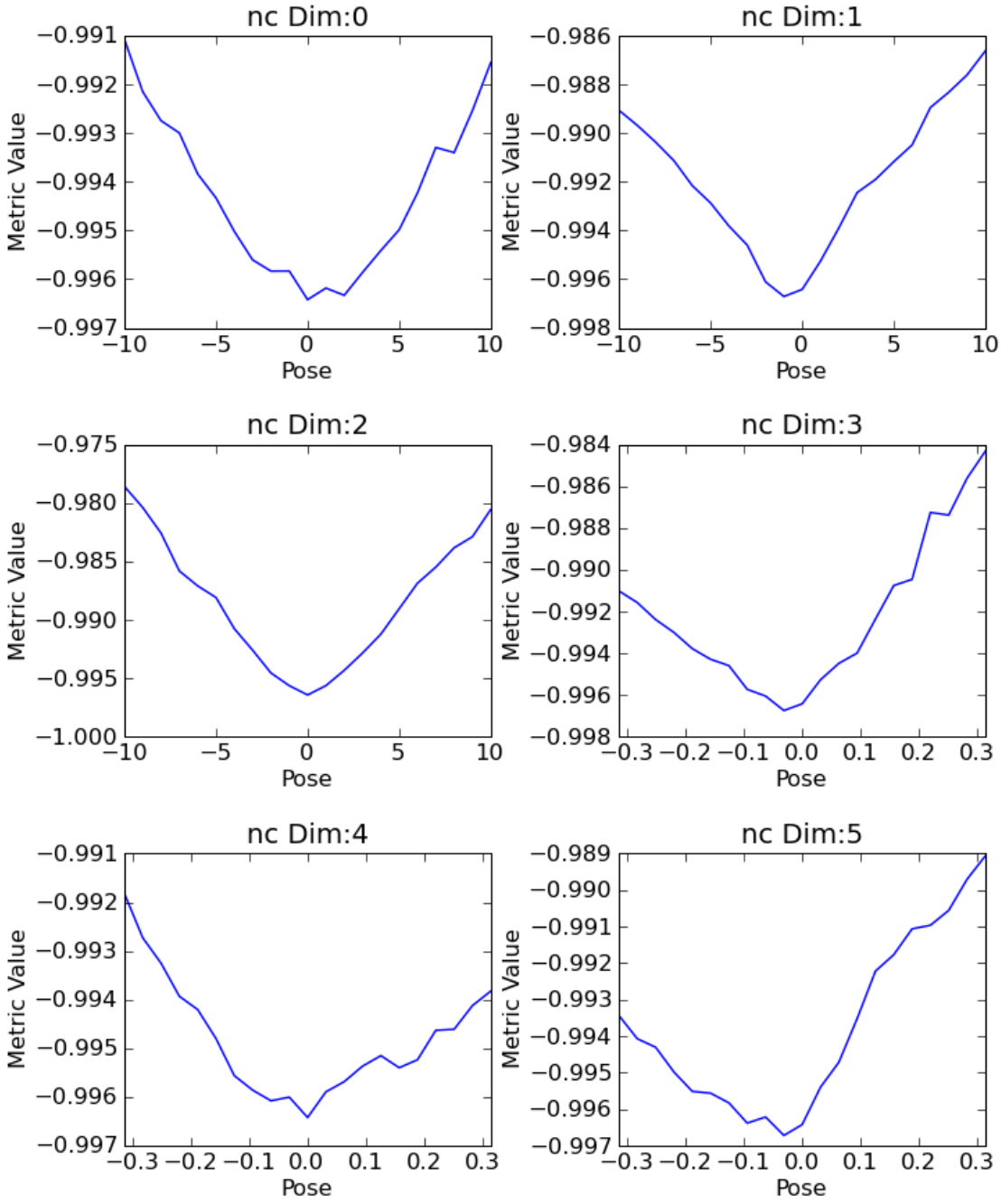

Figure 3-11. Plots of the NC metric function versus pose. Dimensions 0-2 correspond to X, Y and Z translations, and dimensions 3-5 correspond to rotations about the X, Y and Z axes. Translations are in mm, and rotations are in radians.

Normalized cross correlation

The normalized cross correlation (NCC) (54) metric is very similar to NC, except that each image is first normalized to its mean pixel value before determining the product between the two images.

$$NCC(A,B) = -1 \times \sum_{i=1}^{N} \frac{(A_i - A_{mean}) \times (B_i - B_{mean})}{\sqrt{\sum_{i=1}^{N} (A_i - A_{mean})^2} \times \sqrt{\sum_{i=1}^{N} (B_i - B_{mean})^2}}$$

Where:

Ai is the i-th pixel of the fixed image

Amean is the mean intensity of the fixed image

Bi is the i-th pixel of the DRR image

Bmean is the mean intensity of the DRR image

N is the number of pixels considered

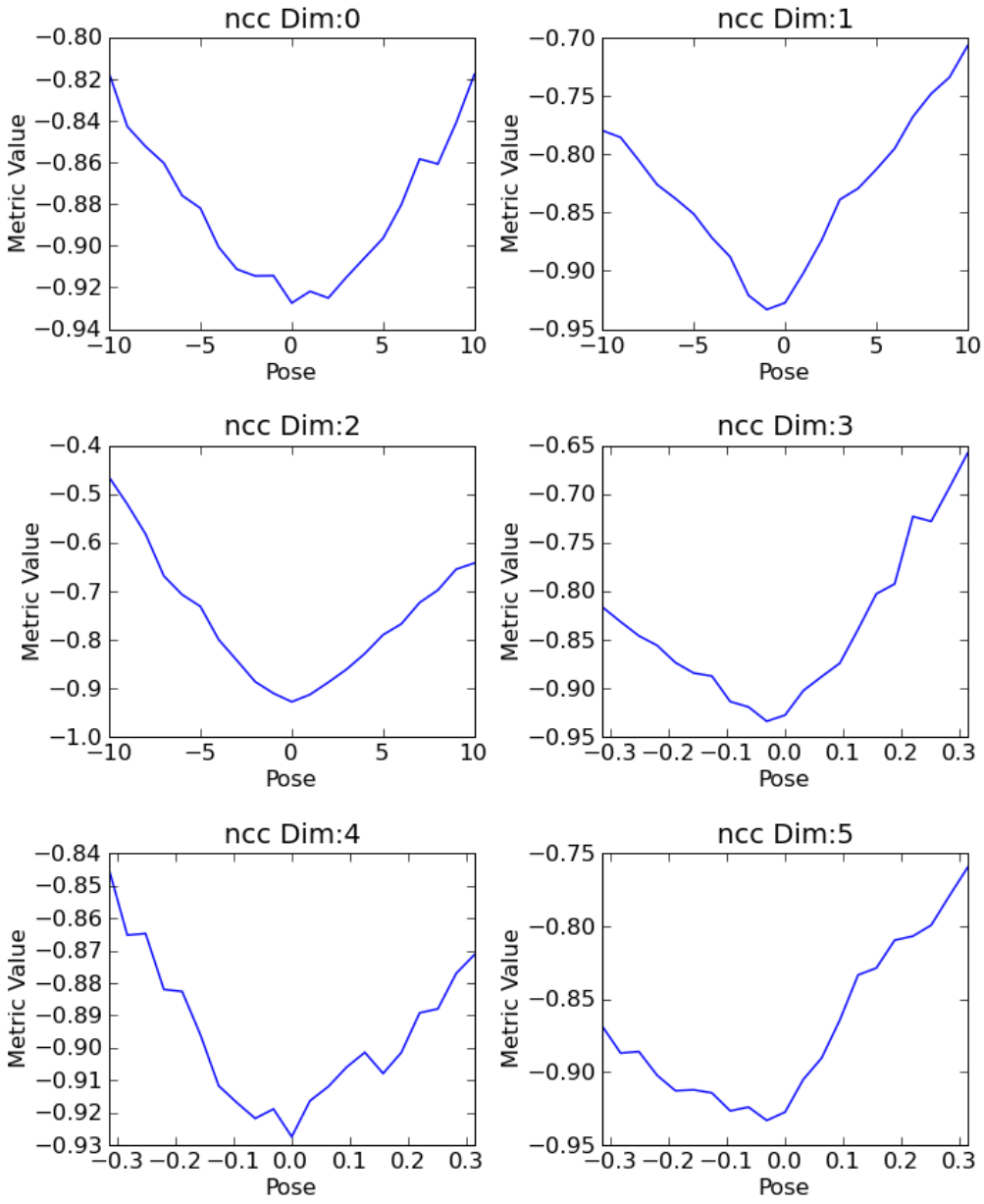

Figure 3-12. Plots of the NCC metric function versus pose. Dimensions 0-2 correspond to X, Y and Z translations, and dimensions 3-5 correspond to rotations about the X, Y and Z axes. Translations are in mm, and rotations are in radians.

Gradient correlation

The gradient correlation (GC) metric has been demonstrated in previous studies to be a useful measurement for comparing DRR images to fluoroscopic images(33). The

GC metric uses edge information from the image by calculating an image gradient using the Sobel filter and Gaussian blur with a standard deviation of 1.4. The GC metric is the same as the NCC, except the input images are gradient images.

$$GC(A,B) = -1 \times \sum_{i=1}^{N} \frac{(A_i - A_{mean}) \times (B_i - B_{mean})}{\sqrt{\sum_{i=1}^{N} (A_i - A_{mean})^2} \times \sqrt{\sum_{i=1}^{N} (B_i - B_{mean})^2}}$$

Where:
A_i is the i-th pixel of the gradient of the fixed image
A_{mean} is the mean pixel intensity value for the gradient of the fixed image
B_i is the gradient image from the DRR image
B_{mean} is the mean pixel intensity value for the gradient of the DRR image
N is the number of pixels considered

For this study, a Gaussian blurring filter (Figure 3-13) was applied to the images before calculating the gradients, a standard deviation of 1.4 was chosen based on preliminary testing. An example of a gradient image of one vertebrae is shown in Figure 3-14.

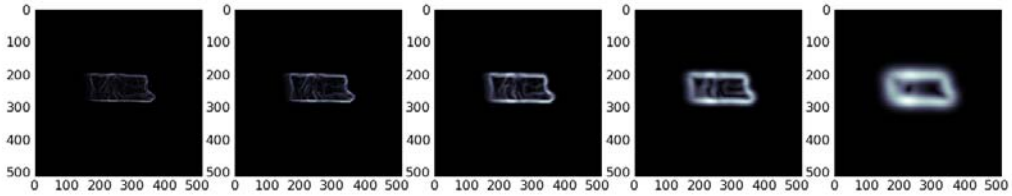

Figure 3-13. Changing the amount of image blur before calculating the edge image accentuates different features of the image. All images were blurred with a Gaussian filter and then a Sobel edge detecting algorithm was applied in the horizontal and vertical directions. From left to right, the images were blurred with a kernel size of: 1, 2, 4, 8, 16.

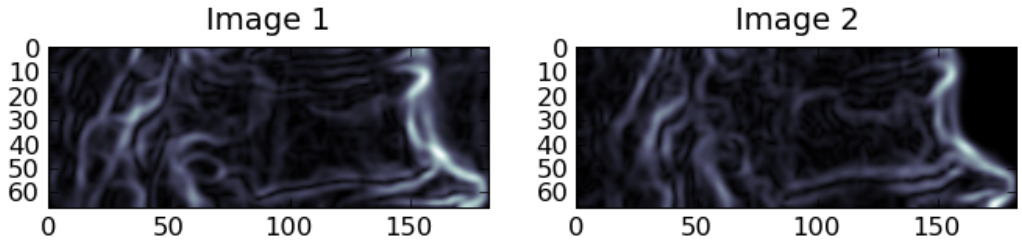

Figure 3-14. An example of edge images from the fluoroscopic image (left) and the DRR image (right) for a vertebrae in optimal alignment. A standard deviation of 1.4 was used in the Gaussian filter for these images.

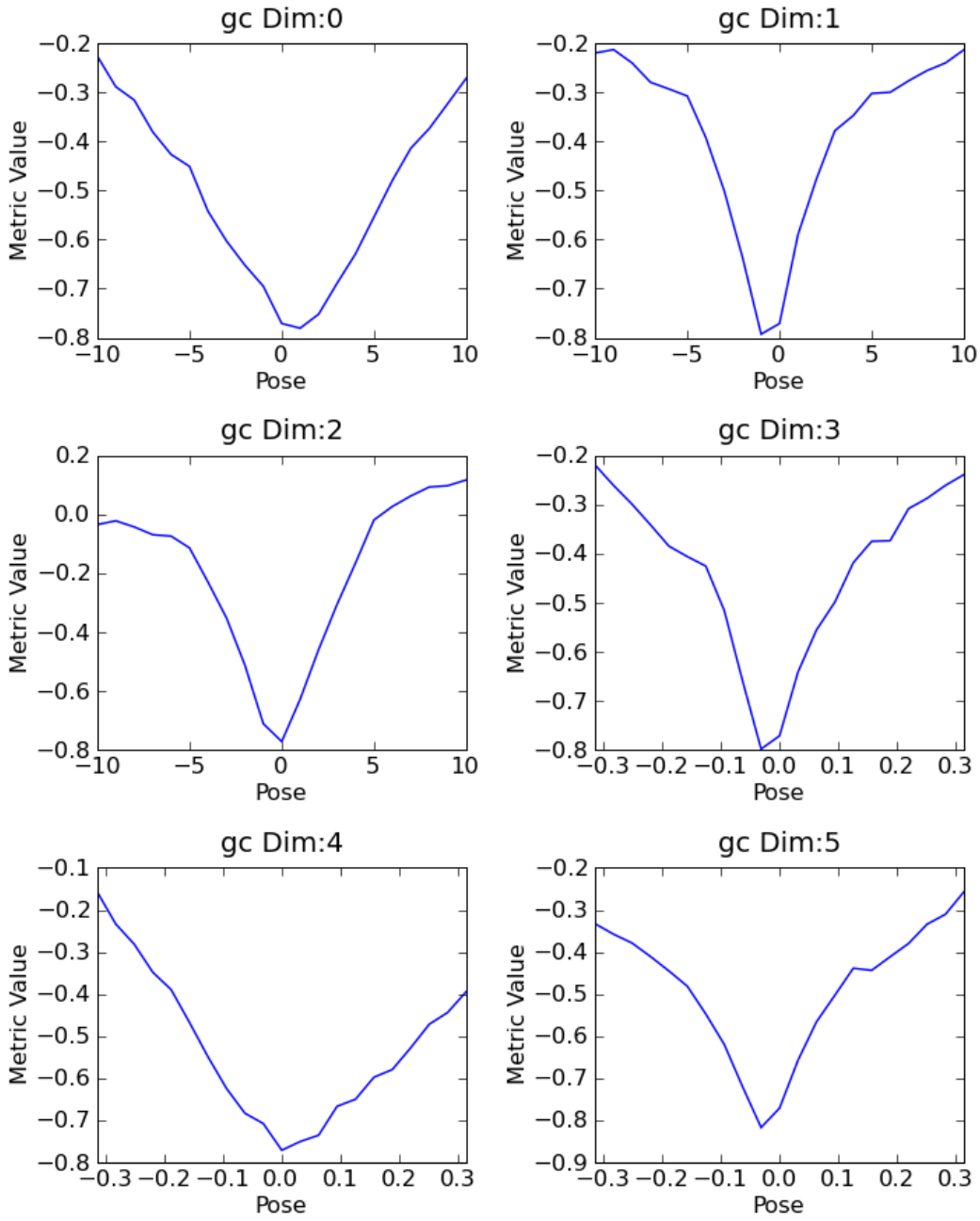

Figure 3-15. Plots of the NCC metric function versus pose. Dimensions 0-2 correspond to X, Y and Z translations, and dimensions 3-5 correspond to rotations about the X, Y and Z axes. Translations are in mm, and rotations are in radians.

Gradient difference

The gradient difference (GD)(54) metric computes the difference between two edge images, using a scale parameter to adjust the intensity between the two images.

$$GD(A,B) = \sum_{i=1}^{N} \frac{\upsilon}{\upsilon + I_{diff}^2}$$

$$I_{diff} = A_{edge} - (scale \times B_{edge})$$

Where:

A_{edge} is the edge enhanced fixed image

B_{edge} is the edge enhanced DRR image

scale is the a scalar parameter (see text for detail)

I_{diff} is the difference image created from A_{edge} and B_{edge}

υ is the variance of the I_{diff}

N is the number of pixels in I_{diff}

The scale parameter is included in the image difference calculation to compensate for different ranges of intensity values in the images being compared. The scale is optimized using brute force over the range max(A)/max(B)/100 to max(A)/max(B) to find the value that minimizes the metric result. Edge images were calculated using a Sobel gradient filter, which was applied in both the horizontal and vertical dimensions.

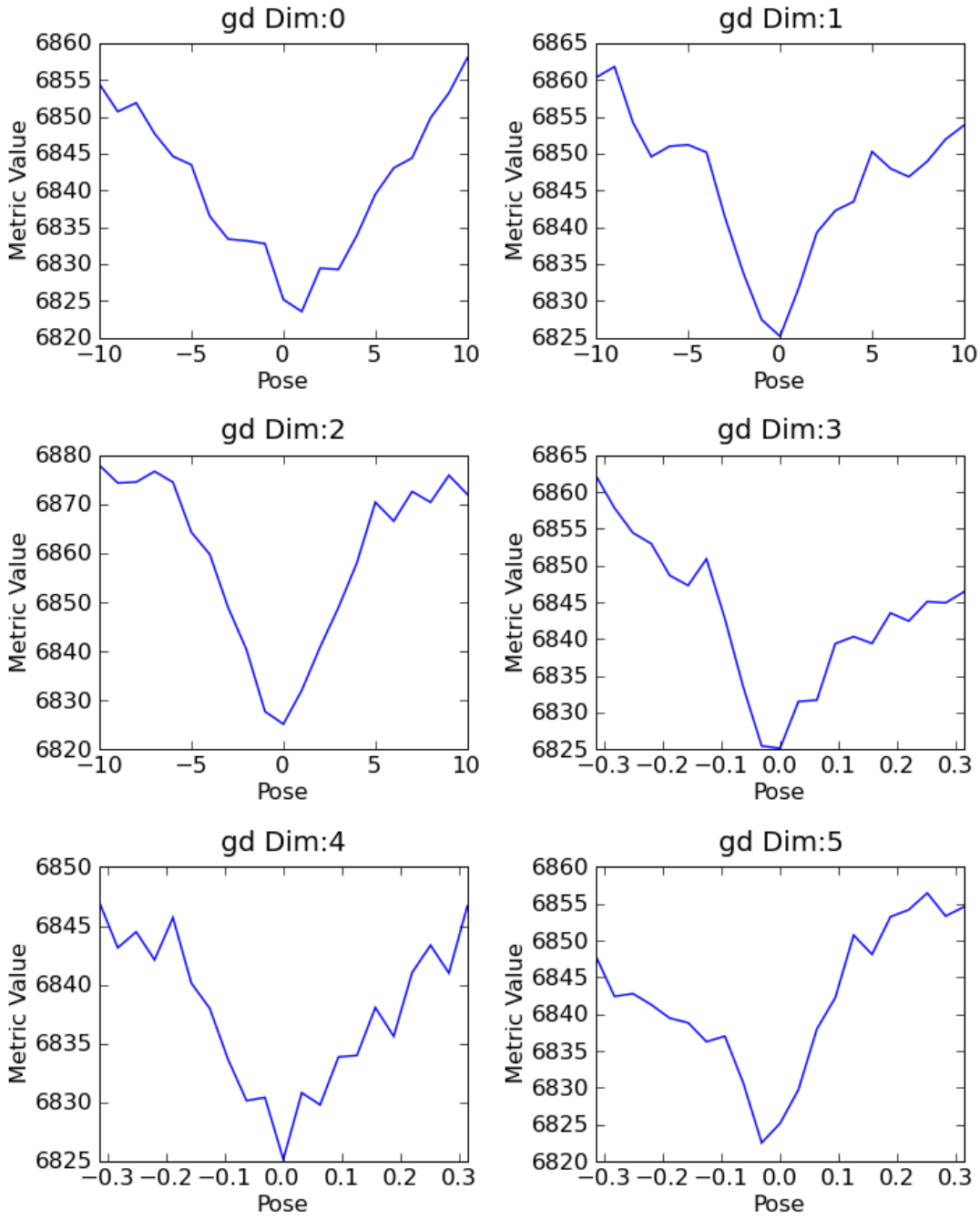

Figure 3-16. Plots of the GD metric function versus pose. Dimensions 0-2 correspond to X, Y and Z translations, and dimensions 3-5 correspond to rotations about the X, Y and Z axes. Translations are in mm, and rotations are in radians.

Mutual information

Mutual information (MI)(53,48) is an example of a class of similarity metrics based on statistical descriptions of intensity probability distributions. The concept of MI is that the information contained in two images is maximized when the images are perfectly aligned. Specifically, this metric calculates the uncertainty of knowing the pixel value in one image given a value in the other image. For example, if the two images are completely independent, the mutual information would be 0, that is knowing one pixel would yield no information about the other image. If the two images are identical, then knowing one pixel would allow the corresponding pixel in the other image to be known exactly, and the mutual information would be high (Figure 3-9). The benefit of using statistical descriptors of the image is that they are insensitive to shifts or inversion (as with MRI and CT) of pixel intensities.

$$MI(A,B) = -1 \times \sum_{i=1}^{N} p(A,B) log \left(\frac{p(A,B)}{p(A)p(B)} \right)$$

Where:

p(A) is the probability density function for the fixed image

P(B) is the probability density function for DRR

P(A,B) is the joint probability density function for the fixed image and DRR

N is the number of pixels considered

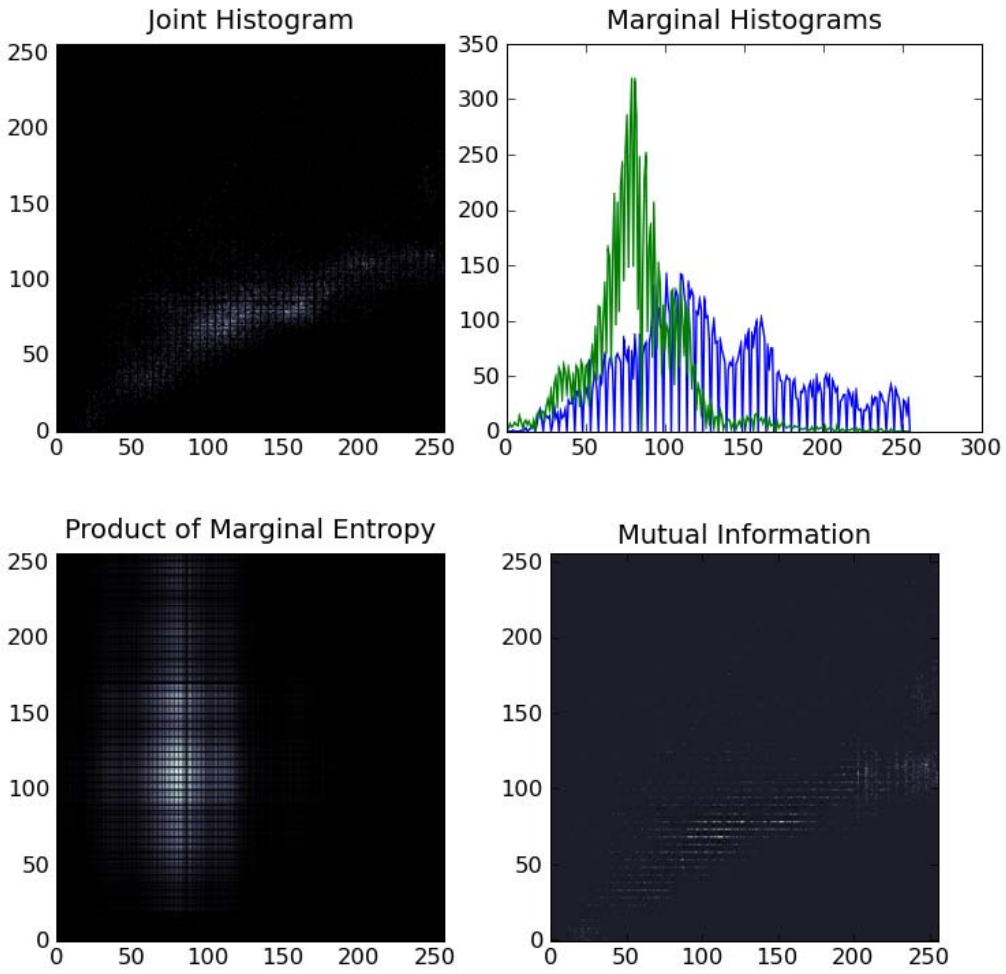

Figure 3-17. Example of Mutual information as applied to a fluoroscopic image and DRR image in optimal alignment. Mutual information is calculated from the probability density functions of each image, which are simply the normalized histograms of the images. The joint histogram is a plot of each image's individual histogram, with the fluoroscopic image on the x-axis and the DRR image on the y-axis. The product of marginal entropy is a measure of the total amount of information contained within both images. Mutual information is the probability of knowing a pixel in one image, given the intensity value for the other image.

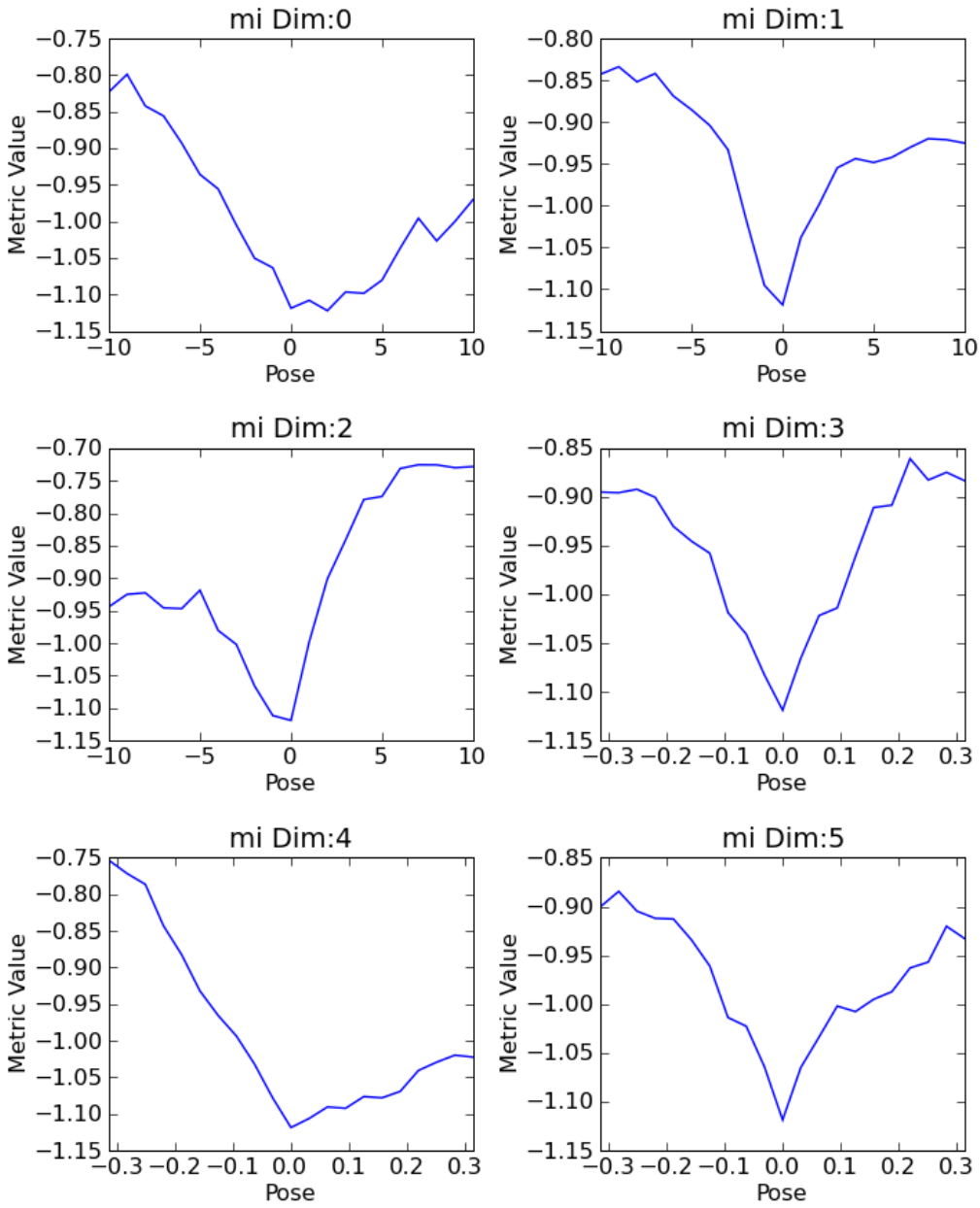

Figure 3-18.. Plots of the MI metric function versus pose. Dimensions 0-2 correspond to X, Y and Z translations, and dimensions 3-5 correspond to rotations about the X, Y and Z axes. Translations are in mm, and rotations are in radians.

Mutual information and gradient correlation

A third image metric was created by combining the MI and GC metric into a single similarity measure (MI+GC), with the theory that the unique characteristics of each would synergistically improve the performance of the combined metric (Figure 3-19).

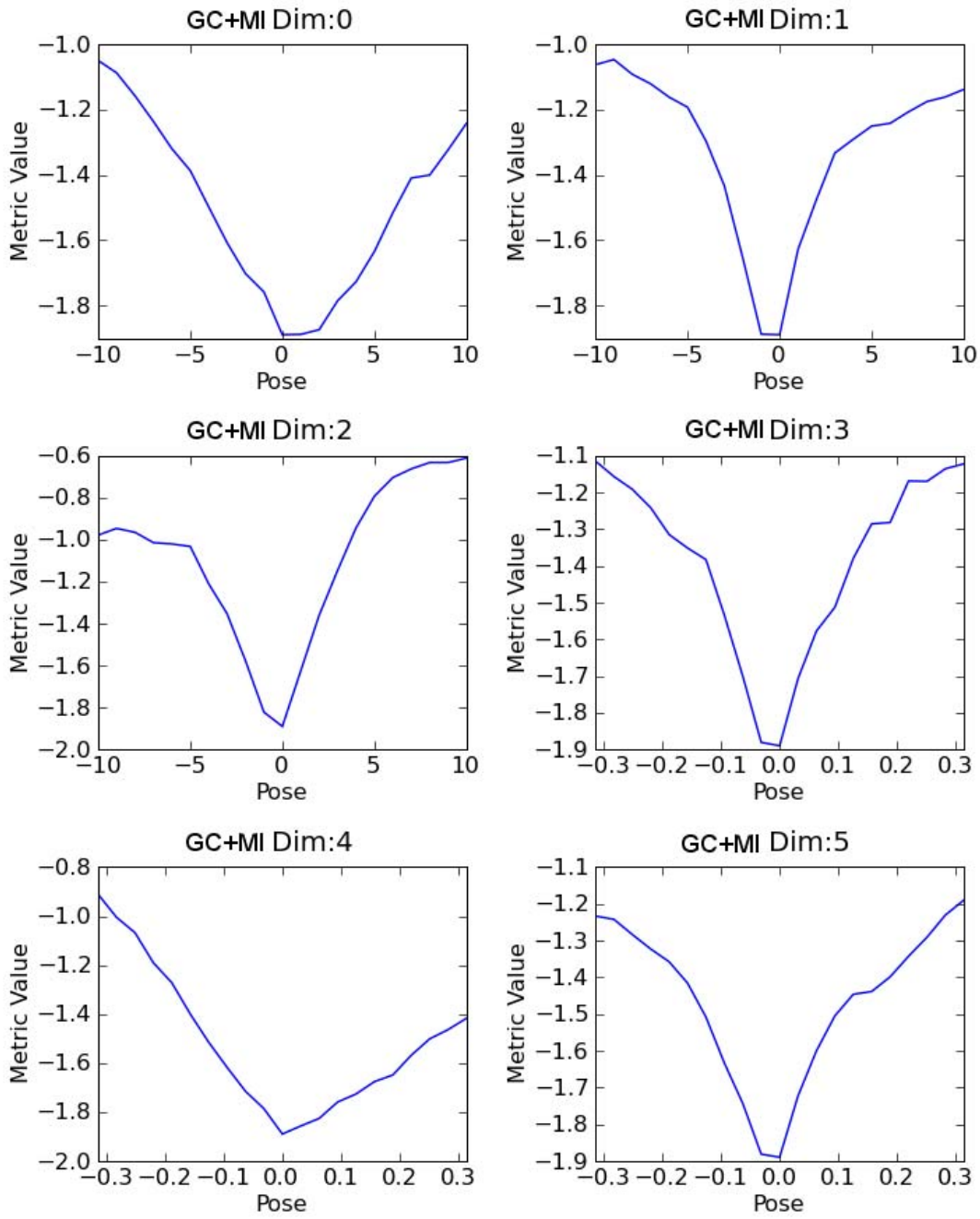

Figure 3-19.. Plots of the GC+MI metric function versus pose. Dimensions 0-2 correspond to X, Y and Z translations, and dimensions 3-5 correspond to rotations about the X, Y and Z axes. Translations are in mm, and rotations are in radians.

The plots of the metric function versus pose provide useful information on the characteristics of the metric. For example, the ratio of the highest value to the lowest value determines the sensitivity of the metric to small changes in pose. The slope of the metric is also important: if the metric begins to slope downward further from the optimimal pose, then it indicates the metric has a large capture range. Based on the results of the metric function versus pose analysis, we chose to use three different metrics (MI, GC, GC+MI) for the remainder of the experiments in this chapter.

Optimizer

The image similarity metric defines the cost function that should return a minimum value when the images are aligned. The choice of an optimizer for finding the minimum value for the cost function has a significant impact on the results of the registration algorithm. The optimizer takes as an input the value of the cost function from which it generates a new pose vector to evaluate in the cost function. The challenge of the optimizer is to relatively quickly descend into the global minimum without getting trapped in spurious local minimum. For this study, a global optimizer, simulated annealing (SA), was initially chosen. SA was selected because its global characteristics would potentially allow for a very large capture range, meaning relatively poor starting poses would still converge to the true solution. The principle of the SA algorithm is to take random parameter steps in the region around the current guess. If a step improves the cost function, it is accepted and used as the starting guess for the next iteration. A fraction of the steps that have a *worse* cost function value are also accepted since the cost function might need to go uphill to escape a local minimum. At each iteration, the step size is reduced (quenched), until it reaches a minimum value. Initial testing with the SA optimizer demonstrated that the stochastic nature of the algorithm made tuning

the parameters very difficult, since sometimes the same parameter set would result in a successful registration and sometimes it would not converge.

The second optimizer that was considered was the regular step gradient descent optimizer (RSGD). The RSGD optimizer calculates a finite-difference gradient of the parameter space at each iteration and takes a step along each parameter dimension proportional to the gradient for that parameter. Because the RGSD optimizer is deterministic, it was easier to determine a parameter set that would consistently converge the optimizer. Ultimately, the RSGD optimizer was used in the registration algorithm. The following parameters were chosen based on pilot testing from a small subset of different starting poses. The size of the step taken at each iteration was reduced by a factor of 0.75 each time the gradient changed sign. The stopping conditions for the optimizer were: step size was less than 0.1, more than 100 iterations or gradient change of less than 1e-4. The optimizer was repeated for five runs, with the best result of the previous run being used as the starting point for the next run. The initial maximum step size was 4 and was reduced by a factor of 0.618 after each run.

Starting Positions

A standard set of starting positions provided with the gold-standard dataset were used as initial guesses for the optimizer. Starting positions are described by the mean target registration error (mTRE), which defines the average displacement error (in mm) over a grid representing the volume of one vertebral body(51). A total of 150 starting positions were uniformly distributed over the range of 0-15 mm mTRE, so that the capture range of the registration algorithm could be determined. Registration success was defined as mTRE in the plane of fluoroscopic image within 2mm. The mTRE is calculated by transforming a grid of points using the pose being evaluated. The mean

distance of these points from the true position is the mTRE, and therefore the error measure is a function of both rotation and translation errors.

Results

A total of six vertebral bodies, three each from two spines, were registered. Each vertebral body was registered at each of the 150 starting positions, so that there were a total of 900 registrations performed for each similarity metric. The starting positions were grouped into 1 cm bins for this analysis, such that each bin contained 60 registrations with which to gauge the success of the algorithm (10 starting positions x 6 vertebrae). A registration was deemed successful if the in-plane mTRE was less than 2mm. The combined gradient correlation and mutual information similarity metric produced successful registrations 88% of the time when starting within 4mm mTRE (Figure 3-11), compared to 75% successful registrations with the standard gradient correlation metric and 30% successful registrations with the standard mutual information metric over the same range of starting positions. For the registrations that were successful, the error was consistently between 1.2-1.6mm regardless of starting position or metric used (Figure 3-12). For evaluating the accuracy at matching each pose parameter (translation and orientation), we defined 1.2 mm and 1.2 deg (for translations and rotations, respectively) as the threshold for success for that parameter. This value was chosen because it represents approximately the overall accuracy of the algorithm as measured in mTRE (Figure 3-12). The percentage of successful final results for individual pose parameters is presented in Table 3-1. X translations are approximately (they represent global axes that are not aligned with the anatomic axes) out of the fluoroscopic plane and are therefore expected to be less accurate than the other parameters.

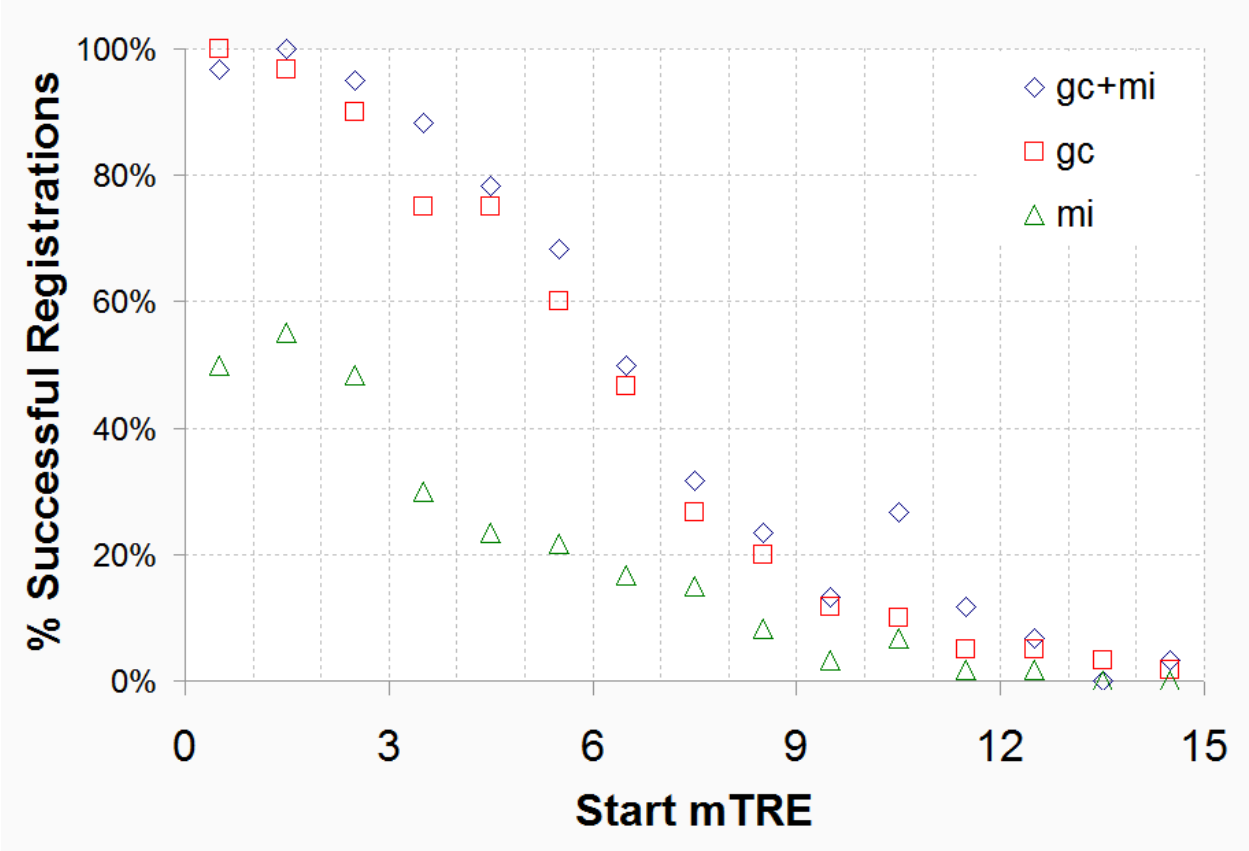

Figure 3-20. Percentage of successful registrations plotted against the amount of error in the starting position. Both the GC and combined GC+MI metric had similar results, with the success rate at approximately 80% when the starting position is within 4 mm mean target registration error (mTRE). Successful registration was defined as within 2mm mTRE for in-plane errors.

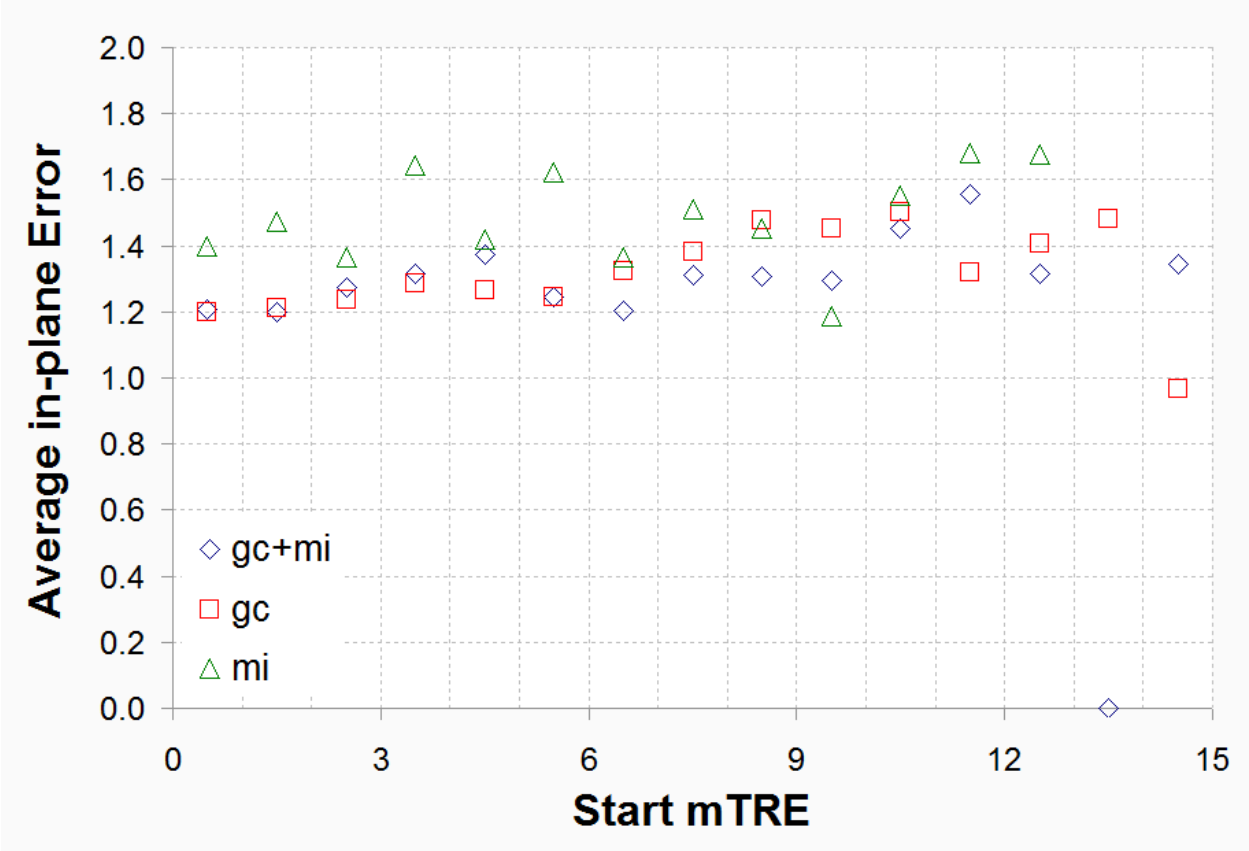

Figure 3-21. For registrations that were successful, the average in-plane mTRE was invariant to the amount of starting error.

Table 3-1. Analysis of registration errors for each pose parameter when using the combined MI+GC metric. For individual parameters, success was defined as being within 1.2 mm or 1.2 deg of the optimum value at the final registration pose. Axes are global and are not aligned with anatomic reference system. Cells that are greater than 95% are highlighted in green, those between 80-95% are yellow and those less than 80% are red.

Starting Error (mTRE)	% of final parameters within 1.2mm/1.2deg					
	Xtrans	Ytrans	Ztrans	Xrot	Yrot	Zrot
0-1	70%	100%	100%	100%	100%	80%
1-2	90%	100%	100%	100%	100%	87%
2-3	80%	100%	100%	100%	100%	77%
3-4	97%	100%	100%	100%	100%	79%
4-5	83%	100%	93%	100%	100%	73%
5-6	74%	100%	93%	100%	100%	74%
6-7	60%	93%	87%	93%	90%	60%
7-8	70%	87%	90%	80%	77%	53%
8-9	63%	90%	80%	80%	80%	73%
9-10	76%	55%	83%	59%	55%	66%
10-11	57%	83%	73%	83%	77%	53%
11-12	73%	60%	73%	77%	80%	43%
12-13	47%	77%	70%	43%	67%	67%
13-14	63%	50%	80%	80%	53%	73%
14-15	57%	70%	77%	87%	50%	70%

Discussion

One of the requirements of this research project was to develop an image registration methodology that could be used to measure the position and orientation of vertebrae. Previous work in our lab has made extensive use of 3D CAD models to register to 2D fluoroscopic images. This technique has worked well for tracking large non-symmetric implants, but early experience demonstrated that surface models of the vertebrae would be insufficient to determine the bone pose. While surface models have proven to be very useful for matching bones with uniform density and minimal internal detail, this is not the case for spinal vertebrae. Figure 3-22 shows a surface model of a spinal vertebra that was created from a CT scan. While the surface model is a high fidelity representation of the anatomical structures, it is not very effective for matching to a 2D radiographic image. In the spine there are a number of internal features that can provide useful landmarks for model to image registration. In particular the areas around the facet joints, pedicles and lateral mass/transverse processes are obscured when the spine is in a neutral position. When the spine rotates about one of the axes parallel to the image plane, there is more overlap of the vertebral bodies as well as the facets, lamina, pedicles. It is difficult to accurately visualize this overlapping region using surface models of the bone. The result is that there is a large uncertainty in finding the true position of the bone model that will generate the unique projection observed in the fluoroscopic image. For this reason we chose to use DRRs for this project so that we would be able to generate projections of the bone volume that were closely matched to the actual fluoroscopic images.

We have previously used a surface model based technique for tracking the motion of cervical spinal arthroplasty implants. Because of the small size of the implants and their symmetrical shape, rotations and translations out of the plane of motion could not be accurately measured. The current technique provides several advantages over tracking the implants alone. Since CT scans are used as models for registration, non-operated vertebrae can be tracked in addition to implants. This is critical for the important application of tracking motion of non-operated vertebrae adjacent to an implant. If it is assumed that the implant is rigidly fixed to the bone it is anchored to, then the vertebrae and implant structure can be used for image registration, which will provide significantly more geometrical information than using the implant alone.

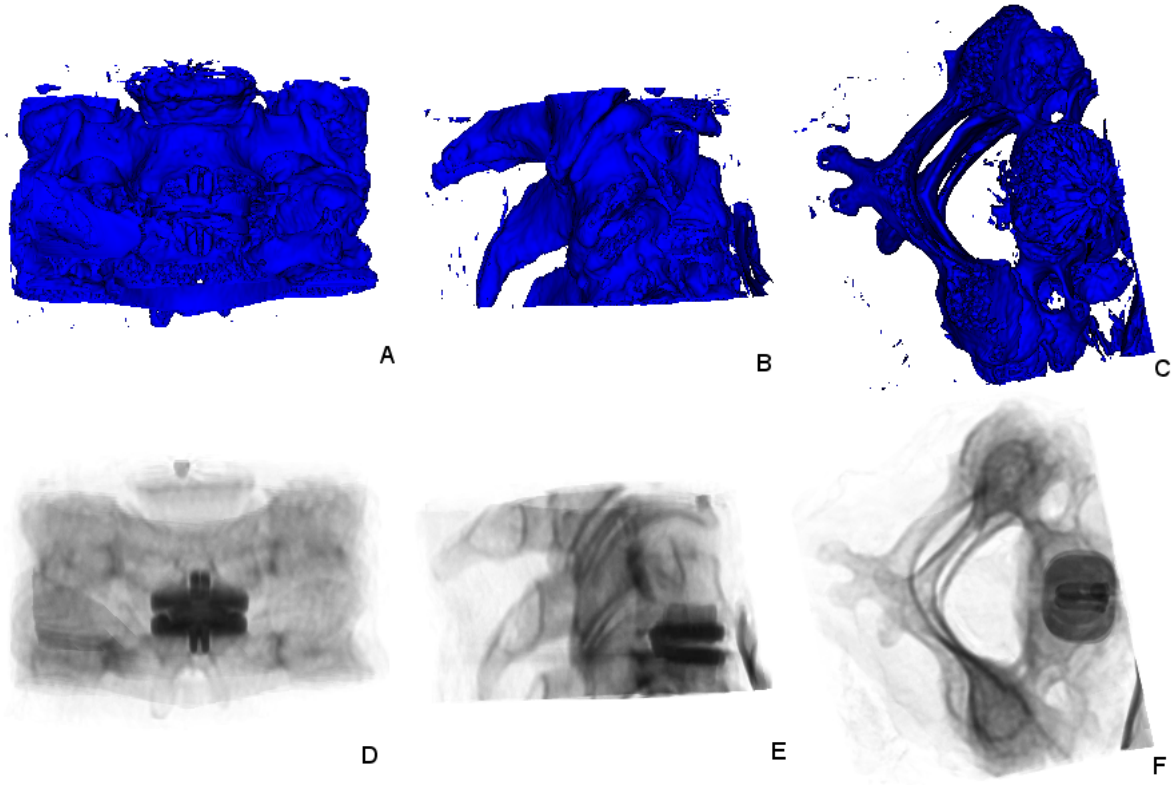

Figure 3-22. Three orthogonal views of a surface model a spinal vertebrae with an implant compared to DRR renderings of the same vertebrae. A) Anterior surface model, B) Lateral surface model, C) Axial surface model, D) Anterior DRR, E) Lateral DRR, F) Axial DRR

Previous research by Penney(33) evaluated 6 different similarity measures for 2D/3D image registration of lumbar spine images. They found gradient difference, gradient correlation and pattern intensity to have the best results, with rotational RMS errors of 0.2-0.5 deg and translation RMS errors of 0.3-0.5 mm in plane and 4-5 mm out of plane. They also found that mutual information had the largest errors, for the particular images used in the investigation. This result is contrary to previous data that suggests mutual information to be highly accurate for 3D to 3D registration. The difference is possibly due to the nature of the images being registered. Mutual information utilizes statistical descriptors of the images, sampling more pixels will generally result in less variability of the probability distribution function. Therefore including more pixels, such as is the case for 3D/3D volumes, can increase its effectiveness. Our results corroborate the observation of Penney(33) in that we found mutual information alone to be less accurate than gradient correlation, but this could be because the region of interest in our registration was relatively small (approximately 75 x 150 pixels).

The gold-standard data used in this study was originally produced and described by Van De Kraats(51). Their investigation evaluated two different similarity metrics, a gradient based method and an intensity based method (gradient difference). The results presented in this chapter are in good agreement with the data reported in their investigation for CT to single plane fluoroscopy for capture region, however we did observe slightly larger errors than they reported for the intensity based method (0.6 mm

compared to 1.2 mm). This difference could be due to differences in generating the DRR images and in the optimizers that were implemented.

In a similar study of 3D/2D CT and MRI to x-ray image registration in the lumbar spine, Tomazevic(55) reported average mTRE values of 0.2-0.5mm (depending on vertebral level) for biplane registration using CT volumes. For their biplane registration setup, they determined a capture region of approximately 6mm mTRE. As in the current study, they also observed a rapid drop-off in successful registrations beyond the capture region. This is in contrast to results in the same paper that show as a steady, almost linear, drop in successful registrations for MRI to x-ray.

One novel contribution of the current research was the evaluation of a unique image similarity metric, by combining the results of gradient correlation and mutual information into a single measurement. The theory behind this metric is that the two different functions would be sensitive to different features in the image and by combining them, the resulting metric would be more robust than either of the individual components alone. Our results demonstrate that when compared head-to-head the gradient correlation metric was significantly more accurate than mutual information alone. Even still, there seems to be a modest synergistic effect by combining the two measures and that the combined metric has a slightly higher success rate.

The time duration of each registration is not as critical for our intended application of tracking kinematics compared to the surgical navigation application. However, increasing the speed can facilitate user interaction during the registration process. For example, if each registration can be completed in a few minutes or less, then a user can oversee the optimizer and stop the registration process and restart it with a new initial

guess if the optimizer is not converging. The generation of DRRs is the bottleneck for our registration algorithm, and this can be significantly sped up with high performance graphics cards. For these experiments, relatively modest consumer graphics cards were used (Nvidia GEForce 9400 GT, Nvidia GEForce 8400 GS and Nvidia GeForce 8600 GT), based on benchmarks, it is expected that a high end graphics card (Nvidia Geforce GTX 285) could increase the speed of DRR generation by at least a factor of 4. Also with the recent introduction of graphics hardware specifically designed for general purpose computing (eg Nvidia Tesla) it might be possible to achieve even greater increases in registration speed.

Conclusion

These results demonstrate that single plane fluoroscopy can be a useful tool and accurate tool for measuring 3D position and orientation of spinal vertebrae when a staring position within 4mm mTRE can be supplied by the user. The range of the capture region could possibly be increased by modifying the image metric or the optimizer. Since all three of the metrics evaluated in this study seem to have a similar drop-off in capture range around 4mm, it is possible that this is an artifact of the optimizer used. By modifying the optimizer to search a larger region, it might be possible to increase the capture region. We are in the process of exploring additional global optimization options that can be implemented efficiently without requiring an excessively high number of iterations to converge. The next step in this project is to apply this image registration technique to measure vertebral motion in dynamic fluoroscopic image series.

CHAPTER 4
MEASUREMENT OF SPINE KINEMATICS BY REGISTERING LATERAL FLUOROSCOPY IMAGES TO DIGITALLY RECONSTRUCTED RADIOGRAPHS

Introduction

It is widely recognized that many spinal disorders have a biomechanical component which is often manifest in either a loss of motion or hyper-motion (instability). The American Medical Association recommends measuring spine range of motion using a goniometer or inclinometer to document permanent impairment associated with chronic low back pain(56). In response to this proposal by the AMA, Nitschke(57) investigated the practical usefulness of these instruments and reported poor reliability when using a goniometer or dual inclinometer to measure thoracolumbar flexion, extension, lateral bending and axial rotation. Clinicians are therefore presented with the dilemma of having a mandate to measure spine motion, but the available tools are unreliable.

At a more basic level, there are still questions regarding the in vivo 3D kinematics of the normal spine. The challenge lies in measuring complex 3D motion of a series of individual non-superficial vertebrae *in vivo*. Most of the solutions available to date fail at least one of these criteria. Numerous methods have been proposed and implemented for quantifying in vivo spine motion. In the following section, we explore the current options and demonstrate that there is a critical need for a technique that can accurately, reliably and non-invasively measure the in vivo intervertebral kinematics of the cervical and lumbar spine.

Review of Current Methods for Measuring Spine Motion

Optical motion tracking is often used for tracking the motion of the whole body (or even multiple bodies) through a large capture volume. Such systems have proven to be very useful for measuring gait mechanics and sports activities, but are inadequate for measuring the motion of individual vertebrae in the spine. There are several limitations to optical motion capture technology. Markers placed on the skin surface suffer from errors due to soft tissue artifact when the soft tissues movement does not coincide with the underlying bone motion. Even in areas of the body where bony landmarks are relatively superficial, such as the medial and lateral condyles of the knee, large deviations between bone motion and marker motion have been documented. In the spine, it is not possible to attach external skin based markers in a way that would allow accurate measurements of the 3D movements of individual vertebrae.

Electromagnetic systems(58-61) have also been used to measure spinal ROM. Our lab has made extensive use of this methodology in cadavers(62-69) where the sensors can be rigidly and invasively attached to the vertebrae. However, for in vivo measurements, this technique is generally limited to external skin based attachment and like optical motion tracking, it suffers from the errors due to soft tissue artifact.

Other specialized systems have been developed to attempt to measure spine motion using externally attached linkages (CA 6000) (70,71) or a series of inclinometers and magnets(72) (CROM) or accelerometers(73,74) (Spinal Mouse). However, these devices only allow the global motion of the spine to be accurately measured and are not able to determine the amount of motion occurring at each individual segment. To asses the extent of spinal disease, it is critical that motion is measured at individual functional spinal units, so that the appropriate levels can be treated. In measuring outcomes, it is

also important to determine whether motion is occurring at the operated level or at adjacent levels.

Another common method for measuring spinal motion that is widely accepted in the clinical environment is by evaluating two dimensional static radiographs at the extents of the range of motion (eg. flexion-extension films). Spine motion that occurs in the plane of the image can be measured directly from the image, however care must be taken when measuring translations that the appropriate reference frames are taken into account and that consistent landmarks are chosen as the basis for measurements. While this method is able to measure the maximum range of motion (ROM), it is not able to describe the dynamic motion of the spine.

Two-dimensional lateral flexion-extension radiographs alone are inadequate to be used as a clinical outcome measure, and have been shown to give limited information on the underlying pathologic condition. (75) The uncertainty associated with measuring flexion-extension ROM from radiographs is estimated at 3-5 deg and fusion is generally defined as motion less than 2-4 deg(76-78). There has been a great deal of controversy clinically over how to define how much measured motion is relevant since difference between a completely fused spine and normal motion can be as little as 6 deg of ROM.

An interesting new technique that could potentially facilitate measuring dynamic kinematics is 4D (3D volume over time) imaging using either MRI(79) or CT(80). However, 4D imaging equipment is still in an early stage of development and not yet capable of tracking *in vivo* spine motions. Dynamic CT has been used in a cadaver study to capture a 3D image at the extent of motion, due to space limitations within the

CT, it would be challenging to perform functional activities while being imaged.(81) During the time required to obtain each 3D image, the subject must remain completely static during the acquisition of the image, or the image will contain motion blur. It is also possible that the kinematics of the joints will be different because of the static requirements than what would be observed during dynamic motion.

Some researchers have used invasive techniques to attach motion sensors tospinous processes using k-wires(82). The invasive nature of this technique makes it unlikely to gain widespread acceptance for measuring motion in healthy individuals. It is also possible that the insertion of pins into the spine might have an affect on an individual's ability to move normally.

Radiostereometric analysis (RSA) provides accurate measurements, but requires invasive surgery to implant metallic beads in the bone. Because it is an invasive technique it is only used in subjects who are already undergoing surgery, in which case the surgeon would have access to the necessary anatomical landmarks to place the beads. In the cervical spine, some investigators have experienced difficulty in using RSA, due to the relatively small size of the vertebral body not allowing sufficient distribution of the beads.(83)

Purpose

There is a critical need for a technique that can accurately, reliably and non-invasively measure the *in vivo* intervertebral kinematics of the cervical and lumbar spine. The increasing use of motion preserving devices in the spine has highlighted the need for accurate kinematic measurement tools to evaluate the performance of these new implants. Furthermore, a fundamental need exists for accurate measurements of

normal and pathologic motion to better inform clinicians, researchers, and implant designers.

Single plane fluoroscopy has been used for over 15 years to quantify the *in vivo* motions of total knee replacement implants, with reported accuracies of 0.5-1.0 deg for rotations in the image plane. This methodology has been modified to incorporate the additional capabilities of registering DRR projection images and shown accuracy of 1.2 mm mTRE for in-plane motion (Chapter 3). The purpose of this project was to determine the accuracy of using an image based 2D/3D registration technique to measure the 3D segmental kinematics of a cervical spine during dynamic motion.

Methods

Specimen Preparation

Three fresh frozen human cadaveric cervical spines were obtained instrumented with a Synthes ProDisc-C total disc replacement (Synthes Spine, West Chester, PA). For specimen 1, the intervertebral implant was placed at C4-C5, for specimen 2 the implant was placed at C6-C7 and for spine 3 the implant was placed at C3-C4. The two vertebrae at the operated level (superior and inferior) were used for the 2D/3D image registration kinematics measurements.

Experimental Protocol

To establish the “Ground Truth” motion of the implants, a four-camera optical motion analysis system (Motion Analysis Corp, Santa Rosa, CA) was used to measure the 3D position of markers attached to anatomic landmarks (Figure 4-1). Three markers were attached to both the superior and inferior vertebrae at the operated level. The anatomic coordinate system for the fluoroscopic system was defined by identifying three landmarks in the CT image: left and right mid-pedicle, and the most anterior point of the

vertebral body at the mid-pedicle level. The origin of the coordinate system is the midpoint between the right and left pedicle markers. The X-axis is defined between the right and left mid-pedicle points and positive to the right. The Y-axis is in the plane of the three landmarks pointing anteriorly. The Z-axis is perpendicular to the X- and Y-axes and is positive in the cranial direction (Figure 4-2).

The cranial and caudal ends of the spine were potted in polystyrene resin (Bondo Inc, Atlanta, GA). The caudal end of the spine specimen was secured in a vice clamp and positioned in the fluoroscopic devices so that a lateral image could be obtained (Figure 4-3). A manipulator handle was attached to the cranial end of the specimen so that the spine could be manually maneuvered thorough a range of motion, while limiting radiation exposure to the investigator. Each spine was then moved through a passive range of motion in orthogonal planes: flexion-extension, lateral bending and axial rotation.

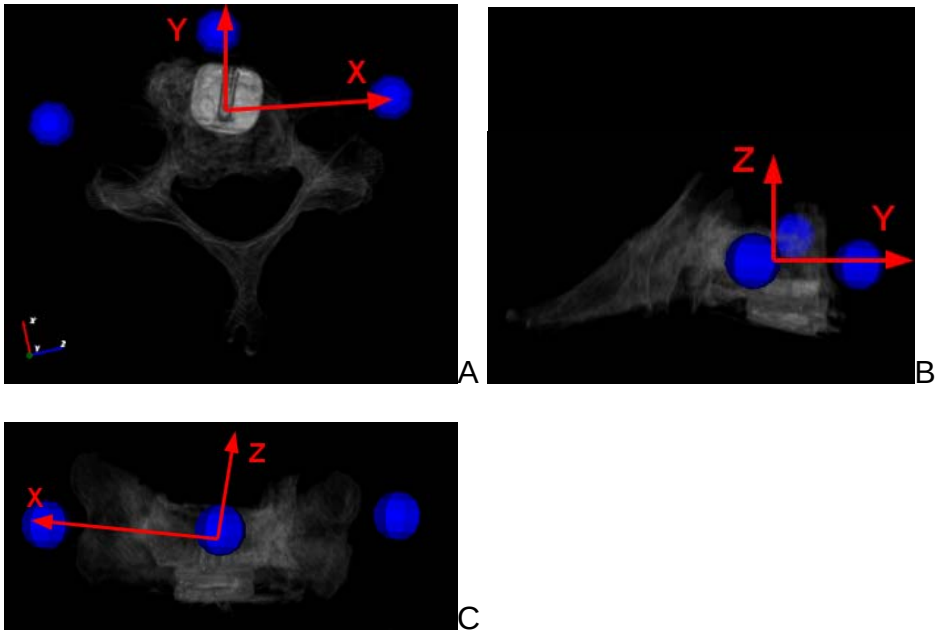

Figure 4-1. Definition of the motion capture reference frame. A) superior view, B) lateral view, C) anterior view.

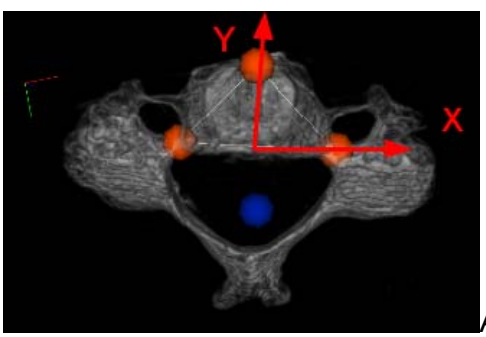

A
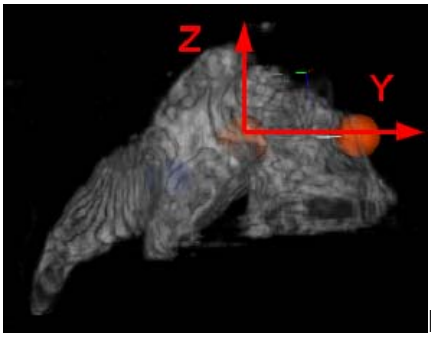

B
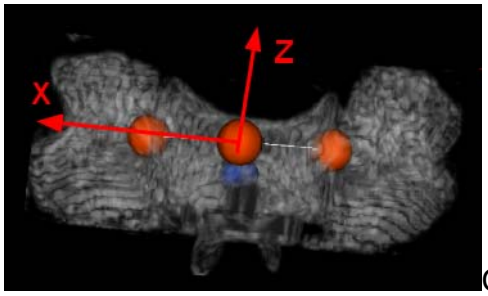

C

Figure 4-2. Definition of the anatomical reference frame in the CT volume. A) superior view, B) lateral view, C) anterior view.

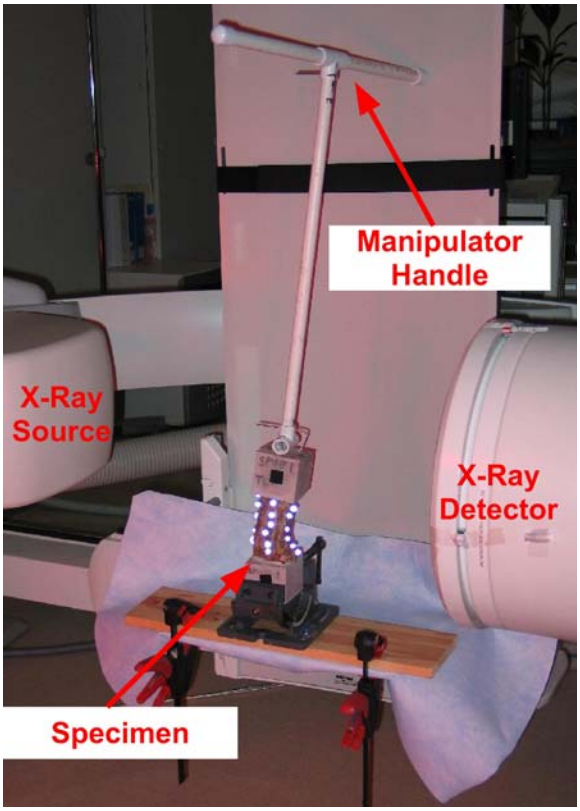

Figure 4-3. Image of the fluoroscopic testing setup. The optical motion tracking markers are visible on the spine specimen.

Imaging Protocol

A Siemans AXIOM-artis fluoroscope was utilized, with the peak energy set to73 kVp, exposure time of 6 ms and frame rate of 7.5 frames/second. The full fluoroscopic images were 1024x1024 pixels, with a pixel size of 0.34x0.34 mm. For analysis, the images were cropped to 512x512, which allowed the vertebrae C3-C7 to be visible during the entire motion sequence. Fluoroscopic images were captured concurrently with the optical motion capture data. Following the motion test, a CT (Siemans, Sensation 16) scan was acquired for each spine. For the CT scan the peak energy was set to 140 kVp and the slice thickness was 0.5 mm, with 0.25 mm overlap between slices. Details of the specimen properties are presented in Table 3-1.

After the CT scans were acquired, the images were processed (ImageJ, National Institutes of Health, USA) to removed overlapping vertebrae, so that a volume could be created which included one and only one vertebra. The volume was cropped to the bounding box of the vertebra. An image mask was created by using a threshold value that removed the soft tissue from the CT images, while leaving the cortical and cancellous bone intact. The mask was applied to the image, leaving the raw intensity values for the bone while eliminating the background and soft tissue. In each image slice, adjacent vertebra were manually airbrushed out of the image using the spraycan tool.

Table 3-1. Specimen properties.

Specimen	CT Pixel Spacing (mm/pixel)	Tested Levels
Spine 1	(0.164, 0.164, 0.5)	C4-C5
Spine 2	(0.279, 0.279, 0.5)	C6-C7
Spine 3	(0.193, 0.193, 0.5)	C3-C4

Data Analysis

In order to measure motion of individual verebra, an anatomical coordinate system was defined for each bone. For the CT volume used in the image registration method this was performed by identifying anatomical landmarks on the image slices. For the motion capture data, the markers themselves were attached to specific anatomic locations so that they would define a comparable reference system to the image registration method. Kinematics were calculated for each individual bone by aligning the dynamic pose to an initial static image at the beginning of each trial.

The motion capture data was collected at a rate of 60 Hz, and the fluoroscopic data was collected at 7.5 Hz. To obtain data on the same time scale, the fluoroscopic data was interpolated to 60 Hz. The data between the two systems was synchronized in the temporal domain by optimizing the linear regression between the motion capture data and the fluoroscopic data. The fluoroscopic data series was shifted in the time domain by one frame, and the linear regression was calculated. The frame which returned the largest R^2 value from the linear regression was chosen as the first frame of the fluoroscopic data. Errors were defined by subtracting the fluoroscopic kinematics from the motion capture kinematics. RMS errors were calculated for each motion. Bias

and precision were also measured by calculating the mean and standard deviation of the error measurements.

The relative joint angles between the proximal and distal vertebral body were also calculated. While these data were not utilized in the uncertainty analysis because of the low magnitude, they provide insight into the accuracy of using a fluoroscopic measurement tool for clinical segmental ROM evaluations. The kinematics of the intervertebral motion are calculated as follows:

$$^{distal}\mathrm{A}_{proximal} = \left(^{fluoro}\mathrm{A}_{distal}\right)^{-1} \times {}^{fluoro}\mathrm{A}_{proximal}$$

Likewise, for the optical motion capture (mocap) measurements:

$$^{distal}\mathrm{A}_{proximal} = \left(^{mocap}\mathrm{A}_{distal}\right)^{-1} \times {}^{mocap}\mathrm{A}_{proximal}$$

Software Development

One of the challenges of image registration is to obtain a good initial pose for the 3D volume to match to the 2D fluoroscopic image. To facilitate this process, a graphical user interface (pyTrack) was built for the image registration algorithm described in the previous chapter. The software was written in the Python programming language using QT for the user interface. This interface allows the user to manipulate the 3D position and orientation of the CT volume and observe the DRR projection overlaid on the fluoroscopic image (Figure 4-13). The user interface provides controls for navigating the data, adjusting the image and DRR display parameters, managing region of interests (ROI's), and for performing image registration. The interface provides several tools to assist the user in determining an initial pose for the CT volume, setting up the registration and viewing the results of the optimization:

- Charts for each pose parameter to allow the user to visualize the trends in motion.
- Windowshade tool that allows the user to interactively split the screen so that the DRR and fluoroscopic image can be viewed at the same time.
- A checkerboard tool that creates a checker pattern alternating between patches of the DRR image and patches of the fluoroscopic image.
- Kinematics charts that display the relative joint angles between any two CT models loaded in the project.
- An ROI tool for interactively drawing, moving and storing region of interest information.
- An optimizer report tool that displays the cost function evaluations and parameter adjustments over the course of the optimization.

In addition to providing a user interface, the pyTrack software also implements a data architecture (Figure 4-14) that allows all of the parameters (data paths, object poses, parameter settings, ROIs, centers of rotation, etc.) related to a project to be saved to an XML file.

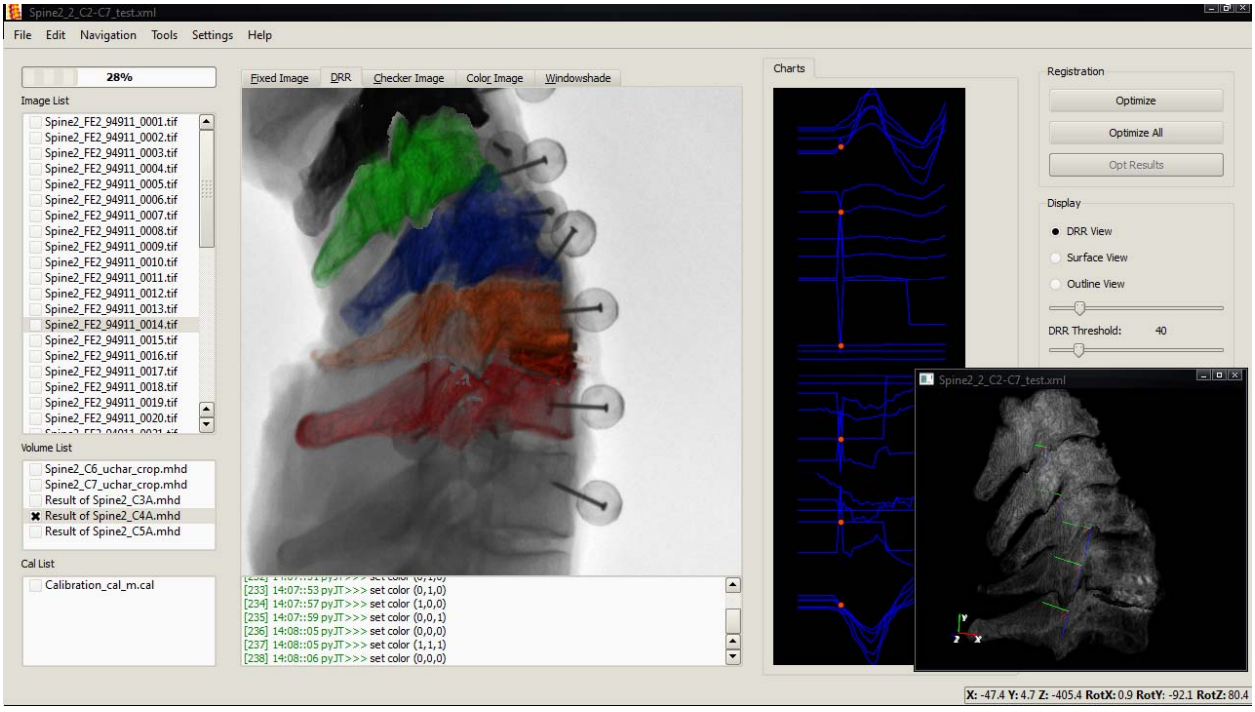

Figure 4-4. Screen capture of pyTrack software user interface for performing 2D/3D DRR image registration.

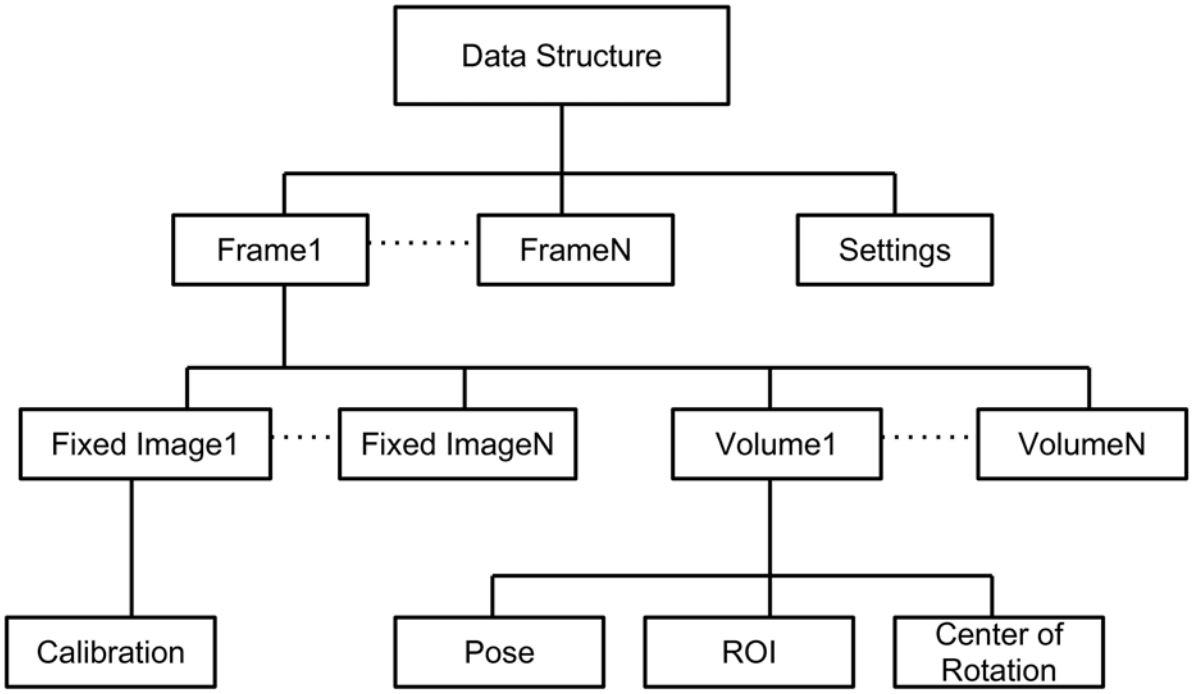

Figure 4-5. Diagram of the pyTrack data structure.

Results

The rotations and translations of two cervical vertebrae were measured in each of three spine specimens using both marker based motion capture and 2D/3D image registration. The kinematics were calculated relative to the starting static pose of each vertebrae. In the figures below, the results for each trial (flexion-extension, lateral bending and axial rotation) are presented in columns and the measured motions in each anatomical plane are presented in rows. Figures 4-6 to 4-6 present the rotation and translation results for the superior vertebrae, for marker based, image based and relative errors, respectively. Figures 4-7 to 4-12 present the rotation and translation results for the inferior vertebrae, for marker based, image based and relative errors, respectively. In the rotation figures, the background for charts of the primary motion direction is colored white, while off-axis motions are shaded gray.

As expected for each motion trial, the largest motions were measured in the direction of motion; however some off-axis, coupled motions were also measured. For example: axial rotation (primary range of motion: 17 deg) was accompanied by a smaller amount of lateral bending (4 deg) and a small amount of axial rotation (8 deg) was measured during lateral bending (primary range of motion: 12 deg) tests.

In all planes of motion, there was less error when measuring the inferior vertebrae compared to the superior vertebrae. This difference was statistically significant for inferior-superior translation ($p=0.021$), flexion-extension ($p=0.026$), and axial rotation ($p=0.015$).

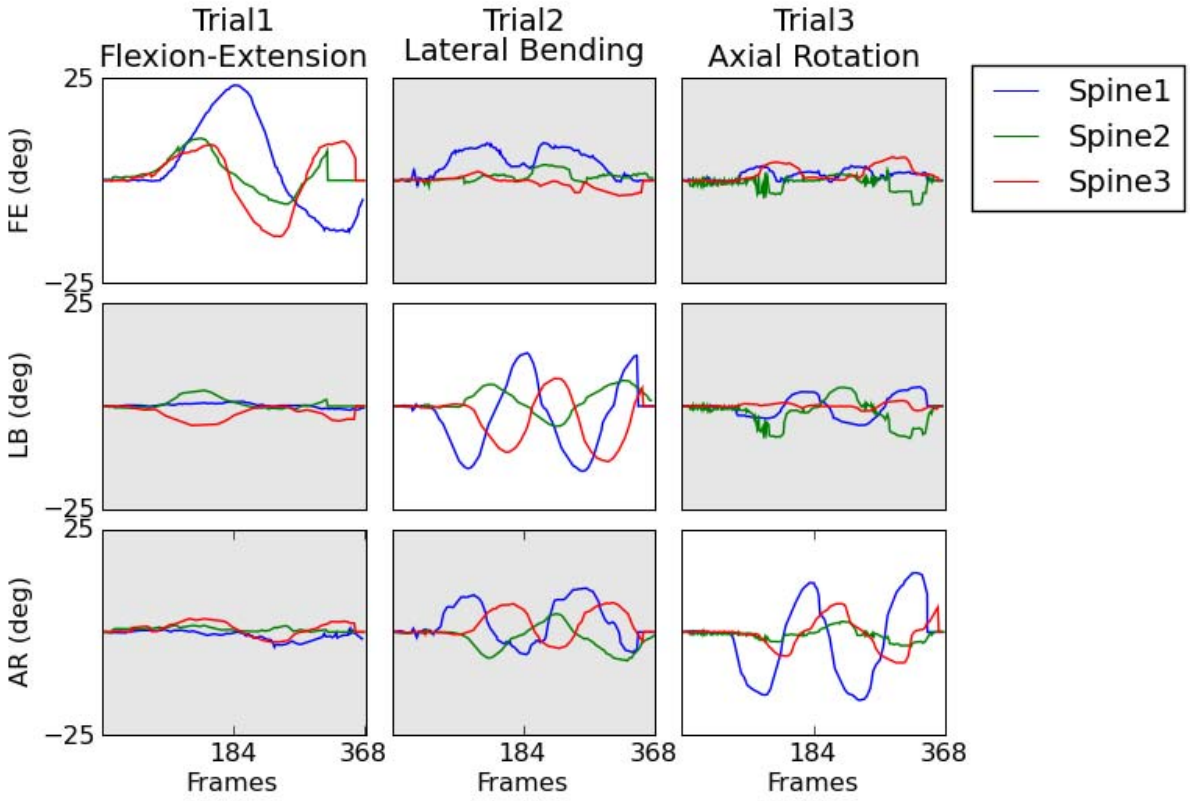

Figure 4-6. Segmental rotation (in degrees) of the superior vertebrae of each spine specimen in primary direction of motion (white background) and the off-axis motions (grey background), measured using marker based optical motion tracking.

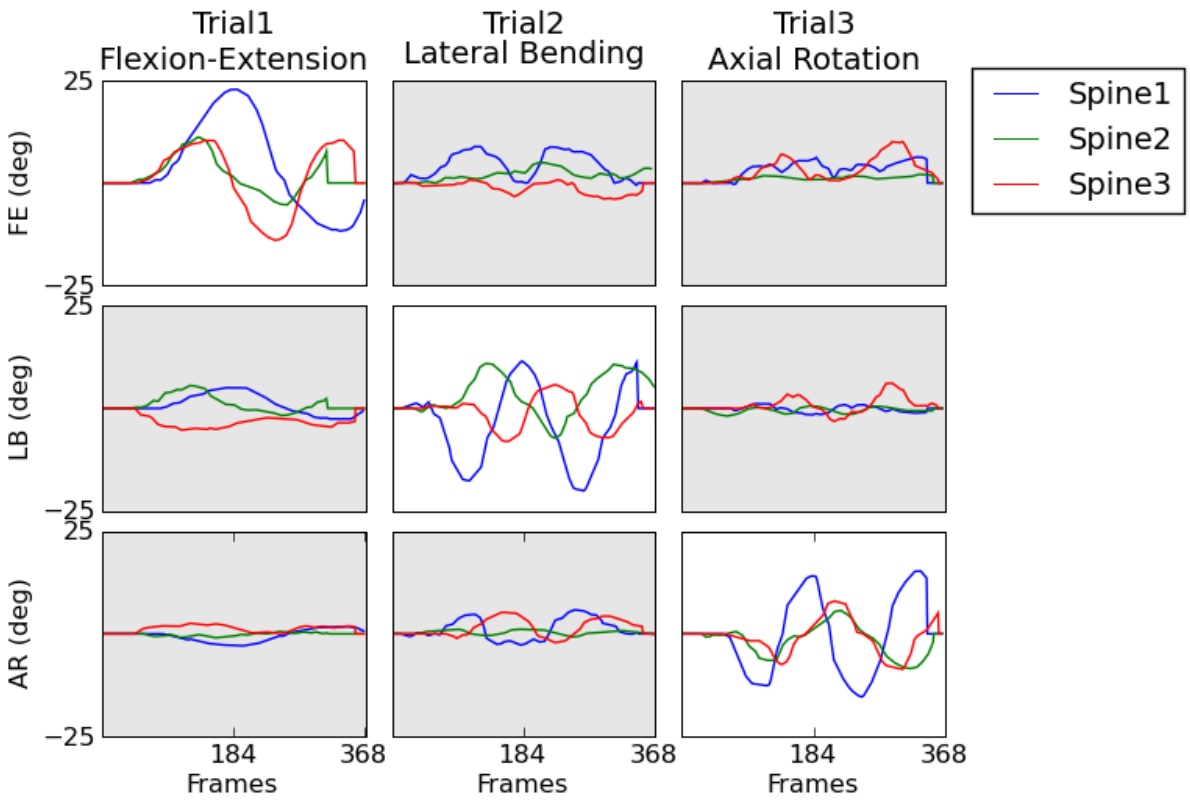

Figure 4-7. Segmental rotation (in degrees) of the superior vertebrae of each spine specimen in primary direction of motion (white background) and the off-axis motions (grey background), measured using image based 2D/3D registration.

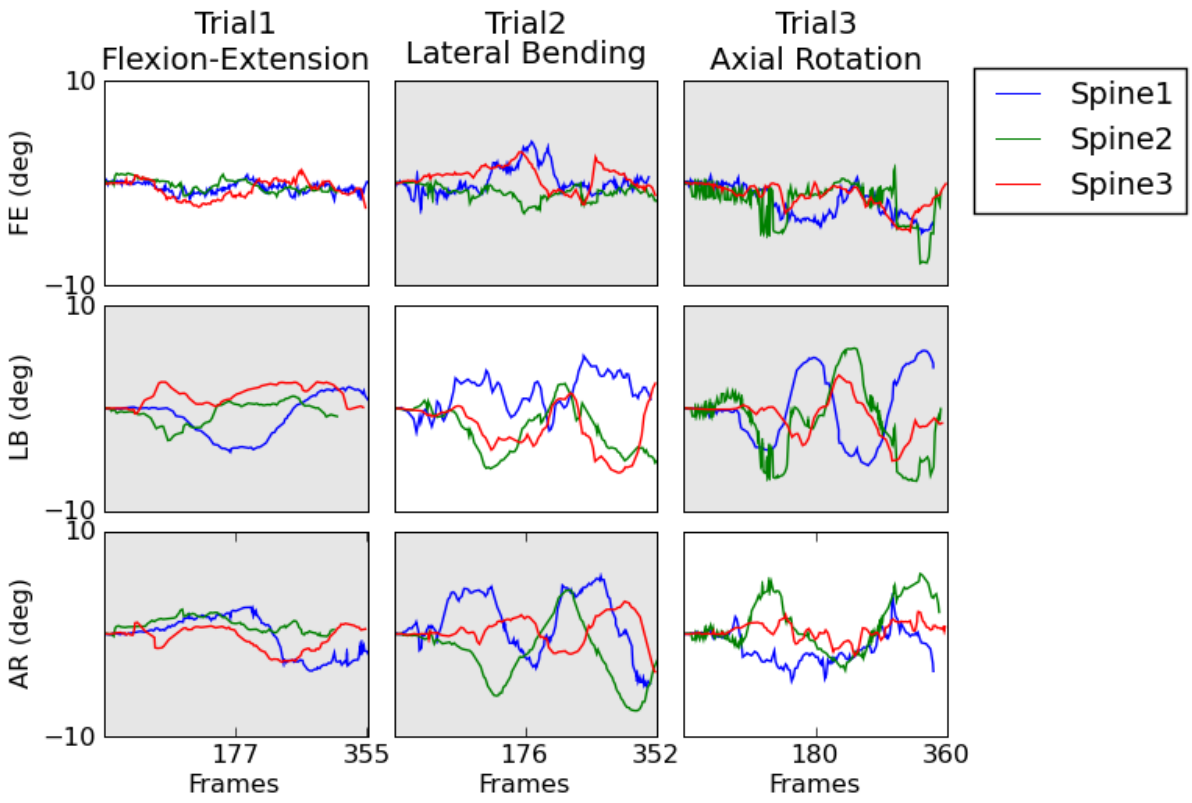

Figure 4-8. Segmental rotation (in degrees) tracking errors of the superior vertebrae of each spine specimen in primary direction of motion (white background) and the off-axis motions (grey background). Errors are calculated by subtracting the image based motion from the marker based motion.

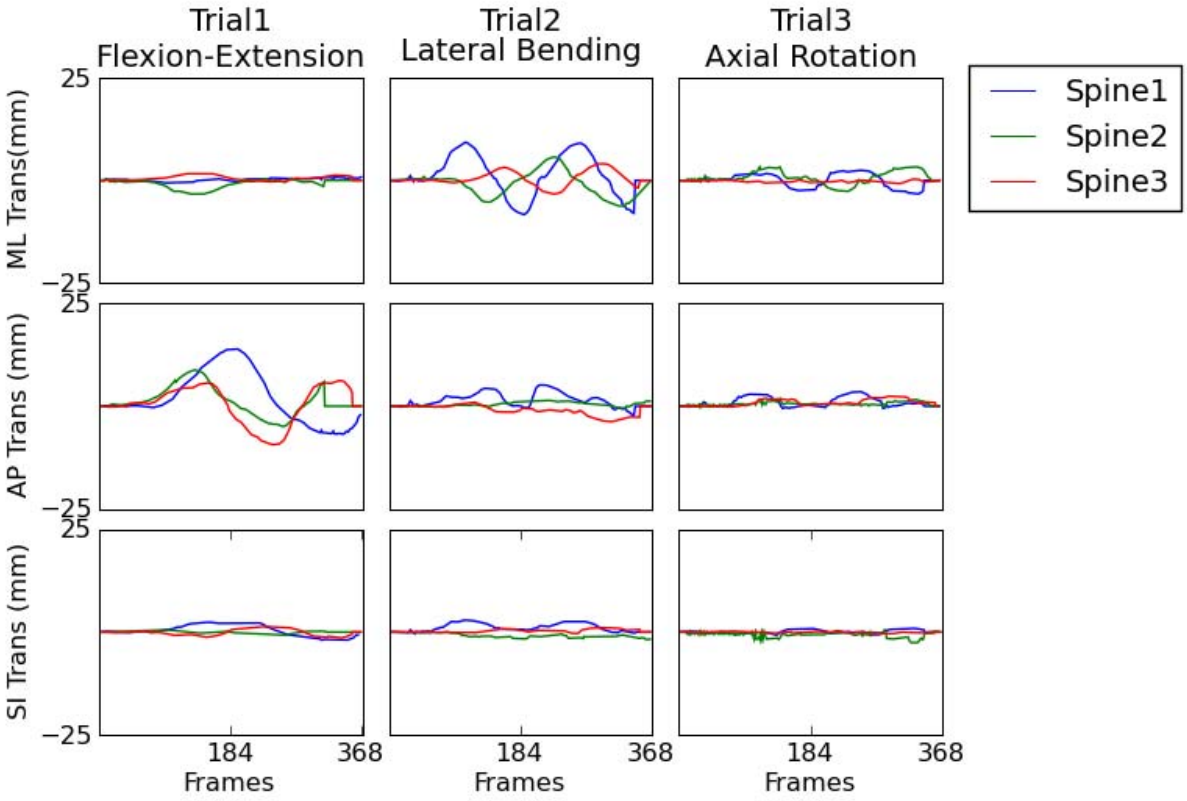

Figure 4-9. Segmental translation (in mm) of the superior vertebrae of each spine specimen, measured using marker based optical motion tracking.

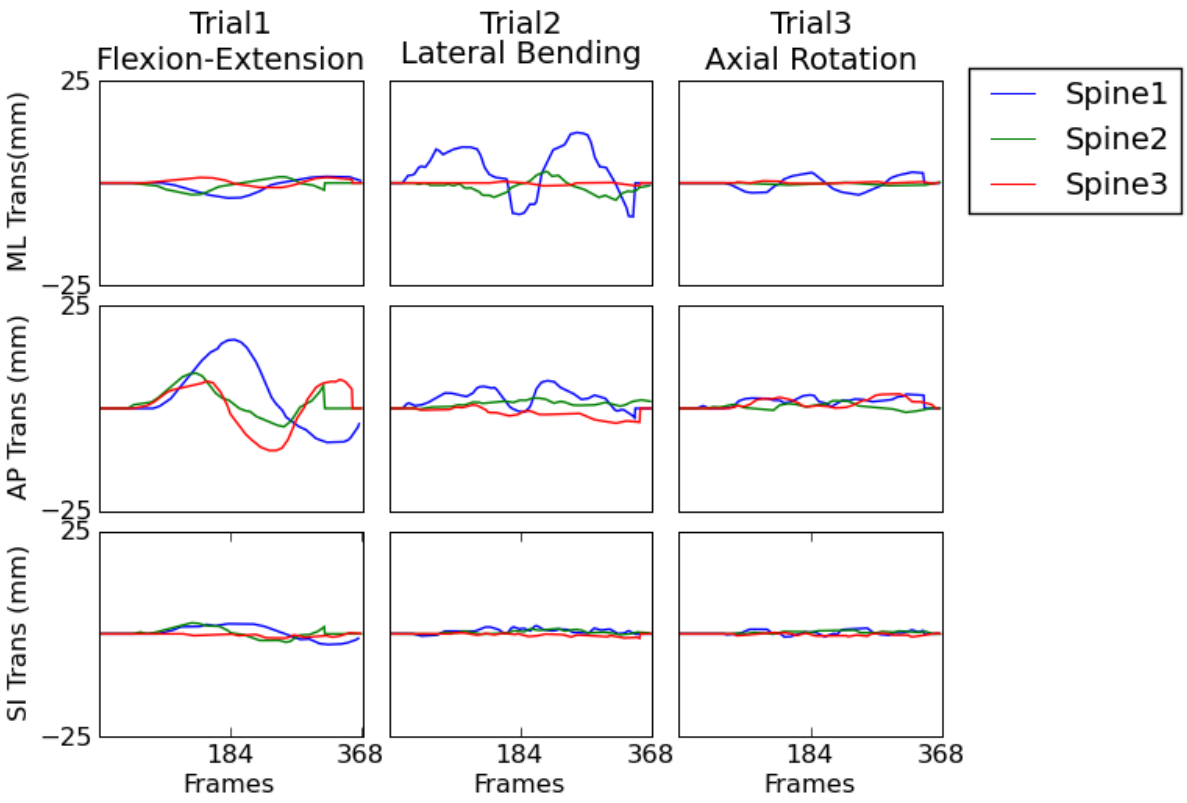

Figure 4-10. Segmental translation (in mm) of the superior vertebrae of each spine specimen, measured using image based 2D/3D registration.

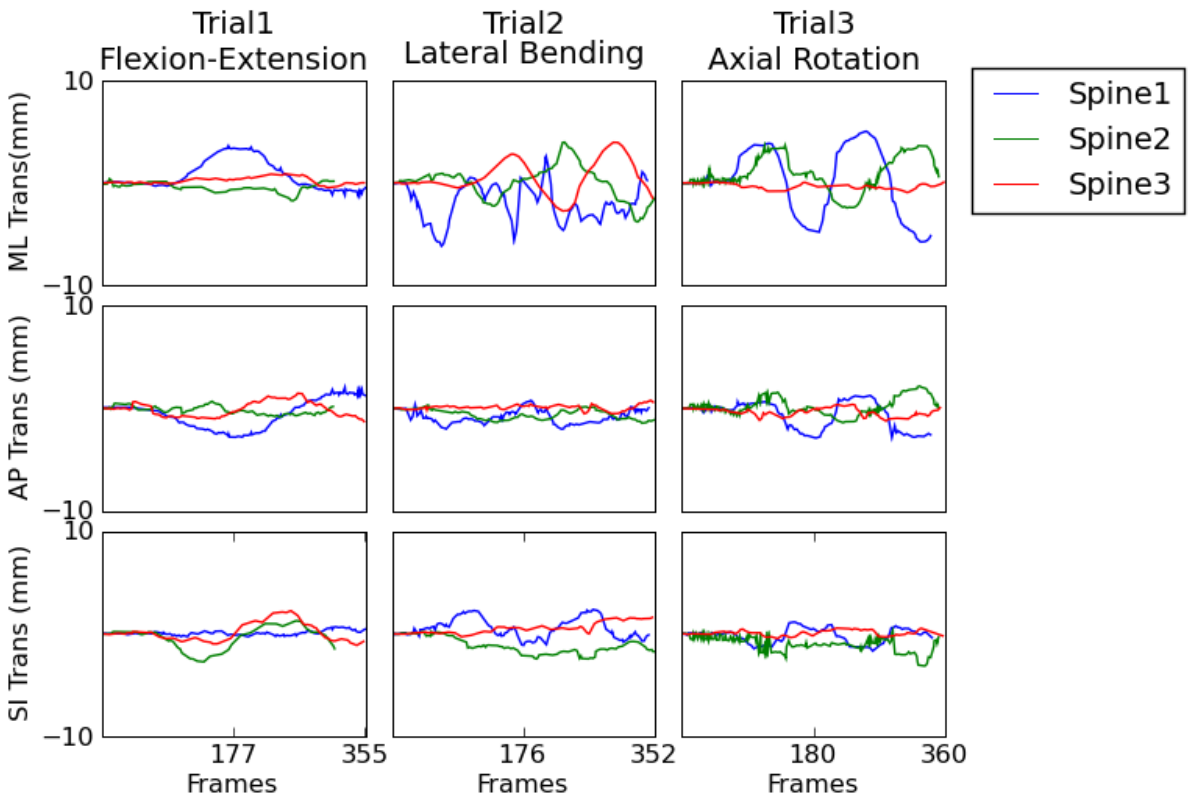

Figure 4-11. Segmental translation tracking errors (in mm) of the superior vertebrae of each spine specimen, measured using marker based optical motion tracking. Errors are calculated by subtracting the image based motion from the marker based motion.

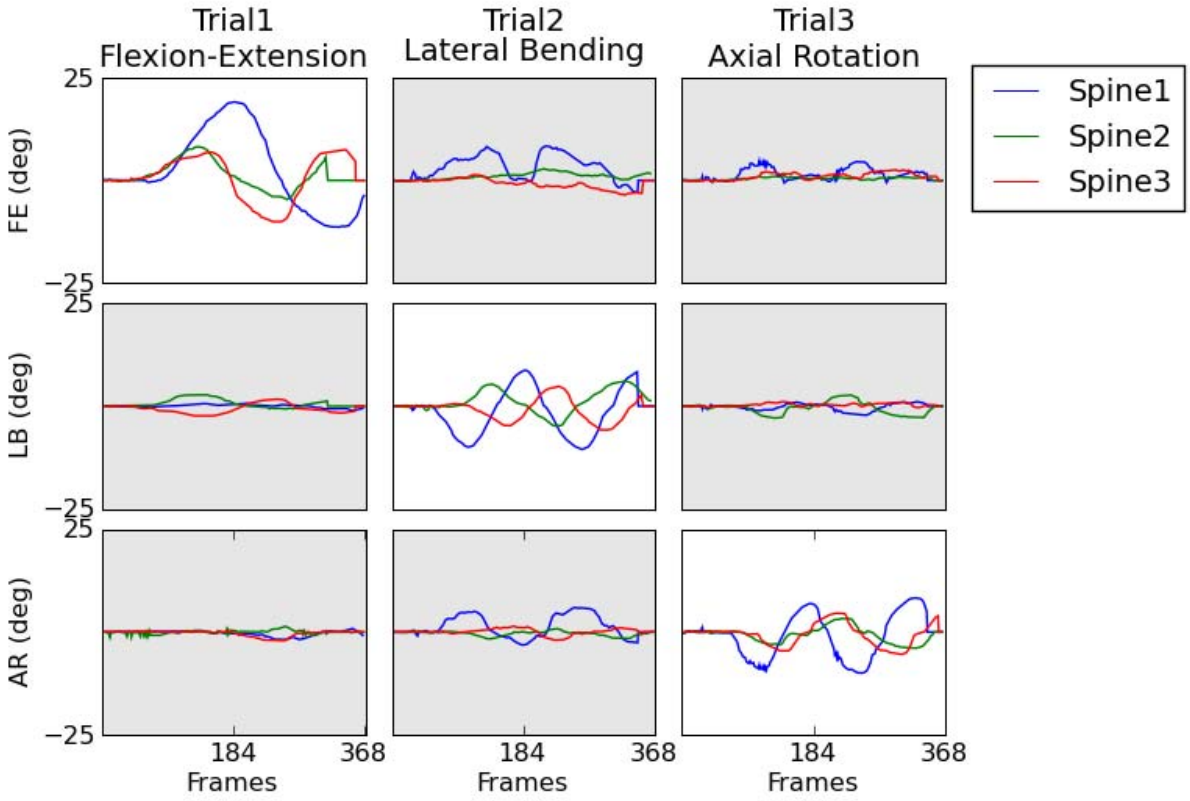

Figure 4-12. Segmental rotation (in degrees) of the inferior vertebrae of each spine specimen in primary direction of motion (white background) and the off-axis motions (grey background), measured using marker based optical motion tracking.

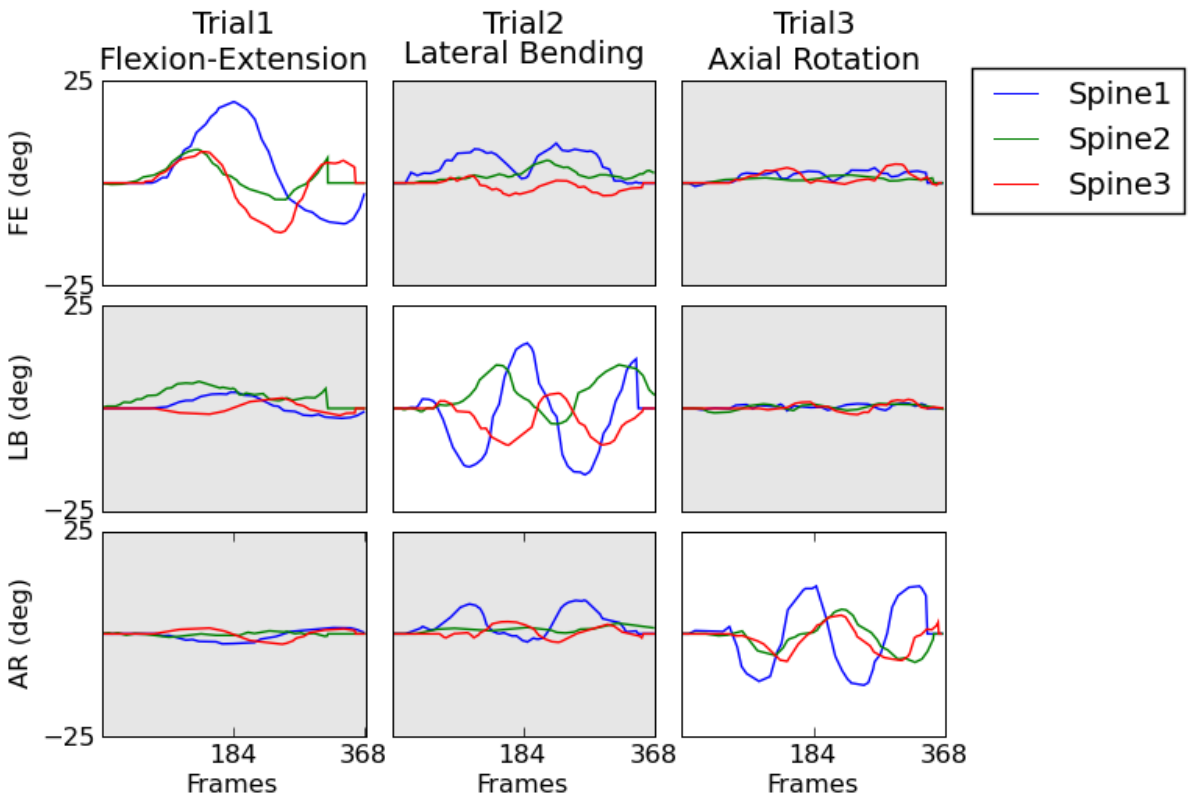

Figure 4-13. Segmental rotation (in degrees) of the inferior vertebrae of each spine specimen in primary direction of motion (white background) and the off-axis motions (grey background), measured using image based 2D/3D registration.

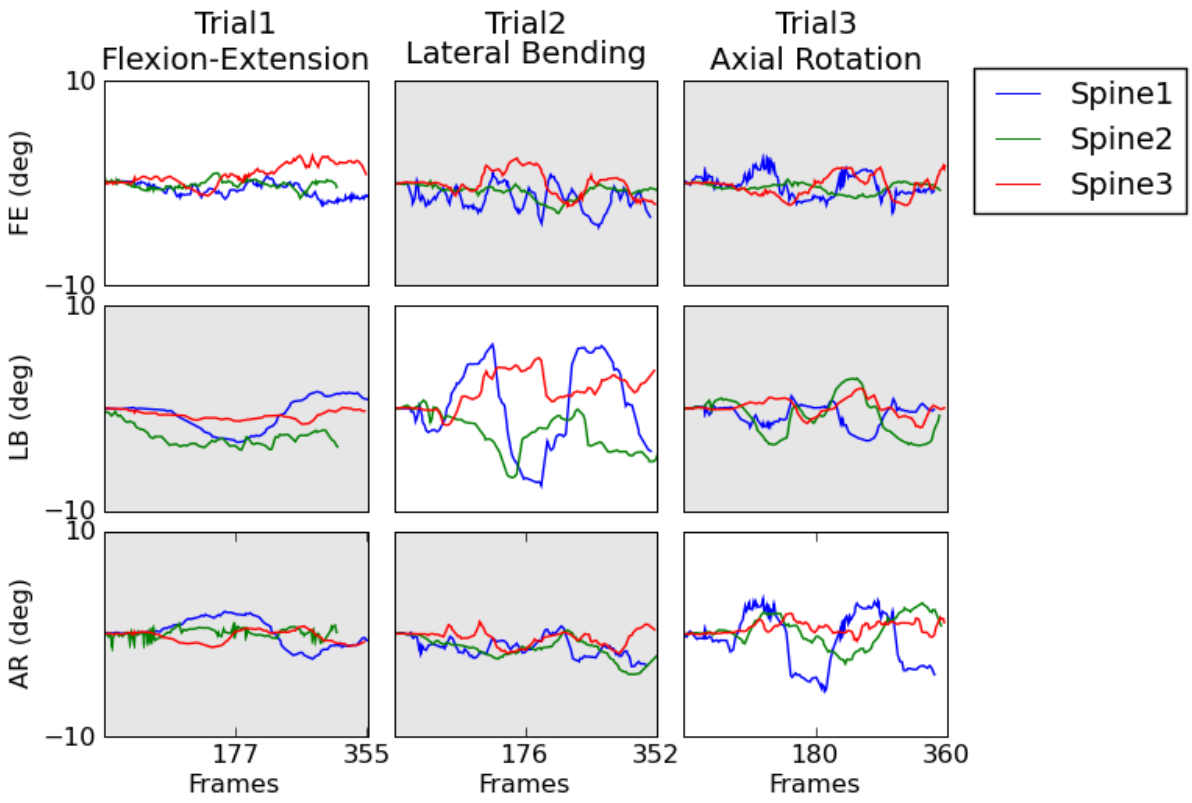

Figure 4-14. Segmental rotation tracking errors (in degrees) of the inferior vertebrae of each spine specimen in primary direction of motion (white background) and the off-axis motions (grey background). Errors are calculated by subtracting the image based motion from the marker based motion.

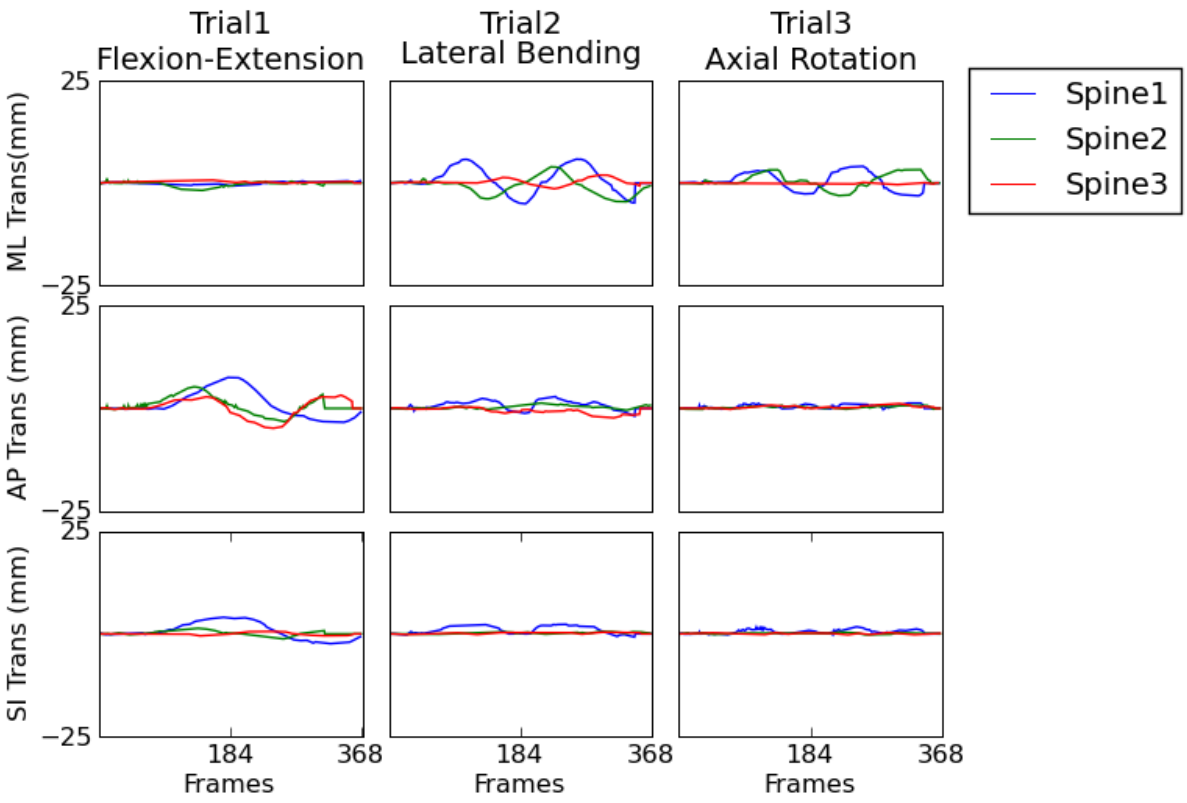

Figure 4-15. Segmental translation (in mm) of the inferior vertebrae of each spine specimen, measured using marker based optical motion tracking.

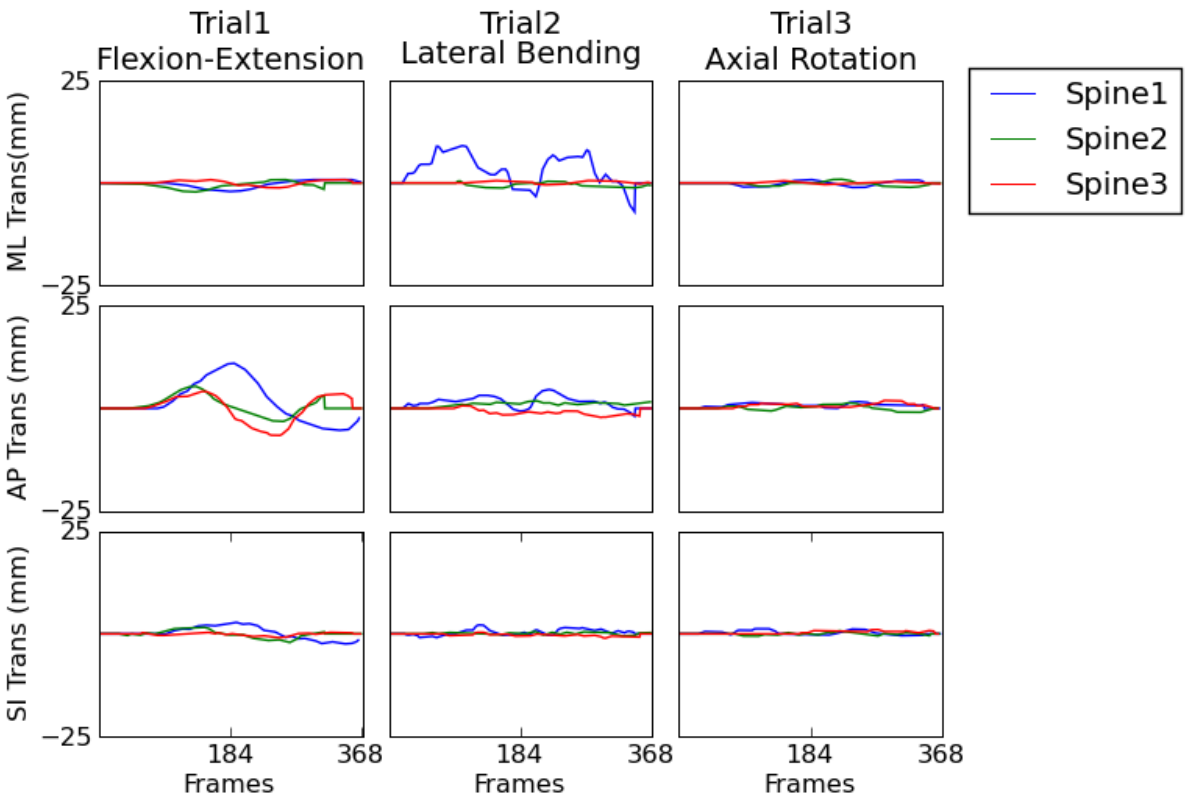

Figure 4-16. Segmental translation (in mm) of the inferior vertebrae of each spine specimen, measured using image based 2D/3D registration.

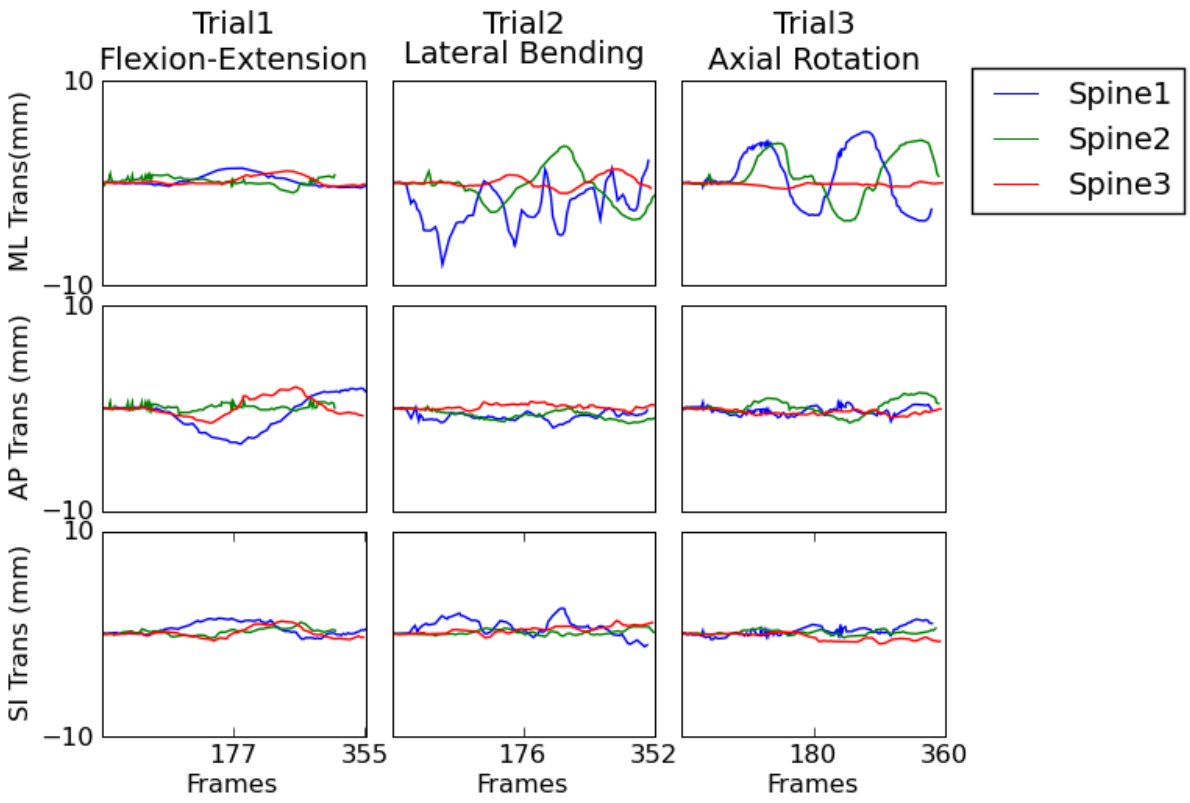

Figure 4-17. Segmental translation tracking errors (in mm) of the inferior vertebrae of each spine specimen, measured using marker based optical motion tracking. Errors are calculated by subtracting the image based motion from the marker based motion.

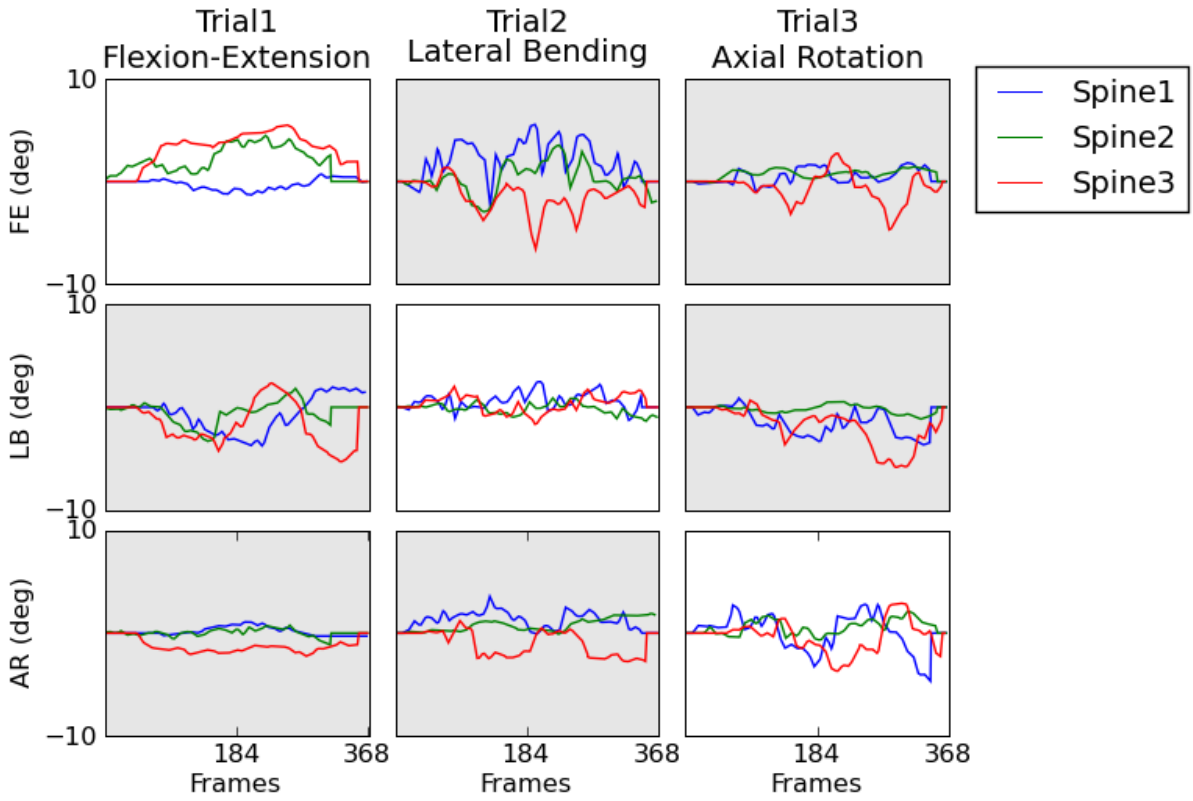

Figure 4-18. Relative joint angles (in deg) calculated from image based motion data.

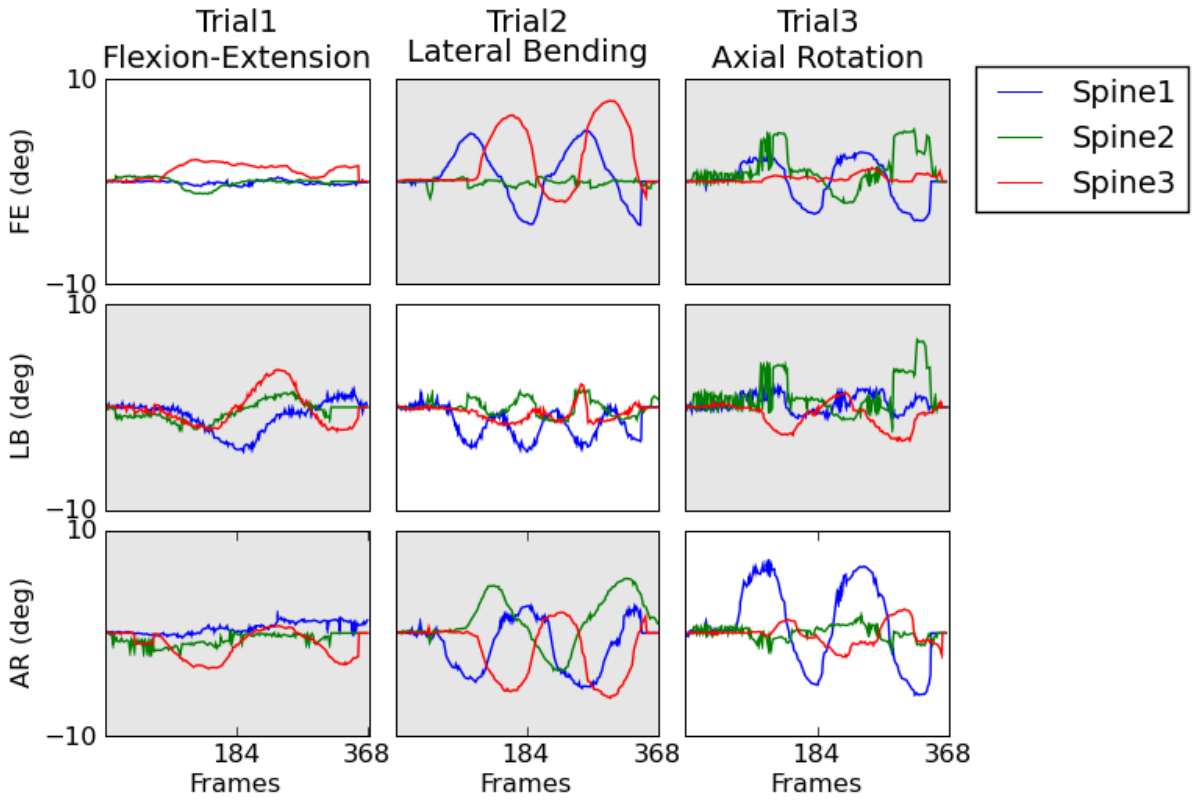

Figure 4-19. Relative joint angles (in deg) calculated from marker based motion data.

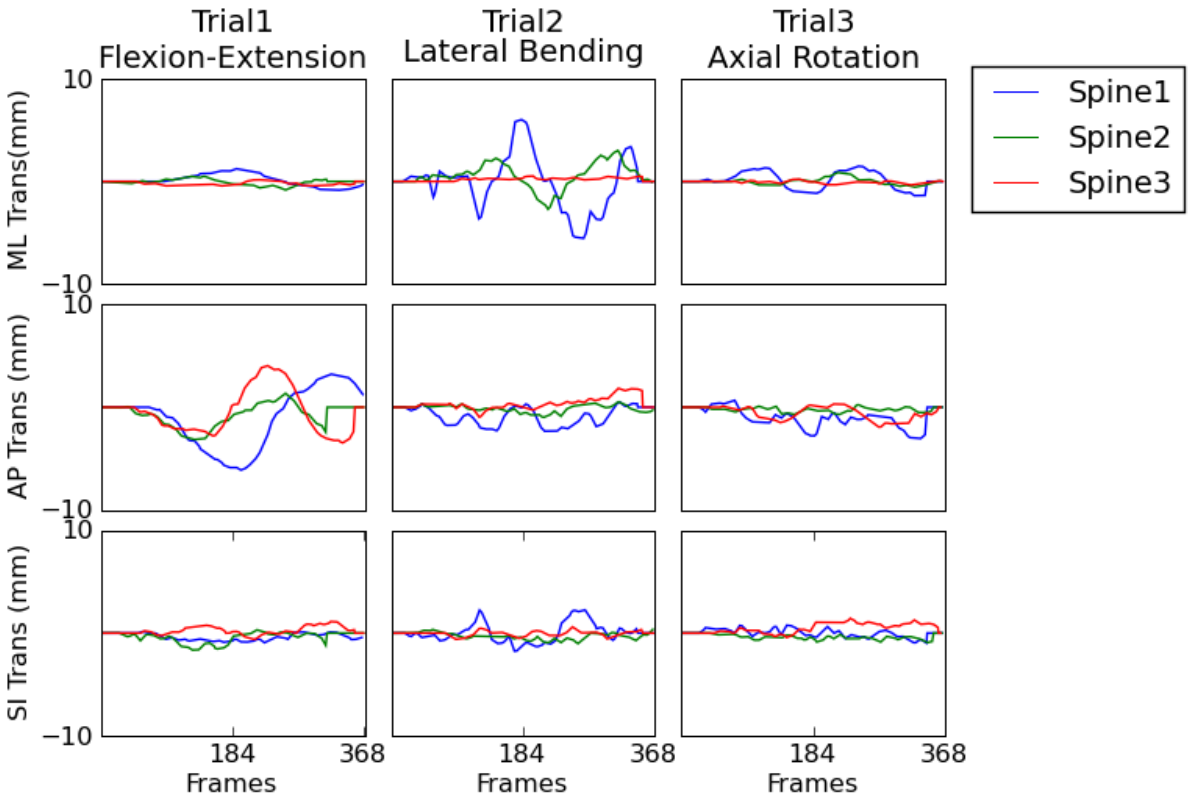

Figure 4-20. Relative joint translations (in mm) calculated from image based motion data.

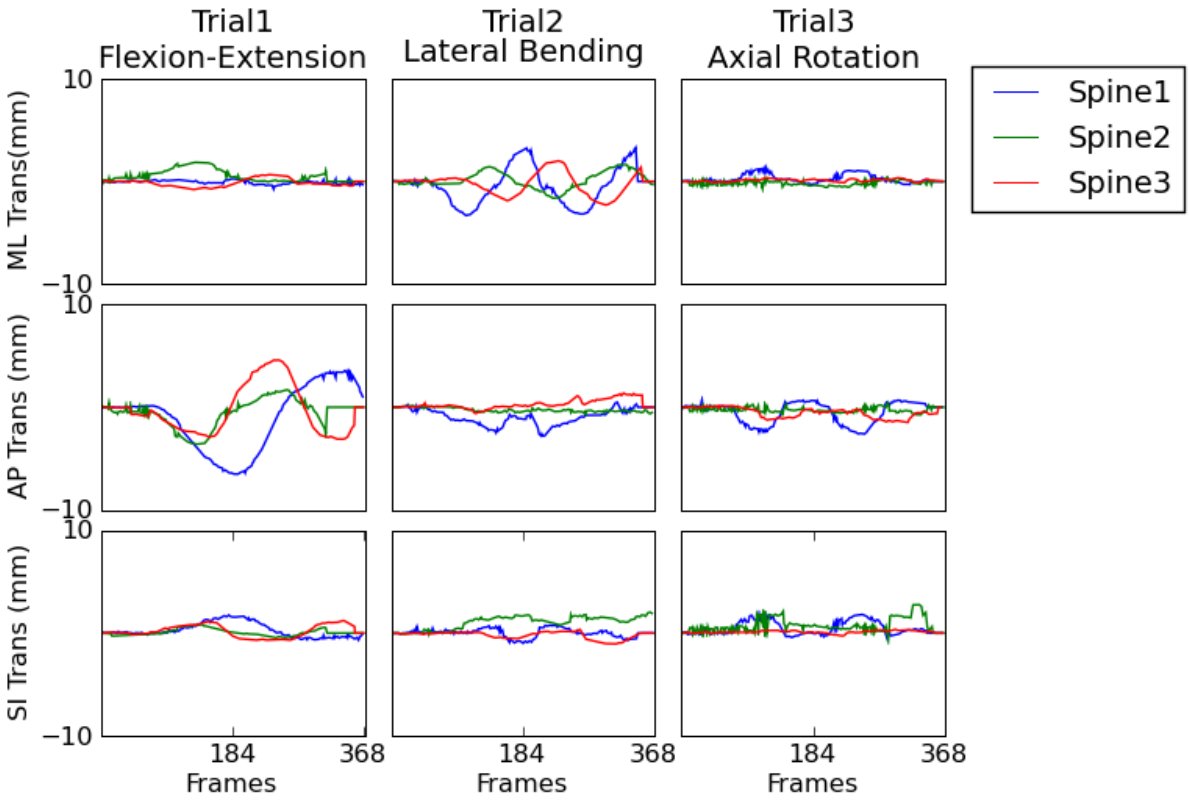

Figure 4-21. Relative joint translations (in mm) calculated from marker based motion data.

Table 4-1. Average **RMS Errors** for translations, average over 3 spines and 2 vertebral bodies.

Trial	Medial Lateral Translation (mm)	Anterior Posterior Translation (mm)	Inferior Superior Translation (mm)
AR Trial	1.84	0.78	0.60
FE Trial	0.70	0.94	0.68
LB Trial	1.90	0.67	0.86
Grand Total	1.48	0.80	0.71

Table 4-2. Average **RMS Errors** for rotations, average over 3 spines and 2 vertebral bodies.

Trial	Flexion Extension (deg)	Lateral Bending (deg)	Axial Rotation (deg)
AR Trial	1.63	2.19	1.73
FE Trial	0.84	1.70	1.12
LB Trial	1.34	2.97	2.05
Grand Total	1.27	2.29	1.63

Table 4-3. Average **bias** for translations, average over 3 spines and 2 vertebral bodies.

Trial	Medial Lateral Translation (mm)	Anterior Posterior Translation (mm)	Inferior Superior Translation (mm)
AR Trial	0.32	-0.21	-0.18
FE Trial	0.20	-0.19	0.12
LB Trial	-0.68	-0.44	0.18
Grand Total	-0.05	-0.28	0.04

Table 4-4. Average **bias** for rotations, average over 3 spines and 2 vertebral bodies.

Trial	Flexion Extension (deg)	Lateral Bending (deg)	Axial Rotation (deg)
AR Trial	-1.02	-0.57	0.05
FE Trial	-0.21	-0.64	0.02
LB Trial	-0.44	-0.49	-0.58
Grand Total	-0.56	-0.57	-0.17

Table 4-5. Average **precision** for translations, average over 3 spines and 2 vertebral bodies.

Trial	Medial Lateral Translation (mm)	Anterior Posterior Translation (mm)	Inferior Superior Translation (mm)
AR Trial	1.74	0.68	0.46
FE Trial	0.60	0.90	0.62
LB Trial	1.56	0.41	0.62
Grand Total	1.30	0.66	0.57

Table 4-6. Average **precision** for rotations, average over 3 spines and 2 vertebral bodies.

Trial	Flexion Extension (deg)	Lateral Bending (deg)	Axial Rotation (deg)
AR Trial	1.21	2.07	1.56
FE Trial	0.67	1.15	1.01
LB Trial	1.03	2.30	1.65
Grand Total	0.97	1.84	1.41

Discussion

Smaller errors were observed for the inferior vertebrae compared to the superior vertebrae. Different vertebrae were measured in each spine: C4-C5 for spine 1, C6-C7 for spine 2, and C3-C4 for spine 3, however there are general trends in the anatomy that might explain the difference in errors. From cranial to caudal, the vertebral bodies become larger and the spinous process becomes more prominent, two features which could be useful for image registration. However, the overall results for the three spines did not follow this pattern, as spine 3 (C3-4) had the smallest errors and spine 1 (C4-5) had the highest errors. Because the caudal end of the spine specimen was fixed to the ground while the cranial end was moved, the more superior vertebrae experienced greater motion than more inferior vertebrae. There is a trend that during larger ranges of motion the errors are higher, and could explain the differences in errors between the superior and inferior vertebrae.

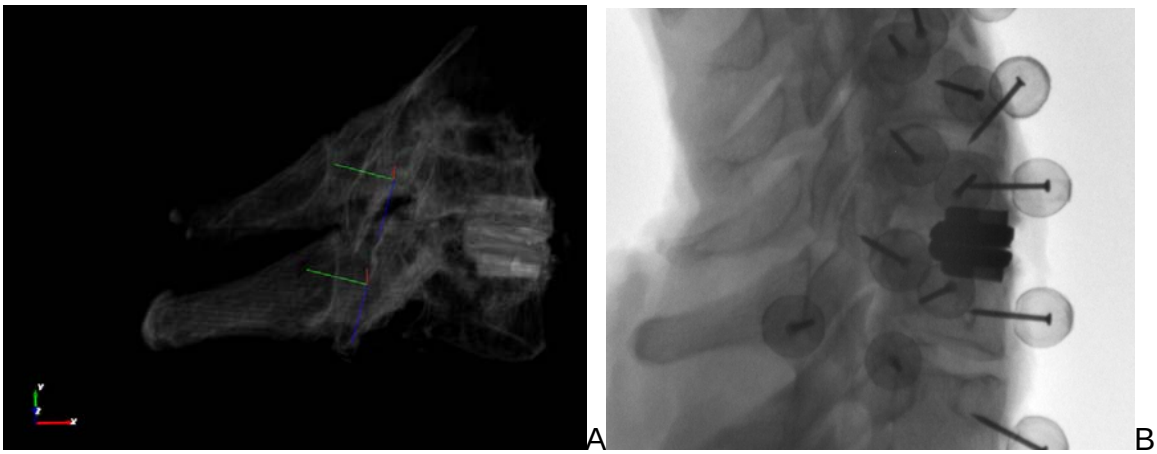

Figure 4-18. Lateral bending motion presents challenges with a lateral fluoroscopic view. A) DRR projection of C6-C7 vertebrae at peak lateral bending pose, B). corresponding fluoroscopic image of the bones in the same pose.

The most common application of 2D/3D image registration for measuring kinematics has been tracking implant motion. There are several differences between tracking implants versus tracking bones. First, while implant CAD models are available from their manufacturer, bone models must be derived from imaging studies. The preferred method for generating these models is through CT scans, however, it has also been demonstrated that slightly less accurate models can be built from magnetic resonance imaging (MRI) scans(5). Second, since implants are constructed from dense, radiopaque, metallic materials, their internal contours (if present) are not easily visible during fluoroscopic evaluation. However, bone has the property of radiolucency that allows internal contours of the structures to be visualized with fluoroscopy. By taking advantage of this additional geometric information, it is theoretically possible to improve image registration results by using DRR projection images, which are a closer match to the fluoroscopic image than a surface model projection.

Accuracy of measurement of spine motions is important clinically, where even small motions can be clinically relevant. For example, the lower limit for normal spine intervertebral spine motion is approximately 7 deg, and fusion is often defined as an intersegmental ROM of less than 3-5 deg. However, many existing methodologies are only accurate to within 2-3 deg, which can lead to a high proportion of mistakes in quantifying fusion success rates. The results of the present study demonstrate improved uncertainties compared to existing methodologies.

One commonly used technique for intervertebral motion analysis in the spine is a 2D quantitative motion analysis (QMA) software program produced by Medical Metrics. This software has been used in a number of clinical trials to asses lumbar and cervical

ROM after disc replacement(19,84,21) or arthrodesis(85). In cadaver testing, Zhou etal(86), report rotational errors of 0.47+/-0.24 deg for flexion extension motions. Although their results demonstrate excellent accuracy and reproducibility, the test setup was constrained to allow only motion in the sagittal plane and the specimen was carefully aligned with the imaging plane. In a clinical scenario, it might be difficult to reproduce that same control over patient alignment, which would decrease the accuracy of this method. Also, this is purely a 2D measurement tool and makes no attempt to quantify axial rotation, or lateral bending. Despite these limitations, the number of studies that utilize this software highlights the critical need for intervertebral motion measurements in the spine.

Tashman has previously reported using DRRs to perform model-based bone tracking using a custom designed high-speed bi-plane fluoroscopy system(87). Their group has published results of tracking glenohumeral(88) and knee motion(50,89,90,87). As in this project, their early papers used DRRs generated directly from CT data using the VTK 3D texture mapping function(87). Some of their more recent studies have made use of a cluster of 24 computers running in parallel to generate ray-traced DRRs(89). Using biplane-fluoroscopy and RSA as a gold standard, they have demonstrated accuracy of 0.385mm RMS error for scapula tracking and 0.374mm RMS for humerus tracking.

There are some limitations to this study. It is not possible to judge whether the motions evaluated in this study are representative of kinematics that would be produced *in vivo* during active muscle activation. However, the motions evaluated in this study were intended to cover a normal passive range of motion for the spine, and for the

purpose of evaluating the measurement methodology, should be similar to the types of motions that would be observed clinically. The use of single plane lateral fluoroscopy inherently presents difficulties in measuring out of plane motion. For the cervical spine, this factor is most problematic during lateral bending motion. In addition to the insensitivity to out of plane motion, lateral bending also produces significant occlusions between adjacent vertebra (Figure 4-13). It is possible that the use of bi-plane fluoroscopy would allow increased accuracy in measuring lateral bending and medial-lateral translation. The presence of motion capture markers in the fluoroscopic views (Figure 4-13B) also creates occlusions with the bones and could decrease the accuracy of image registration, however, during clinical use these markers would not be present.

CHAPTER 5
CONCLUSION

Measuring 3D inter-segmental motion in the spine is a challenging task, but one which can have a significant impact on the clinical care of the spine. Three distinct clinical applications that can directly benefit from improved motion measurements are:

- Diagnosis of disease early in the disease process when conservative therapies might be most advantageous
- Document the level of disability
- Evaluate the effectiveness of treatments

This research project has presented a new methodology for measuring spine motion and reported the measurement uncertainties using both static and dynamic gold-standard data. This method was applied to measuring the 3D motion of an intervertebral cervical disc replacement implant.

Several contributions were made during the course of this work. The feasibility of using surface models to track cervical arthroplasty implants was documented. A new measurement tool was developed which facilitated image registration of CT volumes to fluoroscopic images using DRRs. This is the first reported work that has applied this technique to measuring motion in the cervical spine. A novel image metric was derived and characterized for performing 2D3D image registration.

The next steps in this line of research are to continue to improve the image similarity metric and optimizer to make them more robust to poor image quality and occlusions. Although the present study has focused exclusively on measuring spine kinematics, this technique can readily be applied to other joints such as the shoulder, knee and ankle.

LIST OF REFERENCES

1. Banks S. Personal Communication.

2. Morris H. Human anatomy: A complete systematic treatise. Churchill; 1966.

3. Banks SA, Hodge WA. 2003 Hap Paul Award paper of the International Society for Technology in Arthroplasty Design and activity dependence of kinematics in fixed and mobile-bearing knee arthroplasties. The Journal of arthroplasty. 2004;19(7):809-816.

4. Banks SA, Fregly BJ, Boniforti F, Reinschmidt C, Romagnoli S. Comparing in vivo kinematics of unicondylar and bi-unicondylar knee replacements. Knee Surg Sports Traumatol Arthrosc. 2005;

5. Moro-oka T, Hamai S, Miura H, Shimoto T, Higaki H, Fregly BJ, et al. Can magnetic resonance imaging-derived bone models be used for accurate motion measurement with single-plane three-dimensional shape registration? Journal of Orthopaedic Research. 2007;25(7).

6. Bellemans J, Banks S, Victor J, Vandenneucker H, Moemans A. Fluoroscopic analysis of the kinematics of deep flexion in total knee arthroplasty. Influence of posterior condylar offset. J Bone Joint Surg Br. 2002;84(1):50-3.

7. Kanekasu K, Banks SA, Honjo S, Nakata O, Kato H. Fluoroscopic analysis of knee arthroplasty kinematics during deep flexion kneeling. The Journal of arthroplasty. 2004;19(8):998-1003.

8. Banks SA, Hodge WA. Implant design affects knee arthroplasty kinematics during stair-stepping. Clin Orthop Relat Res. 2004;(426):187-93.

9. Banks S, Bellemans J, Nozaki H, Whiteside LA, Harman M, Hodge WA. Knee motions during maximum flexion in fixed and mobile-bearing arthroplasties. Clin Orthop Relat Res. 2003;(410):131-8.

10. Banks SA, Harman MK, Bellemans J, Hodge WA. Making sense of knee arthroplasty kinematics: news you can use. J Bone Joint Surg Am. 2003;85-A Suppl 4:64-72.

11. Banks SA, Harman MK, Hodge WA. Mechanism of anterior impingement damage in total knee arthroplasty. J Bone Joint Surg Am. 2002;84-A Suppl 2:37-42.

12. Banks SA, Markovich GD, Hodge WA. The mechanics of knee replacements during gait. In vivo fluoroscopic analysis of two designs. Am J Knee Surg. 1997;10(4):261-7.

13. Hilibrand AS, Carlson GD, Palumbo MA, Jones PK, Bohlman HH. Radiculopathy and myelopathy at segments adjacent to the site of a previous anterior cervical arthrodesis. J Bone Joint Surg Am. 1999;81(4):519-28.

14. Goffin J, Geusens E, Vantomme N, Quintens E, Waerzeggers Y, DePreitere B, et al. Long-Term Follow-Up After Interbody Fusion of the Cervical Spine. Journal of spinal disorders & techniques. 2004;17(2):79.

15. DiAngelo DJ, Foley KT, Morrow BR, Schwab JS, Song J, German JW, et al. In vitro biomechanics of cervical disc arthroplasty with the ProDisc-C total disc implant. Neurosurgical Focus. 2004;17(3):44-54.

16. Hilibrand AS, Robbins M. Adjacent segment degeneration and adjacent segment disease: the consequences of spinal fusion? Spine J. 2004;4(6 Suppl):190S-194S.

17. Duggal N, Pickett GE, Mitsis DK, Keller JL. Early clinical and biomechanical results following cervical arthroplasty. Neurosurg Focus. 2004;17(3):E9.

18. Goffin J, Casey A, Kehr P, Liebig K, Lind B, Logroscino C, et al. Preliminary clinical experience with the Bryan Cervical Disc Prosthesis. Neurosurgery. 2002;51(3):840-5; discussion 845-7.

19. Goffin J, Van Calenbergh F, Van Loon J, Casey A, Kehr P, Liebig K, et al. Intermediate follow-up after treatment of degenerative disc disease with the Bryan Cervical Disc Prosthesis: single-level and bi-level. Spine. 2003;28(24):2673-8.

20. Pimenta L, Mcafee PC, Cappuccino A, Bellera FP, Link HD. Clinical experience with the new artificial cervical PCM (Cervitech) disc. Spine J. 2004;4(6 Suppl):315S-321S.

21. Wigfield CC, Gill SS, Nelson RJ, Metcalf NH, Robertson JT. The new Frenchay artificial cervical joint: results from a two-year pilot study. Spine. 2002;27(22):2446-52.

22. Banks SA, Hodge WA. Accurate measurement of three-dimensional knee replacement kinematics using single-plane fluoroscopy. IEEE Trans Biomed Eng. 1996;43(6):638-49.

23. Banks SA, Hodge WA. 2003 Hap Paul Award Paper of the International Society for Technology in Arthroplasty. Design and activity dependence of kinematics in fixed and mobile-bearing knee arthroplasties. J Arthroplasty. 2004;19(7):809-16.

24. Banks S, Bellemans J, Nozaki H, Whiteside LA, Harman M, Hodge WA. Knee Motions During Maximum Flexion in Fixed and Mobile-Bearing Arthroplasties. Clinical Orthopaedics & Related Research. 2003;410:131.

25. Fantozzi S, Benedetti MG, Leardini A, Banks SA, Cappello A, Assirelli D, et al. Fluoroscopic and gait analysis of the functional performance in stair ascent of two total knee replacement designs. Gait Posture. 2003;17(3):225-34.

26. Fregly BJ, Sawyer WG, Harman MK, Banks SA. Computational wear prediction of a total knee replacement from in vivo kinematics. J Biomech. 2005;38(2):305-14.

27. Harman MK, Banks SA, Hodge WA. Polyethylene damage and knee kinematics after total knee arthroplasty. Clin Orthop Relat Res. 2001;(392):383-93.

28. van den Elsen PA, Pol EJD, Viergever MA. Medical image matching-a review with classification. IEEE Engineering in Medicine and Biology Magazine. 1993;12(1):26-39.

29. Maintz JB, Viergever MA. A survey of medical image registration. Medical image analysis. 1998;2(1):1–36.

30. Hill DLG, Batchelor PG, Holden M, Hawkes DJ. Medical image registration. Physics in medicine and biology. 2001;46(3):1-1.

31. Sherouse GW, Novins K, Chaney EL. Computation of digitally reconstructed radiographs for use in radiotherapy treatment design. Int. J. Radiat. Oncol. Biol. Phys. 1990 Mar;18(3):651-658.

32. Lemieux L, Jagoe R, Fish DR, Kitchen ND, Thomas DG. A patient-to-computed-tomography image registration method based on digitally reconstructed radiographs. Med Phys. 1994 Nov;21(11):1749-1760.

33. Penney GP, Weese J, Little JA, Desmedt P, Hill DLG. A comparison of similarity measures for use in 2-D-3-D medicalimage registration. IEEE Transactions on Medical Imaging. 1998;17(4):586-595.

34. Russakoff DB, Rohlfing T, Mori K, Rueckert D, Ho A, Adler Jr JR, et al. Fast generation of digitally reconstructed radiographs using attenuation fields with application to 2D-3D image registration. IEEE transactions on medical imaging. 2005;24(11):1441-1454.

35. Tomazevic D, Likar B, Pernus F. Reconstruction-based 3D/2D image registration. Med Image Comput Comput Assist Interv Int Conf Med Image Comput Comput Assist Interv. 2005;8(Pt 2):231-238.

36. Tomazevic D, Likar B, Pernus F. 3-D/2-D registration by integrating 2-D information in 3-D. IEEE transactions on medical imaging. 2006;25(1):17-27.

37. Aouadi S, Sarry L, INSERM C. Evaluation of a stochastic approach to 2D-3D intensity-based registration. In: Engineering in Medicine and Biology Society, 2007. EMBS 2007. 29th Annual International Conference of the IEEE. 2007. p. 6387-6390.

38. Weese J, Buzug TM, Penney GP, Desmedt P. 2D/3D registration and motion tracking for surgical interventions. Philips Journal of Research. 1998;51(2):299-316.

39. Cullip TJ, Neumann U. Accelerating Volume Reconstruction With 3D Texture Hardware [Internet]. University of North Carolina at Chapel Hill; 1994 [cited 2009 Oct 8]. Available from: http://portal.acm.org/citation.cfm?id=897857

40. Cabral B, Cam N, Foran J. Accelerated volume rendering and tomographic reconstruction using texture mapping hardware.

41. Kniss J, Kindlmann G, Hansen C. Multidimensional Transfer Functions for Interactive Volume Rendering. IEEE Transactions on Visualization and Computer Graphics. 2002;8(3):270-285.

42. Kruger J, Westermann R. Acceleration Techniques for GPU-based Volume Rendering [Internet]. In: Proceedings of the 14th IEEE Visualization 2003 (VIS'03). IEEE Computer Society; 2003 [cited 2009 Oct 8]. p. 38.Available from: http://portal.acm.org/citation.cfm?id=1081432.1081482

43. Westermann R, Ertl T. Efficiently using graphics hardware in volume rendering applications. In: Proc. of SIGGRAPH. 1998. p. 169–178.

44. Banks - IEEE BME 1996.pdf.

45. Ibanez L, Schroeder WJ, Ng L, Cates J. The ITK Software Guide [Internet]. Second. Kitware, Inc.; 2005. Available from: http://www.itk.org/ItkSoftwareGuide.pdf

46. Weese J, Penney GP, Desmedt P, Buzug TM, Hill DLG, Hawkes DJ. Voxel-based 2-D/3-D registration of fluoroscopy images and CT scansfor image-guided surgery. IEEE transactions on information technology in biomedicine. 1997;1(4):284-293.

47. Viola P, Wells III WM. Alignment by maximization of mutual information. International Journal of Computer Vision. 1997;24(2):137-154.

48. Wells WM, Viola P, Atsumi H, Nakajima S, Kikinis R. Multi-modal volume registration by maximization of mutual information. Medical image analysis. 1996;1(1):35-51.

49. Wang F, Vemuri BC, Rao M, Chen Y. Cumulative residual entropy, a new measure of information & its application to image alignment. In: Ninth IEEE International Conference on Computer Vision, 2003. Proceedings. 2003. p. 548-553.

50. Bey MJ, Zauel R, Brock SK, Tashman S. Validation of a New Model-Based Tracking Technique for Measuring Three-Dimensional, In Vivo Glenohumeral Joint Kinematics. J. Biomech. Eng. 2006;128(4):604.

51. van de Kraats EB, Penney GP, Tomazevic D, van Walsum T, Niessen WJ. Standardized evaluation methodology for 2-D-3-D registration. IEEE transactions on medical imaging. 2005;24(9):1177-1189.

52. Hajnal JV, Hawkes DJ, Hill DL. Medical image registration. CRC; 2001.

53. Viola P, Wells III WM. Alignment by maximization of mutual information. International Journal of Computer Vision. 1997;24(2):137-154.

54. Penney GP, Weese J, Little JA, Desmedt P, Hill DLG. A comparison of similarity measures for use in 2-D-3-D medicalimage registration. IEEE Transactions on Medical Imaging. 1998;17(4):586-595.

55. Tomazevic(MRI-CT 3d2d)_IEEE2003.pdf.

56. Gerhardt JJ, Cocchiarella L, Lea RD. The Practical guide to range of motion assessment. American Medical Association; 2002.

57. Nitschke JE, Nattrass CL, Disler PB, Chou MJ, Ooi KT. Reliability of the American Medical Association guides' model for measuring spinal range of motion. Its implication for whole-person impairment rating. Spine. 1999 Feb 1;24(3):262-268.

58. Bull AM, McGregor AH. Measuring spinal motion in rowers: the use of an electromagnetic device. Clin Biomech (Bristol, Avon). 2000 Dec;15(10):772-776.

59. Nelson JM, Walmsley RP, Stevenson JM. Relative lumbar and pelvic motion during loaded spinal flexion/extension. Spine. 1995 Jan 15;20(2):199-204.

60. Pearcy MJ. Twisting mobility of the human back in flexed postures. Spine. 1993 Jan;18(1):114-119.

61. Theodoridis D, Ruston S. The effect of shoulder movements on thoracic spine 3D motion. Clin Biomech (Bristol, Avon). 2002 Jun;17(5):418-421.

62. Rechtine GR, Del Rossi G, Conrad BP, Horodyski M. Motion generated in the unstable spine during hospital bed transfers. J Trauma. 2004 Sep;57(3):609-611; discussion 611-612.

63. Rechtine GR, Conrad BP, Bearden BG, Horodyski M. Biomechanical analysis of cervical and thoracolumbar spine motion in intact and partially and completely unstable cadaver spine models with kinetic bed therapy or traditional log roll. J Trauma. 2007 Feb;62(2):383-388; discussion 388.

64. DiPaola CP, Sawers A, Conrad BP, Horodyski M, DiPaola MJ, Del Rossi G, et al. Comparing cervical spine motion with different halo devices in a cadaveric cervical instability model. Spine. 2009 Jan 15;34(2):149-155.

65. Horodyski M, DiPaola CP, DiPaola MJ, Conrad BP, Del Rossi G, Rechtine GR. Comparison of the flat torso versus the elevated torso shoulder pad removal techniques in a cadaveric cervical spine instability model. Spine. 2009 Apr 1;34(7):687-691.

66. DiPaola MJ, DiPaola CP, Conrad BP, Horodyski M, Del Rossi G, Sawers A, et al. Cervical spine motion in manual versus Jackson table turning methods in a cadaveric global instability model. J Spinal Disord Tech. 2008 Jun;21(4):273-280.

67. Del Rossi G, Horodyski MH, Conrad BP, Di Paola CP, Di Paola MJ, Rechtine GR. The 6-plus-person lift transfer technique compared with other methods of spine boarding. J Athl Train. 2008 Mar;43(1):6-13.

68. Conrad BP, Horodyski M, Wright J, Ruetz P, Rechtine GR. Log-rolling technique producing unacceptable motion during body position changes in patients with traumatic spinal cord injury. J Neurosurg Spine. 2007 Jun;6(6):540-543.

69. Bearden BG, Conrad BP, Horodyski M, Rechtine GR. Motion in the unstable cervical spine: comparison of manual turning and use of the Jackson table in prone positioning. J Neurosurg Spine. 2007 Aug;7(2):161-164.

70. Youdas JW, Carey JR, Garrett TR. Reliability of measurements of cervical spine range of motion--comparison of three methods. Phys Ther. 1991 Feb;71(2):98-104; discussion 105-106.

71. Youdas JW, Garrett TR, Suman VJ, Bogard CL, Hallman HO, Carey JR. Normal range of motion of the cervical spine: an initial goniometric study. Phys Ther. 1992 Nov;72(11):770-780.

72. Fletcher JP, Bandy WD. Intrarater reliability of CROM measurement of cervical spine active range of motion in persons with and without neck pain. J Orthop Sports Phys Ther. 2008 Oct;38(10):640-645.

73. Mannion AF, Knecht K, Balaban G, Dvorak J, Grob D. A new skin-surface device for measuring the curvature and global and segmental ranges of motion of the spine: reliability of measurements and comparison with data reviewed from the literature. European Spine Journal. 2004;13(2):122–136.

74. Post RB, Leferink VJM. Spinal mobility: sagittal range of motion measured with the SpinalMouse, a new non-invasive device. Arch Orthop Trauma Surg. 2004 Apr;124(3):187-192.

75. Dvorak J, Panjabi MM, Novotny JE, Chang DG, Grob D. Clinical validation of functional flexion-extension roentgenograms of the lumbar spine. Spine. 1991;16(8):943.

76. Zdeblick TA. A prospective, randomized study of lumbar fusion. Preliminary results. Spine. 1993 Jun 15;18(8):983-991.

77. Frymoyer JW, Matteri RE, Hanley EN, Kuhlmann D, Howe J. Failed lumbar disc surgery requiring second operation. A long-term follow-up study. Spine. 1978 Mar;3(1):7-11.

78. Lehmann TR, LaRocca HS. Repeat lumbar surgery. A review of patients with failure from previous lumbar surgery treated by spinal canal exploration and lumbar spinal fusion. Spine. 1981 Dec;6(6):615-619.

79. Fujii R, Sakaura H, Mukai Y, Hosono N, Ishii T, Iwasaki M, et al. Kinematics of the lumbar spine in trunk rotation: in vivo three-dimensional analysis using magnetic resonance imaging. Eur Spine J. 2007 Nov;16(11):1867-1874.

80. Li G, Citrin D, Camphausen K, Mueller B, Burman C, Mychalczak B, et al. Advances in 4D medical imaging and 4D radiation therapy. Technol. Cancer Res. Treat. 2008 Feb;7(1):67-81.

81. Zuhlke T, Fine J, Haughton VM, Anderson PA. Accuracy of dynamic computed tomography to calculate rotation occurring at lumbar spinal motion segments. Spine. 2009 Mar 15;34(6):E215-218.

82. Gercek E, Hartmann F, Kuhn S, Degreif J, Rommens PM, Rudig L. Dynamic Angular Three-Dimensional Measurement of Multisegmental Thoracolumbar Motion In Vivo. Spine. 2008;33(21):2326.

83. Ryd L, Yuan X, L\öfgren H. Methods for determining the accuracy of radiostereometric analysis (RSA). Acta Orthopaedica. 2000;71(4):403–408.

84. Duggal N, Pickett GE, Mitsis DK, Keller JL. Early clinical and biomechanical results following cervical arthroplasty. Neurosurgical Focus. 2004;17(3):62-68.

85. Reitman CA, Hipp JA, Nguyen L, Esses SI. Changes in segmental intervertebral motion adjacent to cervical arthrodesis: a prospective study. Spine. 2004 Jun 1;29(11):E221-226.

86. Zhao K, Yang C, Zhao C, An KN. Assessment of non-invasive intervertebral motion measurements in the lumbar spine. Journal of biomechanics. 2005;38(9):1943-1946.

87. You BM, Siy P, Anderst W, Tashman S. In vivo measurement of 3-D skeletal kinematics from sequences ofbiplane radiographs: Application to knee kinematics. IEEE transactions on medical imaging. 2001;20(6):514-525.

88. Bey MJ, Zauel R, Brock SK, Tashman S. Validation of a new model-based tracking technique for measuring three-dimensional, in vivo glenohumeral joint kinematics. J Biomech Eng. 2006 Aug;128(4):604-609.

89. Anderst W, Zauel R, Bishop J, Demps E, Tashman S. Validation of three-dimensional model-based tibio-femoral tracking during running. Medical Engineering and Physics. 2009;31(1):10–16.

90. Tashman S, Kolowich P, Collon D, Anderson K, Anderst W. Dynamic function of the ACL-reconstructed knee during running. Clin. Orthop. Relat. Res. 2007 Jan;454:66-73.

BIOGRAPHICAL SKETCH

The author is married to Suzanne Shunk Conrad and has two lovely daughters, Adeline Ross Conrad ($\cup$) and Esther Maeve Conrad ($e = mc^2$). He was raised by two wonderful loving parents and molded by an encouraging sister.